Reliability Evaluation Including Adequacy and Dynamic Security

Assessment in Renewable Energy Integrated Power Systems

by

Yingying Wang

A Dissertation Presented in Partial Fulfillment
of the Requirements for the Degree
Doctor of Philosophy

Approved April 2020 by the
Graduate Supervisory Committee:

Vijay Vittal, Co-Chair
Mojdeh Khorsand, Co-Chair
Gerald Heydt
Raja Ayyanar

ARIZONA STATE UNIVERSITY

May 2020

ABSTRACT

Power systems are undergoing a significant transformation as a result of the retirements of conventional coal-fired generation units and the increasing integration of converter interfaced renewable resources. The instantaneous renewable generation penetration as a percentage of the load served in megawatt (MW), in some areas of the United States (U.S.) sometimes approaches over 50 percent. These changes have introduced new challenges for reliability studies considering the two functional reliability aspects, i.e., adequacy and the dynamic security or operating reliability.

Adequacy assessment becomes more complex due to the variability introduced by renewable energy generation. The traditionally used *reserve margin* only considers projected peak demand and would be inadequate since it does not consider an evaluation of off-peak conditions that could also be critical due to the variable renewable generation. Therefore, in order to address the impact of variable renewable generation, a probabilistic evaluation that studies all hours of a year based on statistical characteristics is a necessity to identify the adequacy risks. On the other hand, the system dynamic behavior is also changing. Converter interfaced generation resources have different dynamic characteristics from the conventional synchronous units and inherently do not participate in grid regulation functions such as frequency control and voltage control that are vital to maintaining operating reliability. In order to evaluate these evolving grid characteristics, comprehensive reliability evaluation approaches that consider system stochasticity and evaluate both adequacy and dynamic security are important to identify potential system risks in this transforming environment.

The objective of this work is to develop a reliability evaluation approach that evaluates the control capability of a power system to maintain dynamic security in conjunction with resource adequacy evaluation. The developed approach uses sequential Monte-Carlo Simulation (SMCS) as the probabilistic analysis technique of choice. The proposed approach considers the chronological stochasticity in the system and produces probabilistic reliability indices. The dynamic performance of a system can be accurately described and quantified using the developed approach with detailed system models represented in time-domain simulations (TDSs). The evaluation of potential reliability risks in power systems with high wind power penetration is addressed based on the developed approach in this work.

ACKNOWLEDGEMENTS

TABLE OF CONTENTS

LIST OF TABLES

LIST OF FIGURES

NOMENCLATURE

Abbreviations

AC   Alternating current

ASAI   Average service availability index

BPS   Bulk power system

CAIDI   Customer average interruption duration index

CAIFI   Custom average interruption frequency index

CAMX   California-Mexico power area in the WECC system

CCT   Critical clearing time

CE   Cross-Entropy

CEA   Canadian Electricity Association

COV   Coefficient of variation

CREW   Continuous reliability enhancement for wind database

DC   Direct current

EENS   Expected energy not supplied

ELCC   Effective load carry capability

EPRI	Electric Power Research Institute
ERCOT	Electric Reliability Council of Texas
ERO	Electric Reliability Organization
FERC	Federal Energy Regulatory Commission
FOR	Forced outage rate
FOH	Forced outage hours
GADS	Generation Availability Data System
GE	General Electric
IS	Importance Sampling
LOLD	Loss of load duration
LOLE	Loss of load expectation
LOLH	Loss of load hour
LOLP	Loss of load probability
LTRA	Long-term reliability assessment
MARS	Multi-Area Reliability Simulation Program
MCS	Monte Carlo Simulation

MTTF	Mean time to failure
MTTR	Mean time to repair
NREL	National Renewable Energy Laboratory
NERC	North American Electric Reliability Corporation
OPF	Optimal power flow
PID	Proportional-integral-derivative
POI	Point of interconnection
RoCoF	Rate of change of frequency
SAIDI	System average interruption duration index
SAIFI	System average interruption frequency index
SCADA	Supervisory control and data acquisition
SERC	SERC Reliability Corporation
SEP	Stable equilibrium point
SH	Service hours
SMCS	Sequential Monte Carlo Simulation
TADS	Transmission Availability Data System

TDS	Time-domain simulation
TEF	Transient energy function
UFLS	Under-frequency load shedding
UVLS	Under-voltage load shedding
VER	Variable energy resource
VRT	Variance reduction technique
WECC	Western Electricity Coordinating Council
WTG	Wind turbine generator

Variables

A	Availability rate of component outage model
B_{ij}	Imaginary part of the i-th row and j-th column element of the system bus admittance matrix
$D(x,y)$	*Kullback-Leibler* distance between distribution function x and y
$EGAF$	Expected generator tripping occurrence caused by abnormal frequency

EGAV	Expected generator tripping occurrence caused by abnormal voltage
EOAF	Expected abnormal frequency occurrence at generator terminals
EOAV	Expected abnormal voltage occurrence at generator terminals
f	Average failure frequency of transmission outage model
f_u	Transmission outage frequency per kilometer per year
$g(\cdot)$	Probability density function in CE IS
$g_{opt}(\cdot)$	Optimized probability density function in CE IS
H_{ij}	Reliability test function of system state x_{ij}
G_{ij}	Real part of the *i*-th row and *j*-th column element of system bus admittance matrix
I_i	Reliability index obtained from the *i*-th iteration of MCS
$\hat{I}$	Statistical estimate of the expected value of the *I*
KE	System kinetic energy
KE_{corr}	System corrected kinetic energy
L	Length of a transmission line

l_{pd}	Active power frequency index of composite load model
l_{qd}	Reactive power frequency index of composite load model
LS_{TDS}	Load shedding criterion of dynamic security
max	The maximum value operator; the maximum magnitude value for complex numbers.
M_{cr}	Inertia constant of critical generators inertial center
M_{eq}	System equivalent inertia constant
M_i	Inertia constant of generator i
min	The minimum value operator
M_{non_cr}	Inertia constant of non-critical generators inertial center
N	Set of all buses
N_f	Number of failed components in a system state
NG	Set of generator buses
N_j	Number of sampled system states in an iteration of MCS
NL	Set of load buses
N_{MAX}	Maximum iteration of MCS

N_s	Number of successful components in a system state
NT	Set of transmission lines
N_y	Number of simulation iterations of MCS
OCC	Number of unreliable state occurrences in a MCS iteration
OOF_i	Number of occurrences of over-frequency generator tripping actions in the i-th MCS iteration
OUF_i	Number of occurrences of under-frequency generator tripping actions in the i-th MCS iteration
P_0	MW load value at nominal voltage and frequency
p_1	Constant impedance fraction of MW load in load model
p_2	Constant current fraction of MW load in load model
p_3	Constant power fraction of MW load in load model
p_4	Frequency dependent power fraction of MW load in load model
$P(w)$	Wind turbine active power output when the wind speed input is w m/s
P_G	Generator active power output variable

$P_{G,MIN}$	Minimum generator active power output
$P_{G,MAX}$	Maximum generator active power output
P_{L0}	Initial MW load value from power flow
$P_{ns,ij}$	MW value of load not supplied in state x_{ij}
P_r	Rated active power output of wind turbine
$P_i(V,\delta)$	Active power injection at bus i
PD_i	MW load at load bus i
PG_i^{min}	Minimum active power output of generator i
PG_i^{max}	Maximum active power output of generator i
$P_{UFLS,ij}$	MW value of load shedding triggered by under-frequency load shedding relay in state x_{ij}
$P_{trip\_OF,ij}$	MW value of generation trip resulting from over-frequency protection action in state x_{ij}
$P_{trip\_UF,ij}$	MW value of generation trip resulting from under-frequency protection action in state x_{ij}

$P_{trip\_OV,ij}$	MW value of generation trip resulting from over-voltage protection action in state x_{ij}
$P_{trip\_UV,ij}$	MW value of generation trip resulting from under-voltage protection action in state x_{ij}
Q_0	MVAr load value at nominal voltage and frequency
q_1	constant impedance fraction of MVAr load in load model
q_2	Constant current fraction of MVAr load in load model
q_3	Constant power fraction of MVAr load in load model
q_4	Frequency dependent power fraction of MVAr load in load model
$Q_i(V,\delta)$	Reactive power injection at bus i
QD_i	MVAr load at load bus i
QG_i^{min}	Minimum reactive power output of generation i
QG_i^{max}	Maximum reactive power output of generation i
Q_G	Generator reactive power variable
$Q_{G,MIN}$	Minimum generator reactive power output

$Q_{G,MAX}$	Maximum generator reactive power output
S_G	MVA generator output variable
S_L	MVA load variable
S_{L0}	Initial MVA load value from power flow
$S_{mn,MAX}$	Maximum MVA flow on the line connecting bus m and bus n
T_i	Sum of the time durations of states in the ith iteration of MCS
$T_k(V,\delta)$	MVA power flow on transmission line k
T_k^{max}	MVA rating of transmission line k
$T_{mn}(V,\delta)$	MVA flows on the line between bus m and bus n
U	Unavailability rate of component outage model
$\vec{u}$	Original unavailability rate vector of components for CE IS
$\vec{v}$	Motified unavailability rate vector of components for CE IS
U_i	A sampled uniformly distributed random number between $(0,1]$ for component i

UFOC	Expected occurrence of under-frequency load shedding
UFENS	Expected power not supplied from under-frequency load shedding actions
UFLS(x_{ij})	Test function of under-frequency load shedding for state x_{ij}
V	Bus voltage magnitude
$\overline{V}$	Bus voltage
V_{MIN}	Lower limit of bus voltage magnitude
V_{MAX}	Upper limit of bus voltage magnitude
V_i	Voltage magnitude of bus i
V_i^{min}	Lower limit of voltage magnitude at bus i
V_i^{max}	Upper limits of voltage magnitude at bus i
$\overline{V}_m$	Voltage phasor of bus m
$\overline{V}_m^*$	Complex conjugate of $\overline{V}_m$
$\overline{V}_n$	Voltage phasor of bus n
$\overline{V}_n^*$	Complex conjugate of $\overline{V}_n$

$\vec{v}_{opt}$	Optimal unavailability rate vector of components for cross entropy based importance sampling
w	Wind speed input for wind turbine power curve
w_i	Cut-in wind speed in wind turbine power curve
w_r	Rated wind speed in wind turbine power curve
w_o	Cut-out wind speed in wind turbine power curve
$W(X_i)$	Likelihood ratio for optimized probability density function calculation in CE IS
X_i	System state vector in the i-th iteration of MCS
x_{ij}	System state j in the i-th iteration of MCS
Y_{bus}	Bus admittance matrix
Y_{bus}^*	Conjugate transpose of Y_{bus}
Y_{line}	Transmission line admittance
Y_{line}^*	Conjugate transpose of Y_{line}
Z_{th}	Thévenin impedance seeing into the point of interconnection of a generator
ΔZ_{th}	The change of Thévenin impedance Z_{th} after a contingency

β_{MAX}	*COV* criterion for determining MCS convergency
λ	Failure rate of a component
λ_i	Failure rate of component i
μ_i	Repair rate of component i
μ	Repaire rate of a component
$\widetilde{\omega}_{cr}$	Angular speed of the inertial center of the critical generator group
ω_{coi}	Angular velocity of the center of inertia
$\widetilde{\omega}_{eq}$	Equivalent inertia constant and angular speed of the system
ω_i	Angular velocity of the generator i
$\widetilde{\omega}_{non\_cr}$	Angular speed of the inertial center of the non-critical generator group
δ_i	Voltage angle of bus i
δ_{ij}	Voltage angle difference between bus i and bus j
τ_{ij}	Duration time of state x_{ij}
ψ_L	Load adjustment factor setting for OPF

$\psi_{L,MIN}$ Minimum value of load adjustment factor setting for OPF

$\psi_{L,MAX}$ Maximum value of load adjustment factor setting for OPF

Chapter 1

INTRODUCTION

1.1   Background

Power systems are undergoing a significant and rapid transformation, primarily

driven by environmental regulations, incentives for variable energy resources (VERs), and

impacts of fuel prices. The generation fleet is transforming from mainly relying on coal-

fired generation to being primarily natural-gas-fired and renewable generation. In 2018,

natural gas and other gases consisted of 43% of the fuel mix, while renewable resources

consisted of around 5% of the fuel mix in North America [1]. Conventional coal-fired gen-

eration continues to decrease in the system. In certain areas, the rate of transformation is

more rapid and is significantly impacting the planning and operations of power systems. In

the Electric Reliability Council of Texas (ERCOT) system, the instantaneous penetration

of renewable generation exceeded 50% of system load in 2017 [2] and led to changes in

system operation, such as the participation of demand response to maintain reliability.

Transmission systems are correspondingly subjected to expansion as a consequence of the

resource mix. These changes in the system are altering the operational characteristics of

the grid and consequently have raised reliability issues that require comprehensive exami-

nation.

It is worthwhile to review the definition of reliability and the processes of reliability

studies in the industry, to understand the impact of the transformations described above on

systems reliability. Reliability is the term used to describe the ability of a system to deliver

power to consumers within accepted standards and in the amount desired. According to the current definition by North America Electric Reliability Corporation (NERC), reliability consists of two fundamental aspects: adequacy and operating reliability. Adequacy is the ability of the electric system to supply the aggregate electric power and energy requirements of the electricity consumers at all times, taking into account scheduled and reasonably expected unscheduled outages of system components. Operating reliability is the ability of the electric system to withstand sudden disturbances such as electric short circuits or unanticipated loss of system components [1]. Before the term *operating reliability* started to be used by NERC to describe the ability of the system to withstand sudden disturbances, the term *security* was used and is still widely used in literature. The two terms are used interchangeably to represent the system's capability to withstand sudden disturbances.

The maintenance of both adequacy and operating reliability is essential to provide the desired level of reliability in the system. However, in current practice, the two reliability functions have been treated separately, primarily because of historical experiences of different approaches for the assessments of the two aspects. System adequacy examines the sufficiency of generation and transmission resources to meet demand. It is evaluated as a part of the seasonal reliability assessment and long-term reliability assessment (LTRA) in industry practice. Since the number and configuration of generators and transmission lines contribute to the reliability of a system, the LTRA considers proposed generation and transmission additions and projects future electricity demands to analyze the resource adequacy in the next one year to ten years. The analytical approaches for resource adequacy range

from relatively simple calculations of planning reserve margins to rigorous probabilistic reliability simulations that calculate system loss of load probability (*LOLP*) or loss of load expectation (*LOLE*) values. In either approach, the adequacy assessment analyzes the static status of the system supplying demand rather than the system dynamic performance. Whereas the operating reliability of a system is measured by the dynamic response of the system when it is subjected to a disturbance. The operating reliability requires that the system operates within steady-state limits and maintains dynamic security after a disturbance. The assessment of the operating reliability assessment is primarily based on the NERC Transmission Planning Standard [3] that define a range of credible contingencies under which the system needs to maintain reliable operation. System behavior under these credible contingencies is analyzed based on power flow studies or/and dynamic studies.

The traditional process of assessing the adequacy and operating reliability has been challenged by the retirements of conventional coal-fired generation units and the increasing penetration of renewable resources. The main sources of these challenges stem from the uncertain nature of the renewable resources, e.g., wind and solar generation, and the new failure characteristics of the renewable generation units. Moreover, the operating characteristics of power systems have been altered due to the power electronics interface of these renewable resources to the grid. Adequacy assessment has become more complicated due to the variability and uncertainty brought by the renewable energy generation. The traditionally used reserve margin that calculates the gap between future generation and projected load would be insufficient if it is only based on the projected peak demand. The off-peak system conditions can be critical due to the variability of renewable generation.

For instance, in the 2018 LTRA of the Western Electricity Coordinating Council (WECC) system, WECC projected that the reserve margin for the WECC-CAMX (California-Mexico) Region is over 22 percent in 2020 and over 21 percent in 2022. The projected reserve margins in the two years are both above the reserve margin reference showing that there will be adequate resources in the system. However, the loss of load hour (*LOLH*) from probabilistic adequacy analysis is projected to increase from 0.13 hours in 2020 to 2.3 hours in 2022, due in part to the changing resource mix [1]. The finding indicates that the deterministic planning reserve margin metric may not be an accurate means to measure the resource adequacy, especially in areas that have a high penetration of VERs. Probabilistic analysis that studies all hours of the year is necessary to identify system adequacy risks.

Different from the adequacy assessment, which focuses on system steady-state conditions, the operating reliability examines systems performance after contingencies occur. It addresses the system static security, which involves steady-state analysis of the post-disturbance system conditions, as well as the dynamic security, which involves examining rotor angle stability, frequency stability and voltage stability of the system [4]. The contingencies are normally pre-specified based on the transmission planning standard [3], and a qualitative result of operating reliability under these contingencies will be specified in terms of pass or fail. Due to the new resource mix, system operating characteristics are subjected to changes. For example, when a generation unit located near a load center is retired and new generation not in the vicinity of the load area, comes online, the load center will require power imports and dynamic reactive resource replacement to maintain voltage stability. These changes lead to a questioning of the credibility of using the traditionally

used deterministic approach based on pre-specified contingencies to examine operating reliability. To consider the stochastic variability in the system operating conditions, the utilization of probabilistic approaches for operating reliability evaluation needs to be investigated.

The uncertainties associated with the new generation fleet also prompt the need to consider more system conditions in the operating reliability evaluation. Driven by these challenges, some special assessments of the frequency and voltage dynamic stability have been conducted in conjunction with traditional N-1 studies. Comprehensive reliability evaluation approaches are needed to evaluate the system performance considering system stochasticity while addressing both adequacy and operating reliability, to measure the overall reliability impacts of the changing resource mix.

1.2   Motivation and Objectives

Under the fundamental transformation in power systems, reliability studies must be conducted comprehensively to identify potential system risks. It should be ensured that there is sufficient capacity and flexibility in systems to meet the peak demand as well as off-peak hours introduced by generation resources that are limited by the primary energy. From this perspective, probabilistic analysis methods that consider the variability and uncertainty of generation and the availability of the various components in a system is worthy of investigation. Also, since it is impossible to study all possible initial conditions for operating reliability, probability analysis methods provide an efficient approach to consider

the stochasticity in selecting operating conditions to study static and dynamic security. Another benefit of the probabilistic analysis approach is that quantitative results are expected to be calculated rather than qualitative results. The quantitative evaluation results can provide more precise information on the level of unreliability and identify critical system conditions.

A comprehensive reliability evaluation approach should also integrate the assessment of the adequacy and operating reliability into a single process. When a system is subjected to a contingency, the process should evaluate system dynamic security after the contingency occurs to determine whether the system maintains stable transition to a post-contingency status and evaluate the adequacy of the post-disturbance system supplying load within steady-state security limits.

Therefore, the objective of this work is to develop a comprehensive reliability evaluation approach with adequacy and dynamic security integrated into a single framework. The approach will evaluate the generation and transmission adequacy of the system considering steady-state security limits including thermal limits and voltage limits, and dynamic security including short-term rotor angle stability, frequency stability, and voltage stability. The approach will also incorporate renewable generation in the adequacy assessment and dynamic security assessment to evaluate the reliability of power systems with high renewable penetration. Specifically, this work has the following objectives:

1. Designing the Monte Carlo Simulation (MCS) framework: MCS has emerged as a preferred approach for probabilistic analysis in large power systems. MCS deals with the

issue of dimensionality by sampling states based on their probabilities and drawing the inference from the sample with a convergence criterion to ensure sufficient accuracy. One of the objectives of this work is to develop a probabilistic approach for reliability evaluation integrating system adequacy assessment and dynamic security assessment into a single framework.

2. Developing models representing system stochasticities: All relevant stochasticities in the system is investigated to develop appropriate probability model representations. With proper stochastic models, the key factors associated with uncertainty and variability are included in the MCS to sample system states.

3. Developing integrated reliability assessment techniques: For the assessment of a state in integrated reliability evaluation, the examination includes the system dynamic performance after the disturbance and the post-contingency steady-state performance. The assessment techniques that can accurately evaluate the performance and can be incorporated into the integrated reliability measurements are investigated.

4. Developing acceleration techniques for the integrated reliability evaluation process: Dynamic system performance simulation is a time-consuming process. Therefore, tools that can pre-determine the stability or instability of a case can significantly reduce the computational efforts. A pruning process is developed to determine whether stability evaluation is warranted. Another acceleration approach is investigated to improve the computational efficiency of the MCS process.

5. Proposing quantitative integrated metrics: Quantitative metrics that integrate adequacy and dynamic security evaluation results are proposed and a research-grade software that implements the proposed integrated reliability approach and demonstrates the advantages of the proposed approach is developed.

6. Investigating the utilization of the proposed reliability evaluation approach in renewable integrated power systems: Studies are conducted to evaluate the impact of increasing renewable energy integration on system reliability, considering both the impact on system adequacy and dynamic security. The effect of the control capability of the converter-interfaced renewable energy on reliability performance is analyzed.

1.3   Organization of the Dissertation

This dissertation is organized as follows. Chapter 2 discusses a detailed literature review of the existing work in this area. Chapter 3 presents the probabilistic models of components and probabilistic analysis methodology. Chapter 4 presents the test system and system dynamic models for reliability evaluation. Chapter 5 discusses the reliability evaluation approach considering the adequacy and dynamic security being assessed by steady-state analysis and stability analysis, respectively. Two acceleration methods to speed up the integrated reliability evaluation are discussed in this chapter. Chapter 6 presents the results of the application of the proposed methods, along with discussions of the results. Chapter 7 presents the application of the proposed approach for the reliability evaluation of a test system with high wind generation penetration. The impact of increasing wind

power penetration and wind turbine generators (WTGs) participating in grid control are discussed in this chapter. Chapter 8 concludes this dissertation and discusses future work.

Chapter 2

LITERATURE REVIEW

Reliability describes the ability of power systems to deliver electricity to all points of consumption, in the quantity and quality demanded by the customers. After the 2003 Northeast blackout, the Federal Energy Regulatory Commission (FERC) was authorized to designate a national Electric Reliability Organization (ERO) and required the development of mandatory reliability standards. NERC became the nation's ERO and charged with conducting reliability studies of the bulk power system (BPS) in North America. In industry practice, reliability evaluations include resource adequacy evaluation examining static system conditions, operating reliability examining system dynamics, and some special assessments such as studies of maintaining reliability while integrating VERs or gas turbines. Although there are unified reliability requirements throughout the industry, the methodologies used by various entities can be different. Existing work related to the evaluation of system adequacy and dynamic performances is discussed in this chapter.

2.1   Evaluation Techniques for System Adequacy

Adequacy assessment is one of the essential power system studies that evaluate and plan a power system to ensure that an adequate supply of electricity is available to meet current and future needs. Historically, adequacy assessment of power systems has been conducted using deterministic approaches such as percentage reserves in generation capacity planning or N-1 contingency criteria in transmission expansion [5]. The fundamental weakness of deterministic criteria is that it does not reflect the probabilistic or stochastic

nature of system behavior. Driven by this, studies and applications of the probabilistic reliability evaluation approach have become prevalent after the required computational resources became available in the 1990s [6]. Probabilistic evaluation techniques can be classified under two main categories: analytical and simulation techniques, and each has its merits and demerits. The use of analytical techniques or MCS methods depends on the system that the analysis is performed on. Generally, analytical techniques are more efficient in analyzing systems that have small failure probabilities of components or do not have complex operating conditions. Reference [7]–[9] are among the early works that presented analytical approaches for system adequacy evaluation. However, if complex system conditions should be considered or the number of unreliable events is relatively large in a system, MCSs are more preferred. The theory and mathematical models of MCSs are well explained in [5], [10]. In MCS methods, the stochastic behavior of power systems is analyzed through simulation of physical relationships, and the generated results are the expected values of reliability indices. It makes MCS an efficient analysis technique for systems with stochasticity. Particularly, sequential MCS is capable of incorporating the chronological stochasticity in the system, such as the load variation and the increasing integrated wind and PV generation. In [11], a method to calculate equivalent wind capacity is introduced for reliability evaluation based on MCS. The equivalent wind capacity is based on a global annual wind power distribution established in the literature by the convolution of constitutive wind plant generation histograms. Chronological wind speed was used as an input in the adequacy evaluation in [12], [13] in order to accurately represent the stochastic nature of wind generation. The results using the MCS method were compared with the results from the enumeration method in [14]. The authors proposed a hybrid

Monte-Carlo method and an analytical approach. Because of the so-called curse of dimensionality issue (the enumeration number increases exponentially with the number of components), the exhaustive enumeration is computationally intractable. For the assessment of a large power system, the MCS method is preferred.

In current industry practice, probabilistic techniques for generation adequacy analysis have been used at some level in nearly all regions of North America, either by making direct probabilistic assessments that calculate probabilistic reliability indices such as *LOLE* or by identifying an equivalent percent reserve margin. In direct probabilistic assessments, the objective is to test whether existing and future resources are sufficient to assure a *LOLE* of no more than 1 day in 10 years where all relevant factors and uncertainties are included in the simulation. Some universal factors and uncertainties are considered including the forced outages of thermal generators and load uncertainty. While in areas that have abundant wind or hydro resources, wind or hydro generation may also be modeled as stochastic parameters. It is important to note that, in most of the probabilistic analysis of resource adequacy, the transmission system is not considered or simplified as transfer limits. Although the probabilistic approaches for composite generation and transmission system have been well investigated, their applications in the electric power industry are quite limited, and the main reason is the computational burden and the lack of a unified approach.

Extensive work has been done to reduce the computation time in MCSs. High-speed computing and programming paradigms have been explored to improve Monte-Carlo simulation efficiency. Gubbala and Singh in [15] described two random number generation

schemes and three topologies for parallelizing the fixed interval MCS for reliability evaluation of interconnected power systems. In [16], Borges, Falcao, Mello, and Melo demonstrated two parallel methods for composite reliability evaluation using SMCS. In one of the methods, a complete simulation year is analyzed on a single processor and the many simulated years necessary for convergence are analyzed in parallel. In another method, the assessment of the system states in the simulated years is performed in parallel and the convergence is checked on one processor at the end of each simulated year. Other computational techniques such as intelligent agent technology based on which reliability evaluations are assigned to different agents [17], [18], artificial neural networks [19], and object-oriented programming [20] have also been proposed to reduce the computational cost. Another approach to make the MCS method more time efficient is to use variance reduction techniques (VRTs). The objective of VRTs is to mathematically decrease the variance of the estimators of the reliability indices while not affecting their expected value. By decreasing the variance, the number of samples needed for reaching convergence can be reduced so that the convergence is sped-up. Different types of VRTs such as Antithetic Variables [21]–[23], Control Variables [24], [25] and the combination of VRTs [26] have been tested by researchers to increase the MCS efficiency. Importance Sampling (IS) is a relatively new VRT method. Its utilization in the study of real systems has been limited by the fact that it is difficult to find the optimized IS distribution. The application of the Cross-Entropy (CE) method provided a possible solution to that problem. In [27]–[29], the Cross-Entropy based optimization process was proposed in non-sequential MCS to obtain an auxiliary sampling distribution, which helped to minimize the variance of the reliability index

13

estimators. The method has been tested in generation reliability and composite system reliability. The probabilistic approaches with suitable acceleration methods to improve evaluation speed for complex realistic power systems need to be further investigated to promote the application in real systems, so that transmission capability is considered in measuring resource sufficiency to serve load.

2.2   Evaluation Techniques for Operating Reliabilty

Operating reliability assessment aims to provide a judgment on the ability of a power system to operate reliably under disturbances for a range of operating conditions. A variety of issues including voltage issues, frequency issues, and transient stability issues should be considered in the operating reliability assessment. In the power industry, the approaches for operating reliability evaluation used by entities are different. A general practice is to conduct power flow analysis to identify problem areas or paths and then conduct stability studies specifically on these areas or paths. Stability limits on system reliability are playing a more important role because of the transformative changes in systems. As identified in [2], stability challenges are likely to be the most limiting constraints for high renewable penetration conditions and could significantly affect the reliability of the system. Stability limits are necessarily considered in the reliability assessment, in conjunction with adequacy assessment. Using probabilistic approaches is more suitable in the assessment, rather than deterministic approaches.

The approaches currently being used in the industry are mainly deterministic approaches where system performance is evaluated based on pre-determined operating

conditions and credible contingencies. The system stability in deterministic studies is treated as binary (stable or unstable). Various uncertainties associated with operating conditions and with contingencies are not taken into account in these approaches. Probabilistic approaches, on the other hand, consider the probability distribution of stochastic factors in systems, and therefore can better reflect the actual system behavior. Probabilistic approaches provide an alternate way to identify stability limits.

Probabilistic approaches for evaluating system stability have attracted a significant amount of interest in the past. In [30], a practical method of probabilistic reliability assessment for large interconnected power systems was proposed. The probabilistic reliability assessment relies on an enumeration of contingencies and draws from the simulations the quantitative and probability-weighted evaluation of the contingencies impacts. Four distinct types of reliability indices were proposed in this paper. They are the thermal overload reliability index, voltage violation reliability index, voltage instability index and load loss index. Based on the method, the root causes that most jeopardize the system reliability, the weak points and the operating conditions that have the most severe impact on system reliability can be generated. This paper presented the benefit of probabilistic stability analysis: while the deterministic method determines the maximum level of load/transfer increase the system can handle without violating criteria, the probabilistic method determines this maximum level by judging whether reliability indices exceed the threshold. A probabilistic technique was proposed in [31] for measuring the level of security or the level of stress of a power system in an operational environment. It considered not only contingencies that are deemed credible but also the less probable but highly damaging contingencies. Hence,

15

it provides a complete assessment of the state of the system. In these two efforts, the system analysis focuses on the steady-state system conditions and is based on power flow studies.

Work has also been done on the assessment of transient stability, frequency stability, and voltage stability using probabilistic approaches. Authors in [32] presented the results of the probabilistic transient stability assessment on the large scale system of B. C. Hydro. Results in the paper showed that deterministic criteria produce conservative results and do not always correspond to the worst-case scenario. The difference between deterministic and probabilistic transient studies was well explained in the procedures given in the paper. The procedures are shown in Figure 2.1. Billinton, Carvalho, and Kuruganty in [33] presented a probabilistic assessment method of power system transient stability using Lyapunov functions to determine the post-fault stable equilibrium. System risk is represented by the product of transient instability probability and the consequence of the fault, which caused the instability. In [34], a risk-based stability assessment method considering both transient stability and oscillatory instability is presented. The authors proposed a composite risk index which can be obtained as the summation over risks of each event. In [35], the authors presented a methodology to evaluate the probability and consequences of transient instability. A transient stability index based on transient energy components calculated in TDS is used to quantify the transient stability of the system. The Electric Power Research Institute (EPRI) and Iowa State University worked on a series of projects which tackled the risk-based security assessment issue. The identified methodology, software design, and implementation of computing risk in those projects associated with line

16

overload, transformer overload, and voltage out of limits, voltage instability, transient in-

stability, and special protection schemes. These methods are based on the notion that risk

is the product of probability and consequence. The computations were developed in a man-

ner that the risk result is a function of the operating condition, a specified contingency, and

uncertainty related to the operating condition and the system performance following the

contingency [36], [37].
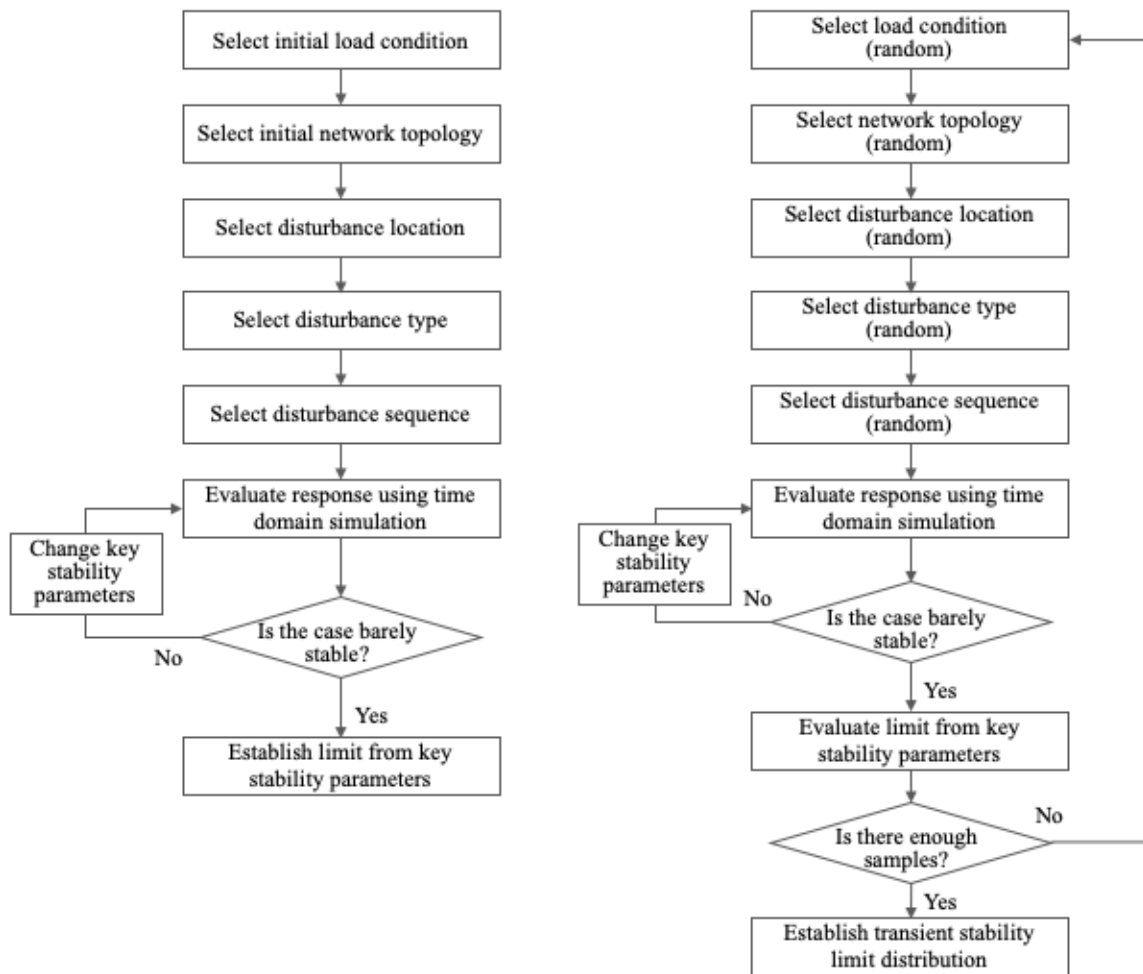
Figure 2.1 Procedures for Deterministic and Probabilistic Transient Stability Studies

A probabilistic index for transient stability based on the probability distribution of the transfer admittance is described in [38] and its application in a practical system considering the probability of fault occurrence, fault location and fault clearing time is illustrated in [39]. Similar probabilistic transient stability evaluation based on the enumeration approach is described in [40]. The probabilistic characteristics of the fault are considered in the same work. Also, a stochastic model of a high-speed reclosing relay is proposed in this paper. The system stability is determined based on whether the fault clearing time is less than the critical clearing time (CCT). In [41], a bisection method is utilized to evaluate probabilistic transient stability and reduce the amount of computation time of the evaluation. An analytical model that addresses the uncertainty of the fault clearing time for probabilistic transient stability assessment of power systems is proposed in [42]. The fault clearing time is compared with the CCT to assess system stability, and a corrected transient energy function-based strategy is developed for case pruning to improve the computational efficacy. In [43], the system risk is calculated using the probability distribution of the transient stability margin and the severity quantifying the impact of a contingency with a variation of stability margin. The authors in [44] presented a conceptual framework for an approach to the probability assessment of power system transient stability using MCS and direct method. The computer program based on this method is described in [45].

More recently, several efforts have been devoted to investigating the probabilistic stability analysis considering the increased uncertainties brought by the integration of VERs. The effects of wind power intermittency on power system transient stability were

studied in [46]. With an equivalent wind farm dynamic model implemented in the test system, the MCS with two indices, namely angle-based margin index and CCT is applied on the test system to evaluate the effects of wind power intermittency and variability on system transient stability. The frequency distribution of transient stability evaluation index, CCT, probability of system transient instability and range of wind speed causing system transient instability are simulated. Reference [47] proposed a probabilistic framework for transient stability assessment of power systems with high penetration of renewable generation. The procedure includes sampling the uncertainties in load and wind/PV generation, running optimal power flow (OPF) to determine generation dispatch, and performing time-domain simulations of a large number of contingencies to calculate transient stability indices. Based on the approach, the impact of renewable energy penetration on transient stability was analyzed. The study based on this approach was extended to assess the impact of intermittent behavior of distributed energy resources on transient stability of power systems [48].

Probabilistic approaches for the evaluation of frequency stability and voltage stability have been studied in [49]–[58]. In [49], a risk assessment approach to analyze power system steady-state voltage, overload, and frequency response adequacy was proposed for operation planning under high penetration of wind power generation. In this approach, the frequency excursion was approximated using a mathematical equation. Therefore, the frequency response adequacy can be performed at the same time with the steady-state voltage and overload evaluation, without performing dynamic simulations. In [50], frequency stability limits were considered in the probabilistic analysis to determine the maximum

penetration level of wind farms. A simplified frequency response model with the inertia and damping considered was used to determine the frequency nadir. Voltage stability has been primarily studied by means of steady-state analysis techniques. In [57], voltage collapse is studied considering the stochastic nature of the load. A probabilistic methodology is developed to provide risk indices of voltage collapse and determine the most likely critical bus and the corresponding point of collapse, based on the MCS method.

The literature survey conducted, shows that, the probabilistic results for transient stability usually were based on the transfer limit calculation [32], probability of system instability [33], [38], [40], [59], [60], expected frequency/ probability of transient instability [39], and transient stability indices such as the maximum rotor angle deviation [47], [48]. The indices for probabilistic analysis of power system frequency stability proposed include the frequency response inadequacy [49], [50], the rate of change of frequency (*RoCoF*), and the frequency nadir [51]. As for probabilistic voltage stability indices, probability/ frequency of voltage instability, reactive load margin, and expected voltage stability margin were used [53], [58]. With the changing resource mix in the system, the adequacy of frequency and voltage support are one of the primary considerations in the industry. The indices used to characterize frequency and voltage support in industry practice are primarily the synchronous inertial response, initial frequency deviation and frequency response in MW/0.1 Hz from pre-disturbance frequency to frequency nadir and settling frequency to measure frequency performance, the number of voltage exceedances and reactive performance to measure voltage performance [61], [62].

2.3   Integrated Evaluation of Adequacy and Dynamic Security in Transformed Grid

With the increasing integration of converter interfaced generation, the inherent system capability to stabilize after disturbance is reducing. The reasons include the reduced inertia to resist frequency deviation, the lowered dynamic reactive power reserve as well as the increased loss of active power and reactive power on long transmission lines. A disturbance after which the system will remain stable and return to a steady-state condition can cause unstable system conditions under low system strength situations [2].

Presently, in the long-term system assessment process, transmission adequacy is evaluated based on power flow analysis from a steady-state perspective while generation adequacy is even more simplified and does not require a power flow study. However, stability challenges are likely to be the most limiting constraints for a system with increasing resource mix change, especially when the generation from new resources needs to be supplied to load through long-distance transmission lines. Steady-state analysis of system performance after a disturbance assumes the system settles in a post-contingency stable equilibrium point (SEP) immediately after the contingency. Hence it neglects system dynamic performance after the contingency and overlooks system risks which would be identified in a stability analysis. New approaches for reliability evaluation that consider stability evaluation in conjunction with steady-state adequacy assessment is, therefore, necessary to identify system risks in the new circumstance. The importance of system dynamic behavior and its significant influence on the overall reliability have been well recognized. However, there is limited work existing in this area of integrating the evaluation of system dynamic performance in conjunction with adequacy analysis.

21

A conceptual framework of a unified approach to probabilistic steady-state and dynamic security assessment was proposed in [63]. The authors introduced the time to insecurity as the metric of system security. The probability distribution of the time to insecurity is obtained from the solution of a linear vector differential equation whose coefficients are expressed in terms of steady-state and dynamic security regions. Reference [64] presented an integrated approach to extend the scope of reliability evaluations to include a probabilistic assessment of system security including transient stability and the effects of cascading sequences. In the proposed method, the system transient stability limit is determined by comparing the fault clearing time with the critical clearing time. If the fault clearing time is within the critical clearing time, the system is seen to be able to maintain transient stability after the contingency. The critical clearing time is different for different contingencies. Comprehensive reliability metrics are presented in the same paper. The probability of transient instability and the mean time to instability are used to measure the dynamic aspect of reliability. *LOLP*, *LOLF*, loss of load duration (*LOLD*), and expected energy not supplied (*EENS*) are used as the composite system indices. A method of composite power system reliability, including both static and dynamic processes through the sequential MCS, is proposed in [65]. In the proposed approach, the reclosing time is compared with fault time to classify fault to be transient or permanent. TDSs are used to analyze the transient stability and OPF is used to determine the amount of load curtailment. The loss of load during restoration under permanent and transient faults is calculated based on a corrective OPF. Conventional indices *EENS* and *LOLP* are calculated from the composite reliability evaluation, and two additional indices were proposed to describe the transient

stability. The two indices were Mean Instability Occurrence Rate and Mean Loss of Load during Restoration.

Reference [66] proposed a framework for extending conventional probabilistic reliability analysis to include transient and voltage stability issues in the adequacy assessment of a composite system. Instead of running TDSs, an intelligent system which is a combination of neural network and a fuzzy neural network is used to predict the transient and voltage stability status. Andrea M. Rei, et al. in [67], presented a method for integrating adequacy and security reliability evaluation using SMCS to capture stochastic features in power systems. Transient stability is evaluated by comparing the critical energy based on CCT and the potential energy boundary surface calculated based on transient energy function (TEF). More recently, Benidris, Mitra, and Singh in [68] proposed an integrated evaluation of the reliability and stability method. A direct method is utilized for transient stability assessment based on computing the energy margin of the system under fault. Three probabilistic transient stability indices are proposed to address system instability in the reliability indices calculation.

Most of the work listed above focused on including the transient stability assessment in the adequacy assessment. A few of the works include frequency stability and voltage stability with conventional reliability evaluation that analyzes resource adequacy. Reference [69] proposed an approach to include the frequency stability limit in reliability evaluation. The integration of wind generation is limited by the frequency stability constraint and the limited wind generation was considered in reliability indices calculation.

23

The frequency deviation was calculated based on a proposed mathematical model. Reference [70] introduced a method to include voltage stability assessment reliability analysis. The probability of voltage collapse was approximated and used as a proportion of the voltage stability margin. Reference [71] proposed a technique to evaluate power system reliability considering aspects of frequency control. The reliability indices under various operating conditions and system contingencies are formulated considering the frequency regulation processes.

The literature survey presented above shows that the merits of a comprehensive reliability evaluation with adequacy and dynamic security integrated are well recognized. The benefits of MCS as a probabilistic approach to incorporate stochastic factors are also presented in much of the literature. Although extensive work has been done on the probabilistic approaches of adequacy or dynamic security assessment, few of the work presented a practical and quantitative approach of an integrated reliability evaluation. The utilization of MCS as a framework for integrating the adequacy and dynamic security assessment, as well as comprehensive reliability metrics evaluation, need to be studied. Quantitative assessment methods for adequacy and dynamic security will also be investigated in this work.

Chapter 3

PROBABILISTIC ANALYSIS OF COMPOSITE SYSTEM RELIABILTY

Power systems are highly complex systems. Random failures in any part of a system can cause the interruption of electricity supply and sometimes cascading failures in the system. Deterministic approaches, including the planning reserve margin for generation capacity and N-1 contingency criteria for transmission planning, have been widely used to ensure reliable power supply to end-users. The primary weakness of deterministic approaches is that they do not respond to or reflect the stochastic characteristics in the system. Many research efforts have been conducted on probabilistic analysis methods to take into consideration these characteristics.

The obstacles to applying these methods in the past were primarily computational efficiency and the lack of data. These obstacles have been significantly overcome in recent years with the computing techniques rapidly improved and the continuous development of high-speed computational capabilities. On the one hand, the importance of components reliability data has been well recognized, and efforts have been dedicated to collecting these data. In North American, both NERC and Canadian Electricity Association (CEA) have been coordinating with utilities to gather reliability data for transmission and generation equipment. CEA publishes reports on the statistical analysis of forced outage performance of transmission equipment annually. Also, NERC has developed the Transmission Availability Data System (TADS) and the Generation Availability Data System (GADS) to collect outage data. Generation availability data collection through GADS has

evolved to be a mandatory industry program for conventional generating units that are equal or above 20 MW.

The availability of data has promoted the application of probability analysis approaches to evaluate system reliability. The probabilistic reliability evaluation of a composite system considers the generation and transmission infrastructures and is generally associated with the following four tasks:

1. Determining components outage models

2. Selecting system states

3. Evaluating the consequences of outages in selected system states

4. Calculating reliability indices.

In this chapter, the probabilistic evaluation approach that includes the four tasks listed above will be discussed.

3.1   Outage Models of System Components

A power system consists of various components, such as generators, lines, transformers, and breakers. Component failures are typically classified as repairable forced outages and non-repairable outages. Since a non-repairable outage usually is an accident and its probability of occurrence is extremely small, these types of outages are generally neglected in system reliability studies. Instead, the repairable forced outages are of main concern in reliability evaluation. Correct component outage models are essential for the

reliability evaluation of power grids, and the outage model for different types of compo-
nents varies. The outage model, as well as the parameters for the outage models, are
obtained mainly from statistical studies of historical data. For the reliability evaluation of
the BPS, components including generators and transmission lines are the primary concerns
since the contingencies that happen on these components directly affect the continuity of
power supply. The outage model of conventional generators, transmission lines, and wind
turbines in this work are described below.

3.1.1   Conventional Generator Outage Model

Generation units can be operated at a full capacity output state, a partial capacity
output state, or a forced outage state. A Markov process model is typically used to represent
the process of a system changing its state. According to the Markov process model, the
probability of a system being in a state at the time period $t +1$ depends on the state of the
system at the time step t and is independent of the states before this time period. Hence, a
system should have two characteristics to describe its state change using the Markov
model, lack of memory and the stationarity of the state. For generation units in power sys-
tems, these criteria are typically assumed to be true. Hence, the change of state of a
generation unit depends on the transition probability, which is the failure rate if the gener-
ation unit is in operation in the current state or the repair rate if the generation unit is
currently in a failure state.

The two-state Markov model to represent generation unit availability is shown in
Figure 3.1. It gives the transition diagram in the form of the transition rate between the two

27

states. The parameter λ and μ in Figure 3.1 represent the failure rate and the repair rate respectively. The state transition can also be represented using a cycle process between the up state and down state with a resident duration for each state, as shown in Figure 3.2. The parameters, mean time to failure (*MTTF*) and mean time to repair (*MTTR*), in Figure 3.2 represent the resident duration of an up state and the resident duration of a down state, respectively. The duration of each state is assumed to follow an exponential probability distribution.
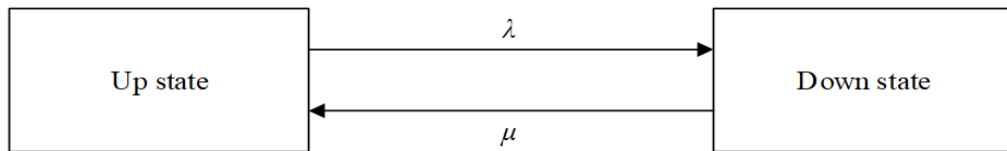
Figure 3.1 Stage Space Diagram of a Repairable Component
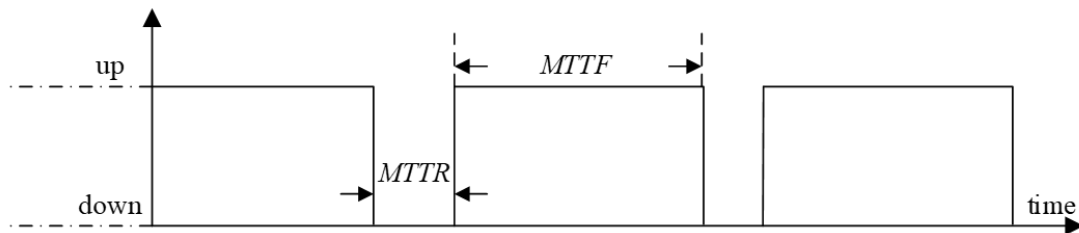
Figure 3.2 Up and Down Process of a Repairable Component

The parameters to characterize the state transition are the failure rate λ and repair rate μ. The conversion between *MTTF*, *MTTR*, λ, and μ are given in (3.1) and (3.2). The availability A and unavailability U which gives the probabilities of whether the unit is in the up state or the down state, respectively can be calculated according to (3.3) and (3.4), where f the average failure frequency (failures/ year),

28

$$\lambda = \frac{1}{MTTF} \tag{3.1}$$

$$\mu = \frac{1}{MTTR} \tag{3.2}$$

$$A = \frac{\mu}{\lambda + \mu} = \frac{MTTF}{MTTR + MTTF} = \frac{f}{\lambda} \tag{3.3}$$

$$U = \frac{\lambda}{\lambda + \mu} = \frac{MTTR}{MTTR + MTTF} = \frac{f}{\mu} \tag{3.4}$$

Reliability parameters of components from various providers can be different. In some dataset, the *MTTF* is not provided, but it can be easily calculated based on (3.3) and (3.4). The parameter derivations are given in (3.5) - (3.8). In some datasets, i.e. NERC GADS data, the forced outage rate (*FOR*) is commonly used to represent component failure frequency. It is worthwhile to note that, based on the definition of *FOR* which is given in (3.9), the *FOR* is not equal to failure rate λ, but represents the unavailability of the component hence is equal to *U*. In (3.9), *FOH* is the forced outage hours, and *SH* is the service hours:

$$f = \frac{MTTR}{MTTR + MTTF} \tag{3.5}$$

$$U = f \times MTTR \tag{3.6}$$

$$f = \frac{\lambda}{1 + \lambda \times MTTR} \tag{3.7}$$

29

$$\lambda = \frac{f}{1 - f \times MTTR} \tag{3.8}$$

$$FOR = \frac{FOH}{FOH + SH} \tag{3.9}$$

In some research efforts, the three-state Markov model is used to represent the generation unit state transition, in which case the derated generation output state is considered. However, since the generation output is always dispatched, a two-state Markov model is more practical to describe whether a generation unit is in a forced outage or operation and let the generation dispatch determine the output. The two-state model is used in some commercial reliability analysis software packages. For example, in the General Electric (GE) Multi-Area Reliability Simulation Program (MARS), a thermal unit is modeled as a two-state Markov model, and the unit is assumed to be always available to provide capacity unless it is in an outage. To give a general indication of the component reliability parameters, selected generating unit failure data from [5] are listed in Table 3.1.

3.1.2 Transmission Outage Model

For composite reliability evaluation where both generation and transmission limits are considered, the ability to meet demand will be limited when the transmission fault exists even if the generation capacity is adequate. The outage cycle for a transmission line is modeled using a two-state Markov model that assumes the state duration follows an exponential distribution. The transition between two states follows the same process as shown in Figure 3.1 and Figure 3.2.

Table 3.1 Generating Unit Failure Data

Generating unit type	Unit capacity (MW)	Failure rate (occurrence/year)	Mean outage time (hours/occurrence)
Hydraulic units	100-199	3.76	71.35
	200-299	6.14	74.94
	300-399	6.03	41.46
	400-499	2.82	64.50
	500 and above	2.42	112.58
Fossil units	100-199	14.53	37.72
	200-299	13.79	25.72
	300-399	16.54	46.55
	400-599	8.79	45.30
Nuclear units	400-599	3.40	369.35
	600-799	4.90	27.17
	800 and above	4.49	111.64

The parameters for the transmission outage model, however, are affected by many factors, such as weather, transmission line type, voltage level, and therefore is a complicated problem. The transmission outage statistic data in available data sources is generally represented as the outage frequency (per length per year) and mean duration of repair. For transmission lines with different length, the frequency of outage can be calculated according to (3.10),

$$f = f_u L \tag{3.10}$$

where f_u is the outage frequency per length per year, L the length of a transmission line. When the average failure frequency and *MTTR* are known, the other parameters can be calculated according to (3.3) - (3.8).

Different types of line fault have different impacts on the system. For example, a three-phase fault generally has a more severe impact compared to a single line-to-ground fault. To take into consideration the fault type stochasticity, the probabilities of different fault types are modeled for transmission outages. Four types of line fault are considered, including three-phase faults, double line-to-ground faults, line-to-line faults, and single line-to-ground faults. The probability of occurrence for the four fault types are 6.2% (three-phase), 10.0% (double line-to-ground), 8.8% (line-to-line) and 75% (single line-to-ground), as provided in [37]. To provide a general indication of the reliability parameters for transmission lines, a selected set of transmission reliability parameters from [72] is listed in Table 3.2.

Table 3.2 Transmission Line Fault Data

Voltage (kV)	Failure Frequency[a]	Mean Duration (hour)	Unavailability (%)
110-149	0.9150	20.7	0.216
150-199	1.1347	2.8	0.036
200-299	0.3771	44.9	0.193
300-399	0.3618	186.8	0.772
500-599	0.2475	27.2	0.077

[a]Number of transmission line failure occurrences per 100 kilometers per year.

3.1.3   Wind Turbine Outage Model

The penetration of renewable energy generation, specifically, wind power genera-tion, has been growing and should not be overlooked in system reliability evaluation. The time-dependent variability of wind generation needs to be addressed in reliability evalua-tion. Also, with more WTGs in the system, the forced outage of WTGs will have more impact on the system. Since the WTGs failure data are available, the WTG forced outage should be considered in evaluating the resource adequacy.

The failure of each wind turbine is typically considered as an independent event. The outage model of a wind turbine can be modeled as Markov components with up and down states. This outage model is regarded as the same as the outage model of conventional generators. Yet, the parameters λ and μ of wind turbines usually are quite different as com-pared to conventional generators. A substantial effort from both industry and research institutions has been made to develop databases and conduct statistical analyses of wind turbine failures and reliability. For example, a large monitoring program is being pursued by Fraunhofer Institute for Wind Energy Systems (Fraunhofer IWES) Germany to establish a database that contains detailed information about the reliability and availability of wind turbines. In the U.S., a CREW (continuous reliability enhancement for wind) database was developed by Sandia National Laboratories to benchmark the current U.S. wind turbine reliability performance. It collects the Supervisory Control and Data Acquisition (SCADA) data in wind farms, downtime and reserve event records, and daily summaries of generat-ing, unavailable, and reserve time for each turbine. Besides, WTG availability data have been collected in the NERC GADS. Generally, from these databases, the *MTTF* and the

average failure rate for the outage model can be obtained, and other WTG availability parameters can be calculated based on simple conversions. The benchmarks of CREW metrics for wind plant availability data from [73] is given in Table 3.3.

Table 3.3 Wind Plant Availability Data

	2013 Benchmark	2012 Benchmark	2011 Benchmark
Operational availability	97.6%	97%	94.8%
Utilization	83.0%	82.7%	78.5%
Capacity factor	36.1%	36.0%	33.4%
Mean time between events (hours)	39	36	28
Mean downtime (hours)	1.3	1.6	2.5

Three-state models for WTG availability have also been proposed in some works [12], [74]. The three-state model subdivides the up state to be a rated and a de-rated state. However, since the wind turbine output mainly depends on a current wind speed value, the two-state model considering the variable wind speed is sufficient to represent the de-rated state. Reference [11] presented a method to compute the two-state wind generation based on a historical wind power distribution in the study area with the probability of zero total wind power generation being considered as the forced outage rate. In [75]–[77], the probabilistic analysis is conducted using wind speed distribution, and the wind power

generation is then generated based on the nonlinear relation with wind speed. Autoregressive moving average models, Markov Chain MCS models, and normal distribution models are used for wind speed modeling. In recent years, with the availability of a more extensive database of historical wind speed data, more studies focus on using chronological wind speed as an input in the adequacy evaluation [12], [13]. The use of chronological historical data and SMCS can accurately capture the stochastic nature of wind generation as well as its correlation with the load. In some industry practices, the variable renewable energy generation is treated as a negative load, and the value of effective load carrying capability (ELCC) is evaluated to avoid the complexities of detail models [78], [79]. Some industry entities consider wind stochasticity based on historical wind power generation data in the adequacy assessment. For example, SERC Reliability Corporation (SERC) represents wind and solar profiles for the units using hourly generation time series [80].

In this work, an 8760-hour (365-day) wind speed data obtained from the National Renewable Energy Laboratory (NREL), National Wind Technology Center Information Portal [81], is introduced and incorporated with the power curve of wind turbines to represent the stochastic WTG output. According to the proposed model in this work, the wind turbine up or down state is determined first. When the wind turbine is in the up state, its output is determined based on the current wind speed and the power curve performance of the wind turbine. The calculation of the active power output knowing the wind speed is based on the following equation,

$$P(w) = \begin{cases} 0 \, , \, 0 \leq w < w_r \\ \frac{w^3 - w_i^3}{w_r^3 - w_i^3} P_r \, , \, w_i \leq w < w_r \\ P_r \, , \, w_r \leq w < w_o \\ 0 \, , \, w \geq w_o \end{cases} \tag{3.11}$$

where, w is the current wind speed (m/s), $P(w)$ is the active power output under the current wind speed (MW), P_r is the rated active power (MW), w_i is the cut-in wind speed (m/s), w_r is the rated wind speed (m/s), and w_o is the cut-out wind speed (m/s)

3.2   Probabilistic Approach for Reliability Evaluation

3.2.1   Probabilistic Analysis Approach

After developing the component outage models, three procedures need to be followed in reliability evaluation: (i) selecting system states, (ii) evaluating system states, and (iii) calculating the indices. In probabilistic reliability evaluation, system states are selected based on probability distributions. There are generally two types of probabilistic approaches for system states selection: analytical-based methods and simulation-based methods. The widely used methods for those two types are state enumeration and MCS, respectively.

The state enumeration method selects system states based on the probability of each component state. The probability of each system state and the consequence of each state are evaluated. The method can be used for the whole system or a selected subset of a system. The procedure for using an enumeration approach to perform reliability evaluation is depicted in Figure 3.3. For a large power system, when it is not possible to enumerate every

36

system states, the enumeration approach can be conducted based on a pre-selected contingency set.
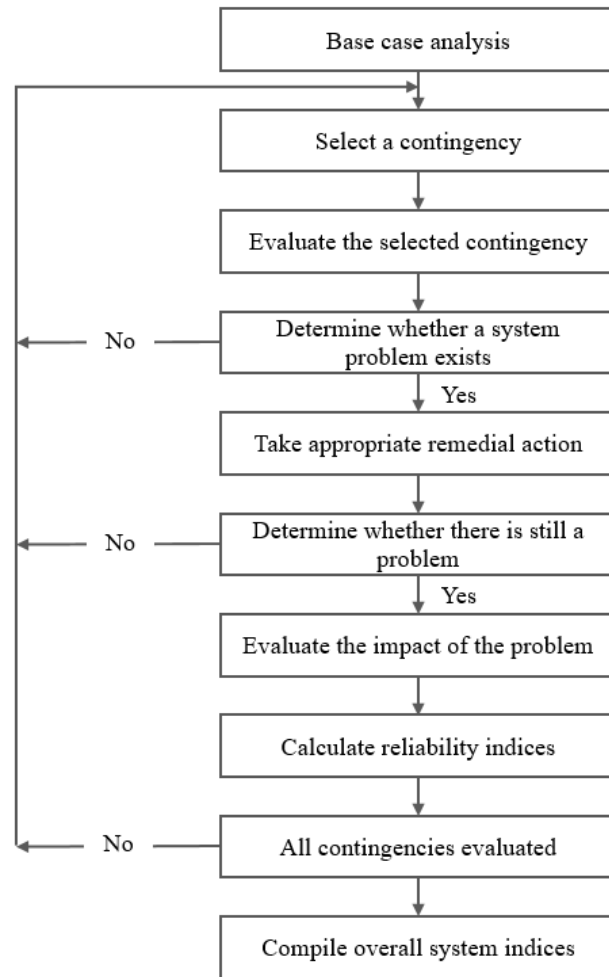
Figure 3.3 Flow Chart for Reliability Evaluation Using State Enumeration Procedure

Evaluation results from a state enumeration method are typically calculated as the summation over the production of probability and consequence of each state. The probability of a system state can be calculated according to (3.12),

$$P(s) = \prod_{i=1}^{N_f} P_{f,i} \prod_{j=1}^{N_s} P_{s,j} \tag{3.12}$$

where N_f and N_s are the numbers of failed and successful components in state s respectively. The overall system reliability can be obtained based on the probability of each selected state and its reliability condition.

The major drawback of the state enumeration approach is the *curse of dimensionality* problem: for a system with n components and each component with two states (up or down), the total number of system states is 2^n. Considering a system with 1000 components, the number of states is 2^{1000}. Sampling such a large number of states is impractical. Therefore, although the enumeration method is very straightforward, this method is only suitable for small systems. For a large power system, the MCS is the preferred method.

The advantage of MCS over the enumeration method is that the number of samples needed to reach a required accuracy in MCS does not depend on the size of the power system but rather on its reliability. There are two types of MCS: sequential MCS and non-sequential MCS. The non-sequential MCS sometimes called the state sampling approach, is based on sampling the probability of the component appearing in that state. However, neither the non-sequential MCS nor the state enumeration approach can simulate the chronology of time-dependent events. To take into consideration the load uncertainty and wind power variability, SMCS is a more suitable approach for system states sampling, since it is easy to integrate stochastic factors with chronological characteristics into state sampling. Also, SMCS allows the representation of the correlation between wind power generation

and load. The approach of SMCS is based on sampling a probability distribution of component state durations and includes the following steps:

Step 1: Specify the initial states of all components. Usually, all components are assumed to be in the up state initially.

Step 2: Sample the duration of each component residing in its present state. The state duration distribution is assumed following an exponential distribution. Therefore, the duration of an up state or a down state is sampled according to the following equations,

$$T_{up,i} = \frac{1}{\lambda_i} \ln U_i \qquad (3.13)$$

$$T_{down,i} = \frac{1}{\mu_i} \ln U_i \qquad (3.14)$$

where U_i is a uniformly distributed random number between $(0,1]$ corresponding to the i th component, λ_i the failure rate of the i th component, and μ_i the repair rate.

Step 3: Repeat *Step 2* in the time span considered (years) and record sampling values of each state duration for all components. The chronological state transition processes of each component in the given time span can be obtained. The illustration of the component state transition process is given in Figure 3.4.

Step 4: By combining the state transition processes of all components, the chronological system state transition cycles can be obtained.
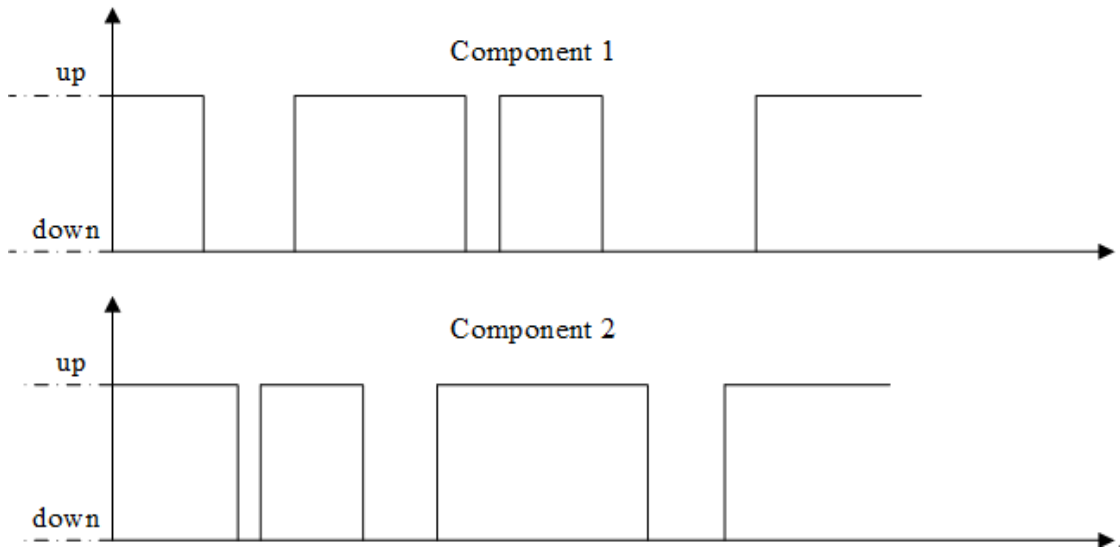
Figure 3.4 Chronological State Transition Processes of Components
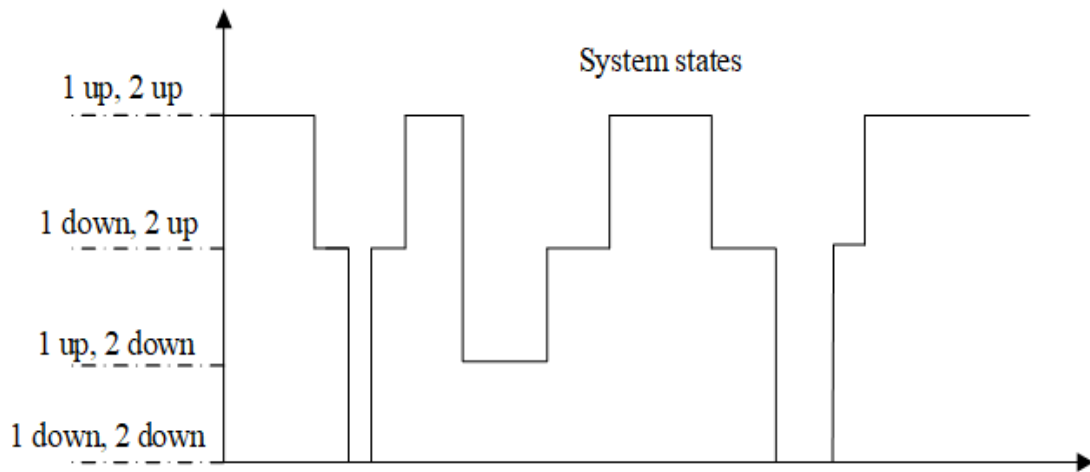
Figure 3.5 Chronological System State Transition Process

For example, combining the transition process of component 1 and component 2 in

Figure 3.4, the system transition process can be formed, as shown in Figure 3.5. The state

of each component and the duration of each system state are obtained. In power system reliability evaluation, all system states are then subject to assessment.

3.2.2   Stochastic Load Representation

The electrical load variation in a power system is a stochastic process. It is difficult to describe this stochasticity with a simple mathematical formulation. Primary load data are typically used in reliability evaluation, and it will provide a minimum amount of data that is needed to establish an hourly chronological load profile. Most primary load data consist of the percentage of maximum monthly load or weekly load in a year, the load in 24 hours in a typical day in each season, and the maximum load in each day in a week. With the percentages of these data available and the annual peak load is known, the hourly chronological load profile can be established.

In the SMCS method, system states can be selected chronologically so that the load variation can be reflected as the simulation progresses. Since the load data used in this work changes every hour, the system state transition happens at least once an hour. In this work, the load curve is combined with generator output, as well as each component state, to formula the system states.

3.3   System Analysis Techniques

For the two aspects of reliability considered, the analysis techniques are different. Techniques for adequacy assessment evaluates steady-state system conditions. In adequacy assessment, the system is assumed to reach a stable equilibrium point after contingencies,

and the dynamics of the transition from the pre-contingency state to the post-contingency state are neglected. Because of the involvement of the transmission system, the analysis techniques for composite system adequacy is more complicated than techniques needed for generation adequacy, and techniques that are capable of network analysis are necessary. Direct current (DC) power flow analysis and alternating current (AC) power flow analysis can be used to calculate line flows and bus voltages following contingencies. From the power flow analysis, it can be identified if there is any overloading, voltage violation, or an isolated bus. When these issues are identified by power flow analysis, OPF analysis can be used to model remedial actions and further analyze system steady-state conditions after the automatic controls. To analyze system dynamic behavior after contingencies, TDS based on numerical integration is the most fundamental and widely used approach. Also, angle stability, frequency stability, and voltage stability can be evaluated in TDSs.

3.3.1   AC Power Flow Analysis

The basic power flow equations in polar coordinates are given in (3.15) and (3.16). The power flow on a transmission line can be calculated according to (3.17)-(3.20),

$$P_i(V,\delta) = V_i \sum_{j=1}^{N} V_j (G_{ij} \cos \delta_{ij} + B_{ij} \sin \delta_{ij}) \tag{3.15}$$

$$Q_i(V,\delta) = V_i \sum_{j=1}^{N} V_j (G_{ij} \sin \delta_{ij} - B_{ij} \cos \delta_{ij}) \tag{3.16}$$

$$T_k(V,\delta) = \max\left\{T_{mn}(V,\delta), T_{nm}(V,\delta)\right\} \tag{3.17}$$

where, $P_i(V,\delta)$ and $Q_i(V,\delta)$ are the active and reactive power injection at bus i. $T_k(V,\delta)$ is the MVA power flow on the transmission line between bus m and bus n. N is the set of all buses in the system; G_{ij} and B_{ij} are the real and imaginary parts of the i th row and j th column element of the bus admittance matrix; δ_i and δ_j is the angle of bus i and bus j respectively, and δ_{ij} is the angle difference of bus i and bus j; $T_{mn}(V,\delta)$ and $T_{nm}(V,\delta)$ are the MVA flows at the two ends of line k. m and n are the two buses of line k. The MVA flow from bus m to n is calculated as

$$T_{mn}(V,\delta) = \sqrt{P_{mn}^2(V,\delta) + Q_{mn}^2(V,\delta)} \tag{3.18}$$

$$P_{mn}(V,\delta) = V_m^2(g_{m0} + g_{mn}) - V_m V_n(b_{mn}\sin\delta_{mn} + g_{mn}\cos\delta_{mn}) \tag{3.19}$$

$$Q_{mn}(V,\delta) = -V_m^2(b_{m0} + b_{mn}) + V_m V_n(b_{mn}\cos\delta_{mn} - g_{mn}\sin\delta_{mn}) \tag{3.20}$$

where, $g_{mn} + jb_{mn}$ is the primitive admittance of line k and $g_{m0} + jb_{m0}$ is the admittance of the circuit to the ground at bus m.

For each bus, there are four variables, which are the active power P_i, reactive power Q_i, voltage magnitude V_i, and voltage angle δ_i. To solve the power flow equations, two of the four variables for each bus have to be pre-specified. That is the reason of nominating bus type in a power flow study: a PQ bus means the P and Q are known for this bus and normally is a load bus. A PV bus means the P and V are known for this bus and normally is a generator bus, also a slack bus or swing bus which has known V and δ needs to be specified in a system or an area to adjust the power balance of the system or area.

The power flow equations can be solved by the successive linearization method. This is the well-known Newton-Raphson model. Based on the Newton-Raphson model, (3.15) and (3.16) can be linearized to the following matrix equation,

$$\begin{pmatrix} \Delta P \\ \Delta Q \end{pmatrix} = \begin{pmatrix} H & N \\ J & L \end{pmatrix} \begin{pmatrix} \Delta \delta \\ \Delta V / V \end{pmatrix} \tag{3.21}$$

The Jacobian coefficient matrix is a $(n + m - 1)$ dimensional square matrix where n and m are the numbers of all buses and load buses. The elements of the Jacobian matrix are calculated according to (3.22)-(3.29) [5],

$$H_{ij} = \frac{\partial P_i}{\partial \delta_j} = V_i V_j (G_{ij} \sin \delta_{ij} - B_{ij} \cos \delta_{ij}) \tag{3.22}$$

$$H_{ii} = \frac{\partial P_i}{\partial \delta_i} = -Q_i - B_{ii} V_i^2 \tag{3.23}$$

$$N_{ij} = \frac{\partial P_i}{\partial V_j} V_j = V_i V_j (G_{ij} \cos \delta_{ij} + B_{ij} \sin \delta_{ij}) \tag{3.24}$$

$$N_{ii} = \frac{\partial P_i}{\partial V_i} V_i = P_i + G_{ii} V_i^2 \tag{3.25}$$

$$J_{ij} = \frac{\partial Q_i}{\partial \delta_j} = -N_{ij} \tag{3.26}$$

$$J_{ii} = \frac{\partial Q_i}{\partial \delta_i} = P_i - G_{ii} V_i^2 \tag{3.27}$$

$$L_{ij} = \frac{\partial Q_i}{\partial V_j} V_j = H_{ij} \qquad (3.28)$$

$$L_{ii} = \frac{\partial Q_i}{\partial V_i} V_i = Q_i - B_{ii} V_i^2 \qquad (3.29)$$

The AC power flow analysis based on the theory discussed above has been widely used for many years and is available for use in large system analysis in serval power system analysis software tools, such as GE PSLF, Siemens PTI PSS/E, and PowerWorld Simulator.

3.3.2 DC Power Flow Analysis

DC power flow equations relate the real power to bus voltage angle and are based on the following assumptions [5]: 1) branch resistances are much smaller than branch reactance, 2) voltage angle difference between two buses of a line is small, 3) susceptances between the buses and the ground can be neglected, 4) all bus voltage magnitudes are assumed to be 1.0 p.u, 5) and the reactive power is ignored. Based on these assumptions, power flow equations can be simplified. The active power flow in a branch can be calculated according to the following equations:

$$P_{ij} = \frac{\delta_i - \delta_j}{x_{ij}} \qquad (3.30)$$

$$P_i = B'_{ii}\delta_i + \sum_{j \in R_i} B'_{ij}\delta_j \qquad (3.31)$$

$$B'_{ij} = -\frac{1}{x_{ij}} \qquad (3.32)$$

$$B'_{ii} = -\sum_{j \in R_i} B'_{ij} \qquad (3.33)$$

where, x_{ij} is the reactance of the line connecting bus i and bus j.

DC power flow analysis is widely used in composite system adequacy evaluation mainly because most of the essential reliability indices are associated with active power load curtailments, and the analysis speed is much faster than AC power flow, especially for large systems. However, when voltage and reactive power considerations are essential in the evaluation, AC power flow needs to be used rather than DC power flow.

3.3.3   Optimal Power Flow Analysis

As indicated in Figure 3.3, if the system is identified to have problems such as an overflow in a branch, controls and remedial actions will be invoked to bring the system back to normal operating conditions. These controls and remedial actions can be phase shifter adjustment, generation re-scheduling, and load curtailment, as well as bus voltage adjustment, capacitor/reactor adjustment. These controls and remedial actions are modeled and analyzed in OPF analysis. The objective of the OPF problem is to minimize the load curtailment via the remedial actions, and it should be subjected to system operating constraints and the limits of control capability. The primary constraints include the node balance, generation output limits, branch thermal limits, and bus voltage limits. The constraints can be mathematically described as follows:

46

$$P_i(V,\delta) = PG_i - PD_i, \forall i \in N \tag{3.34}$$

$$Q_i(V,\delta) = QG_i - QD_i, \forall i \in N \tag{3.35}$$

$$P_{g,j}{}^{\min} \le P_{g,j} \le P_{g,j}{}^{\max}, \forall j \in NG \tag{3.36}$$

$$Q_{g,j}{}^{\min} \le Q_{g,j} \le Q_{g,j}{}^{\max}, \forall j \in NG \tag{3.37}$$

$$|T_k(V,\delta)| \le T_k^{\max}, \forall k \in NT \tag{3.38}$$

$$V_i^{\min} \le V_i \le V_i^{\max}, \forall i \in N \tag{3.39}$$

where, $P_i(V,\delta)$ and $Q_i(V,\delta)$ are the active and reactive power injection at bus i, PD_i and QD_i are the active and reactive load at bus i, PG_i and QG_i are the active and reactive generation input at bus i, $P_{g,j}$ and $Q_{g,j}$ are the active and reactive output of generator j, $P_{g,j}^{min}$, $P_{g,j}^{max}$, $Q_{g,j}^{min}$, $Q_{g,j}^{max}$ are lower and upper limits of active and reactive output of generator j. T_k is the MVA power flow on transmission line k; T_k^{max} is the rating limit of line k; V_i^{min} and V_i^{max} are the lower and upper limits of the voltage magnitude at bus i; N, NG, and NT are, respectively, the sets of all buses, generator buses, and transmission lines in the system.

3.4   Summary

The first important step in a probabilistic reliability assessment is the methodology for system state generation. In this chapter, the details of using sequential MCS as the

probabilistic analysis framework for the integrated reliability evaluation approach are discussed. With the modeling of the traditional generator and transmission outage occurrence, chronological wind power generation, and wind turbine outage, the stochasticity is addressed in the generation of system states. The models and methodologies discussed in this chapter provide the basis for conducting a probabilistic analysis of power systems with wind power integrated.

Chapter 4

TEST SYSTEM AND DYNAMIC MODEL

TDS is the tool of choice to simulate system dynamic behavior after a contingency. Accurate dynamic models are vital for correctly simulating system dynamic behavior in TDSs. Dynamic models of the conventional generator, WTG, and protection system are discussed in this chapter. The test system used in the studies is given in this chapter. All dynamic models are constructed in GE PSLF in this work.

4.1   Test System and Base Case Scenario

A synthetic test system is used to perform the reliability evaluation study in this work. The single line diagram of the test system is shown in Figure 4.1 [89]. The test system consists of 11 conventional power plants with each power plant represented by a conventional generation unit, 10 wind farms with 1120 type-3 aggregated WTGs, 20 transmission lines, and 6 loads at different buses. The test system is divided into 5 zones with loads primarily concentrated in zone 4 and zone 5, while the generation resources are mostly located in zone 1and zone2.

Detailed generator models, including the machine, governor, and exciter models for synchronous generators, the generator, converter, and converter control model for type-3 WTGs, are constructed in the test system. The test system has major features of a realistic power system for transient stability and reliability studies from a system planning perspective. Table 4.1 lists a summary of the test system. The detailed power flow solution of the base scenario is provided in Appendix A.
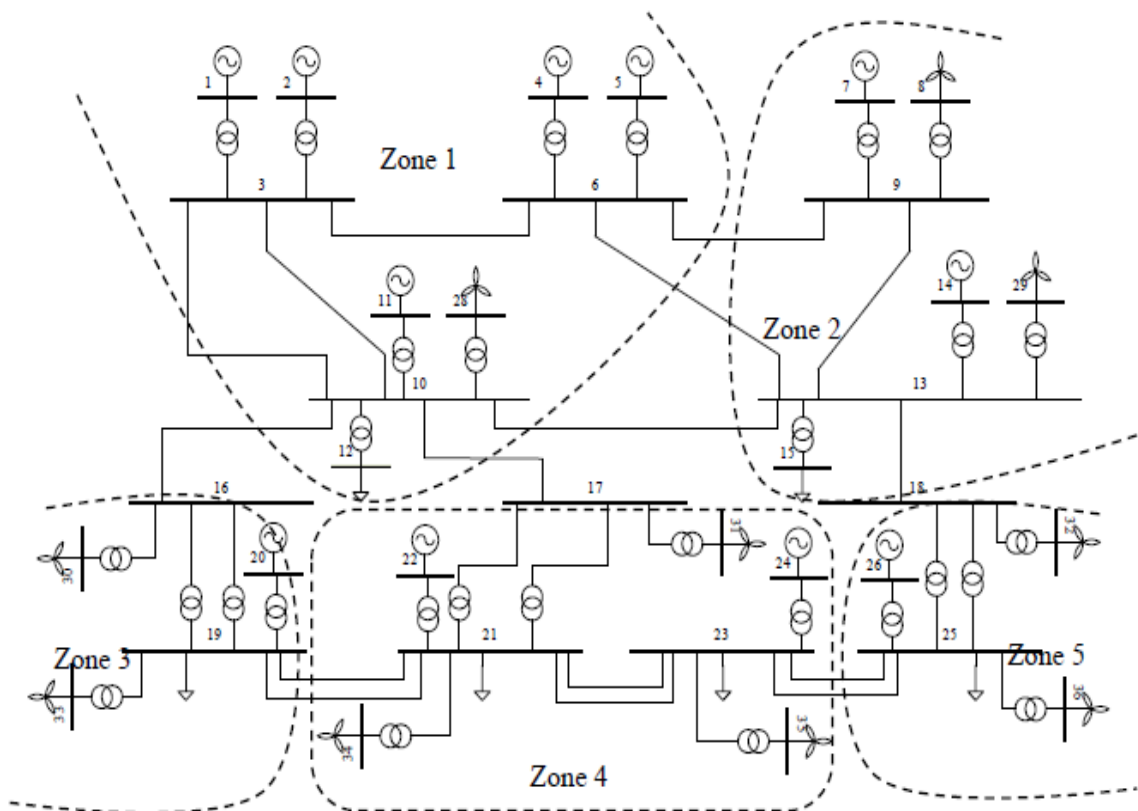
Figure 4.1 Online Diagram of the Synthetic Test System [89]

Table 4.1 Synthetic Test System Summary [89]

Buses	36
Power Plants	11 Conventional Units
	10 Wind farms (1120 ×1.5 MW WTGs)
Lines	30
Total Synchronous Generation	17,000 MW installed capacity
Wind Generation	1,680 MW installed capacity

In the base power flow scenario, the system generation rating is 21771 MVA, which includes WTGs rating of 1871 MVA. The system has a peak demand of 14463 MW. The

WTGs have a maximum 1680 MW active power output in the base case power flow scenario while the total output of synchronous generators is 12956 MW. The wind power penetration is around 11% of system load.

4.2   System Dynamic Modeling

In TDSs, power systems are represented as differential algebraic equations. The differential equations describe the dynamic behaviors of each component in the system, such as a generator or a load, while the network connection of the components is represented using algebraic equations. The TDSs are essentially solving these equations using numerical integration. Therefore, the mathematical representation of each component in the system directly determines the system dynamic analysis results from TDSs.

4.2.1   Synchronous Generator Dynamic Model

The $E^{''}$ model, which is the most detailed model among all the simplified generator models, has been widely used for stability studies in practice. It is also known as the 'voltage behind subtransient reactance model'. In this model, the transformer voltage terms in the stator voltage equations are neglected compared to the speed voltage term. Also, it is assumed that the variation of ω is considered negligible in the stator voltage equations and the subtransient reactance along the d and q axis are equal. The $E^{''}$ model can be represented by (4.1) - (4.6). Detailed derivations are available in Chapter 4 of [82]. This $E^{''}$ model in GE PSLF is the GENROU model. Since the dynamic behavior of the conventional generators directly determines system reliability after disturbances, all synchronous generators in the test system are modeled using the detailed model - GENROU in this work,

51

$$\dot{\lambda}_D = \frac{1}{\tau_{d0}^{''}}\sqrt{3}E_q^{'} - \frac{1}{\tau_{d0}^{''}}\lambda_D + \frac{1}{\tau_{d0}^{''}}(x_d^{'} - x_l)i_d \tag{4.1}$$

$$\sqrt{3}\dot{E}_q^{'} = \frac{\sqrt{3}}{\tau_{d0}^{'}}E_{FD} + \frac{(x_d - x_d^{'})(x_d^{'} - x_l)}{\tau_{d0}^{'}(x_d^{'} - x_l)}i_d - \frac{\sqrt{3}}{\tau_{d0}^{'}}\left[1 + \frac{(x_d - x_d^{'})(x_d^{'} - x_d^{''})}{(x_d^{'} - x_l)^2}\right]E_q^{'} + \frac{(x_d - x_d^{'})(x_d^{'} - x_d^{''})}{\tau_{d0}^{'}(x_d^{'} - x_l)^2}\lambda_D \tag{4.2}$$

$$\dot{\lambda}_Q = \frac{-1}{\tau_{q0}^{''}}\sqrt{3}E_d^{'} - \frac{1}{\tau_{q0}^{''}}\lambda_Q + \frac{1}{\tau_{q0}^{''}}(x_q^{'} - x_l)i_q \tag{4.3}$$

$$\sqrt{3}\dot{E}_d^{'} = \frac{-(x_q - x_q^{'})(x_q^{'} - x_l)}{\tau_{q0}^{'}(x_q^{'} - x_l)}i_q - \frac{\sqrt{3}}{\tau_{q0}^{'}}\left[1 + \frac{(x_q - x_q^{'})(x_q^{'} - x_q^{''})}{(x_q^{'} - x_l)^2}\right]E_d^{'} - \frac{(x_q - x_q^{'})(x_q^{'} - x_q^{''})}{\tau_{q0}^{'}(x_q^{'} - x_l)^2}\lambda_Q \tag{4.4}$$

$$2H\dot{\omega} = T_m - E_q^{''}i_q/\sqrt{3} - E_d^{''}i_d/\sqrt{3} - D\omega \tag{4.5}$$

$$\dot{\delta} = \omega - 1 \tag{4.6}$$

As one of the major control systems that directly affect a synchronous generator behavior, the excitation system controls not only the output voltage but also other aspects, such as the power factor and current magnitude. To simulate the behavior of synchronous machines accurately, the excitation systems of the synchronous machines should be modeled in sufficient detail. The static exciter is one of the commonly used exciter types. In this type of excitation systems, voltage is transformed to an appropriate level, and rectifiers provide the necessary direct current for the generator field. The type ST1A excitation system model with instantaneous control element output limits, as defined in [83], is used in this work. The ST1A excitation system is represented using the EXST1 model in the PSLF model library. The block diagram of the EXST1 model is provided in [84].

Governors, another type of essential control system, need to be accurately modeled for large scale stability studies. It controls turbine mechanical output in response to turbine rotating speed. The GGOV1 model is a general-purpose governor model used for a variety of prime movers controlled by proportional-integral-derivative (PID) governors. The GGOV1 model in PSLF is used to model the governor for gas turbines in the test system. The TGOV1 model in PSLF is used to model steam turbines and governors, and the HYGOV model in PSLF is used to model the hydro turbines and governors. The HYGOV model is capable of representing plants with straight-forward penstock configurations and electro-hydraulic governors that mimic the droop characteristics of traditional dashpot-type hydraulic governors. Reference [84] provides the block diagram of each model. The three types of the governor are used to represent different turbine and governor characteristics of gas turbine generators, steam turbine generators, and hydro turbine generators. The dynamic model data for synchronous generators in the test system are provided in Appendix A.

4.2.2   Wind Turbine Generator Dynamic Model

The integration of WTGs has produced significant changes in the system dynamic performance because the decoupling of generators and the grid through converters. The WTGs inherently do not participate in voltage and frequency control of the grid. Nevertheless, modern wind turbines are generally equipped with the functions of active power and reactive power control so that they are capable of participating in grid control. GE, as one of the major WTG manufactures, implemented these control functions in their WTGs. The models for the WTG with control ability are available in the GE PSLF model library. In

this work, the GE type-3 WTG models in PSLF are used to study the effect of WTGs controls on system reliability in the grid with increasing wind penetration.

The GE type-3 WTG models in PSLF consist of three parts, as shown in Figure 4.2: the generator/converter model, the converter control model, and the turbine control model.

- Generator/ converter model: The generator/converter model is represented using the GEWTG model in PSLF. It injects real and reactive current into the network in response to control commands and represents low and high voltage protective functions (e.g., low voltage ride through capability).

- Electrical control model: The electrical control model is represented using the EXWTGE model in PSLF. It includes both closed and open-loop reactive power controls based on the inputs from the turbine model (P_{ord}) and the supervisory VAr controller (Q_{ord}), or voltage regulation with either a simplified emulator of GE's Wind-CONTROL system or a separate, detailed model. This model sends real and reactive commands to the generator/converter model.

- Turbine and turbine control model: The turbine and turbine control model is represented using the WNDTGE model in PSLF. It represents the mechanical controls, including blade pitch control and power order (torque order in the actual equipment) to the converter; under-speed trip; rotor inertia equation; wind power as a function of wind speed, blade pitch, rotor speed; and active power control.

Control capabilities include fault ride through, active power control, voltage/ reactive power control have made modern WTGs more grid-friendly. These capabilities are

becoming more critical as wind power penetration is growing. The fault ride through function is modeled in the GEWTG model, which enables WTGs to remain connected to the grid for events that are less severe than the defined thresholds and time durations. The thresholds and time durations of the fault ride through function can be set case by case, according to the actual grid code requirements.
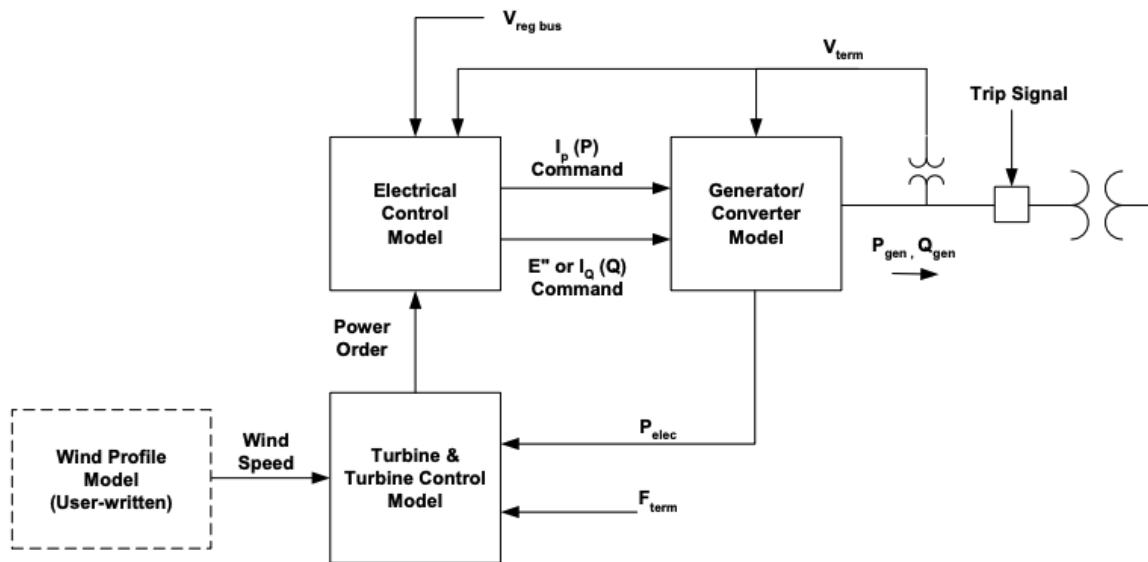
Figure 4.2 GE WTG Dynamic Model Connectivity [84]

The Active Power Control (APC) function is modeled in the WNDTGE model. This function of WTGs provides a margin by generating less power than is available from the wind. The APC function will provide the reserve power in response to frequency going below the normal value or less power in response to frequency exceeding the nominal value. The margin setting usually is 5% of maximum power and can be adjusted. This active power control function is more or less controversial because of the power reservation

and the resulting production loss. Another control function enables WTGs to provide iner-

tial response similar to synchronous generators and thereby participate in frequency control

when a disturbance occurs in the system. The WindINERTIA function in the WNDTGE

model is used to simulate such an inertial response capability for wind turbines in response

to low frequencies. The control functions of APC and WindINERTIA are modeled in the

WTG model in this work. The frequency response curve used in this work is shown in

Figure 4.3 [84].
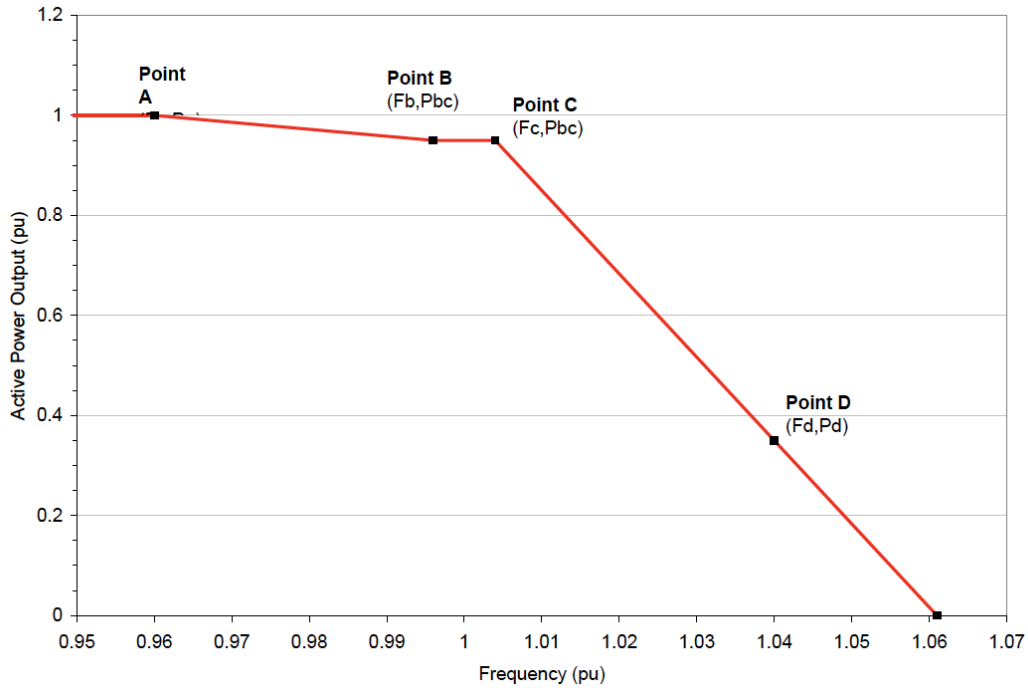
Figure 4.3 Frequency Response Curve [84]

Reactive power control is implemented in the WindCONTROL function in the

EXWTGE model. It monitors a specified bus voltage and compares it with the voltage

reference, and based on that, determines the reactive power control command. The Wind-CONTROL function is modeled in this work to perform voltage control in the simulations.

The detailed representation of the reactive power control model is shown in Figure 4.4. Three modes of reactive power control including power factor control, voltage control, and reactive power control can be used by setting proper parameters. The parameters for the type-3 WTG dynamic model in the test system are provided in Appendix A.
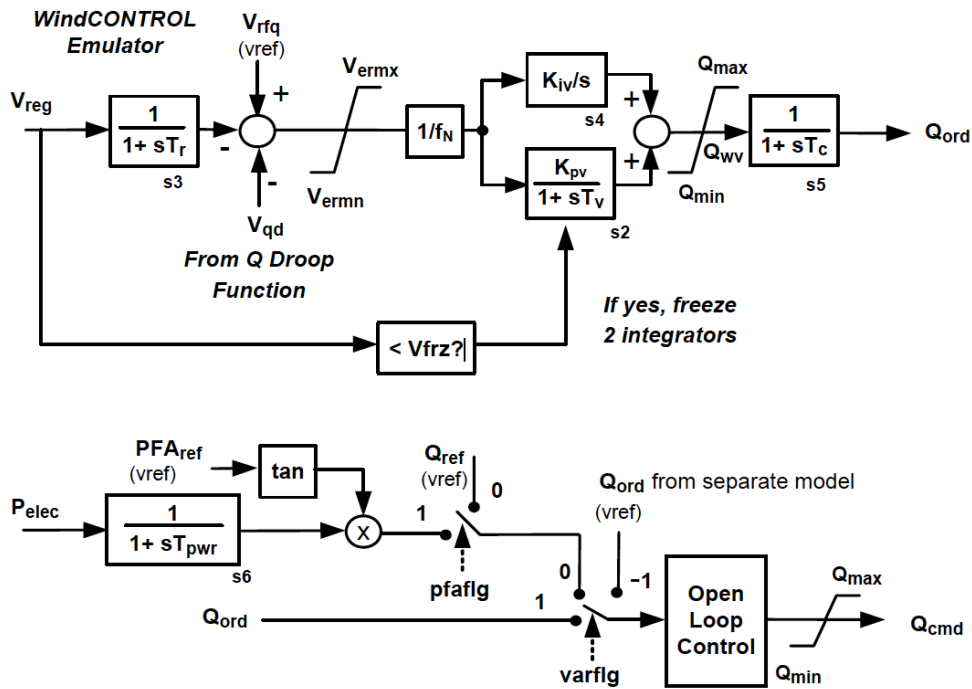
Figure 4.4 Reactive Power Control Model [84]

4.2.3   Load Model

After the Western North America blackout on August 10, 1996, load modeling has been recognized to be very important for accurately capturing system dynamic behavior. Load models can be represented as a dynamic model and a static model. Static load models

are extensively used in large scale system analysis since a historically significant portion of system loads are resistive heating, incandescent lighting, fluorescent lighting. Static loads represent a load as either constant power, constant current, or constant impedance and typically are represented by a polynomial model or an exponential model. Constant impedance loads have been considered the most grid-friendly because of a reduction in voltage results in a linear decrease in current and a quadratic decrease in power consumption. For constant current loads, a reduction in voltage results in a linear reduction in power and hence is also supportive of the power system during disturbance conditions. In different power systems, the composition of load models in the systems varies because the composition is highly dependent on local customer behavior. In this work, the loads in the test system are modeled as constant impedance, using the ALWSCC load model in PSLF. The representation of the load model is given in (4.7) - (4.8):

$$P = P_0(p_1V^2 + p_2V + p_3 + p_4(1 + l_{pd}(f - 1)))$$ (4.7)

$$Q = Q_0(q_1V^2 + q_2V + q_3 + q_4(1 + l_{qd}(f - 1)))$$ (4.8)

where p_1 and q_1 represent the constant impedance in p.u., p_2 and q_2 represent the constant current in p.u., p_3 and q_3 represent the constant power in p.u., p_4 and q_4 represent the frequency dependent power in p.u., l_{pd} and l_{qd} represent the real power and reactive power frequency index, p.u., and P_0 and Q_0 are the total load at the bus at nominal voltage and frequency.

4.2.4   Modeling of System Protection

One obstacle to using probabilistic approaches for system dynamic behavior assessment is the quantification of system dynamic behavior. In this work, in addition to the modeling of generation units and load, the protection systems are modeled in TDSs so that system dynamic behavior can be quantified in terms of load shedding and generation tripping results from these stability preserving protection systems. The protection systems that are modeled in TDS include:

- Under-frequency load shedding (UFLS)

- Under-voltage load shedding (UVLS)

- Over/ under-frequency generator tripping

- Over/ under-voltage generator tripping

4.2.3.1 Under-Frequency Load Shedding

The primary requirement of UFLS is to trip excess load to obtain generation-load balance following a disturbance such as tripping of lines or generators. Since generator turbines cannot operate at low frequencies (56-58 Hz), it is necessary to maintain the frequency near the nominal frequency (60 Hz). Slow changes in load can be compensated by governor action if generators have an available spinning reserve, and equilibrium can be reached. However, during transient outages, the excess load is fed by the available kinetic energy of the rotating machines, and frequency starts dropping. The only way to stabilize the system under such conditions is progressively shedding a portion of loads at pre-determined load centers at certain frequency thresholds.

The LSDT1 model in PSLF is used to represent the UFLS protection system. The setting of the load shedding relay is set according to the NERC reliability standard [85]. Table 4.2 shows the UFLS criteria for the Eastern Interconnection for utilities with net peak loads greater than 100 MW. These criteria are used in the LSDT model.

Table 4.2 UFLS Parameter Settings

Frequency Thresh-old (Hz)	Total Nominal Op-erating Time (sec)	Load Shed at Stage (%)	Cumulative Load Shed (%)
59.5	0.05	10	10
59.2	0.05	20	30
58.8	0.05	20	50

4.2.3.2 Under-Voltage Load Shedding

Voltage stability has become more important in power systems nowadays, mainly because the generation is remote from load centers and more motors and electronic loads are present in the systems. The objective of UVLS is to shed selected loads when the volt-age drops to a pre-specified level for a pre-defined time to recover voltage and avoid a widespread system voltage collapse. Developing a UVLS strategy requires coordination between protection engineers and system planners. System planners need to conduct nu-merous studies using P-V curves as well as other analytical methods to determine the amount of load that needs to be shed to retain voltage stability.

Since the voltage problem is more area dependent, there is no unified requirement on UVLS schemes. For areas with fast voltage decay characteristics, UVLS protection

should be set to be more sensitive. For example, WECC has identified the voltage collapse risk in the system and has extensively investigated the implementation of UVLS protection. Typically, automatic UVLS detects local voltage conditions and sheds the first stage load when the voltage drops to 89% to 94% of the normal voltage. The time delay for UVLS should be in seconds instead of cycles and can be as fast as in 1 to 5 seconds or as slow as over 15 seconds. The setting of UVLS in this work is given in Table 4.3. In any real system studies, the UVLS setting should be carefully studied based on the P-V curve, Q-V curve, as well as studies in TDS.

Table 4.3 UVLS Parameter Settings

Voltage Threshold (p.u.)	Time delay (sec.)	Breaker delay (sec.)	Load Shedding Fraction at stage (%)	Cumulative Load Shedding Fraction (%)
0.90	0.75	0.05	30	30
0.75	1.00	0.05	50	80

4.2.3.3 Over/ under-Frequency Generator Tripping

The over-frequency and under-frequency generator tripping play a crucial role as a defensive line for frequency emergency control measures, as well as essential protection systems to avoid generators being damaged. If any area has a load deficit, the generators start speeding up. The generator turbines are designed to operate near nominal frequency, and operation at an off-nominal frequency can damage the turbine blades. To protect the costly turbine generators, the NERC reliability criteria for UFLS [85] provides the guide-lines for over-frequency and under-frequency generator tripping schemes.
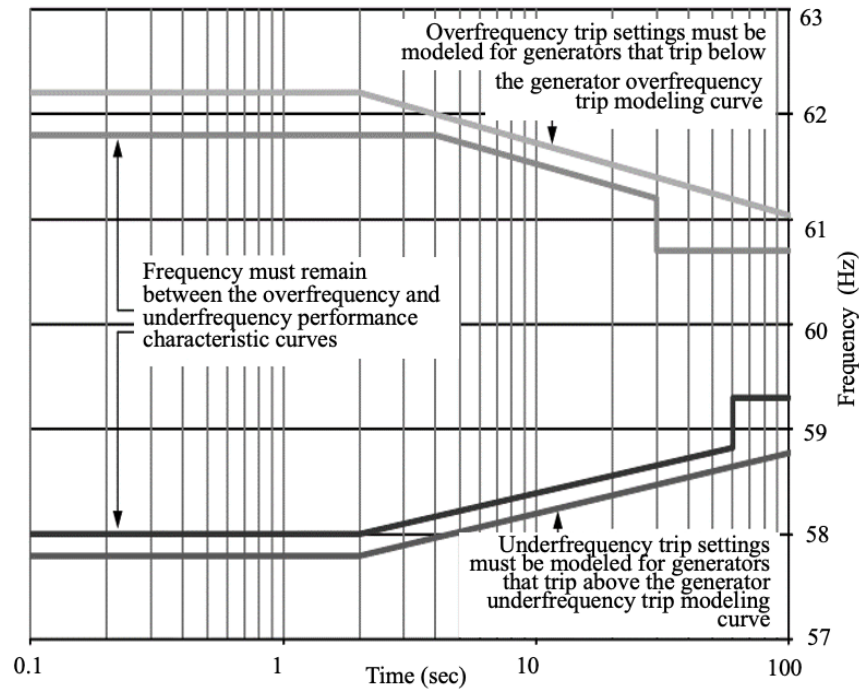
Figure 4.5 Design Performance and Modelling Curves for Over and Under Frequency Generator Trip [85]

Figure 4.5 shows the generator over-frequency and under-frequency performance characteristics and tripping modeling criteria. In this work, the generators are modeled with over-frequency and under-frequency relays that would be tripped when there is a violation of the over-frequency threshold of 61.2 Hz or the under-frequency threshold of 58.2 Hz. The GP1 model in PSLF is used as the generator protection model in this work. GP1 is a multifunction model and can be used to represent protection systems, including under/ over frequency protection, under/ over voltage protection, field over-current, stator over-current, and reverse-power protection.

4.2.3.3 Over/ under-Voltage Generator Tripping

Generators are designed to operate at a continuous minimum terminal voltage of 0.95 p.u. of rated voltage while delivering power at rated voltage and frequency. Generators operating in the under-voltage condition can reduce the stability limit of the system, and result in excessive reactive power import and malfunctioning of voltage-sensitive equipment. In the TDS, if the generator terminal voltage reduces to 0.90 p.u. for 1.0 s, the generator will be tripped. Generator overvoltage protection is also needed to prevent insulation breakdown due to sustained terminal overvoltage. The generator insulation is capable of operating at a continuous overvoltage of 1.05 p.u. of its rated voltage. If the generator terminal voltage increases to 1.15 p.u. for 0.5 s, the generators will be tripped. The over/ under- voltage generator tripping protection is modeled in GP1 in PSLF.

4.3   Summary

The test system and the dynamic models are presented in this chapter. Based on these models, system dynamics after disturbances can be studied in TDSs and further be quantified based on results from the protection actions. The integrated reliability evaluation approach that includes the assessment of system adequacy and dynamic security in a single process is illustrated in chapter 5.

Chapter 5

INTEGRATED RELIABITLIY EVALUATION AND ACCELERATION

TECHNIQUES

This chapter describes the integrated approach to reliability assessment addressing system adequacy and dynamic security. The assessment methods for system adequacy and dynamic security, namely power flow analysis, OPF analysis, and TDS, respectively, are discussed. The outcomes of the integrated reliability evaluation procedure are comprehensive reliability indices that reflect power system reliability impacts from both adequacy and dynamic behavior perspectives. To improve the computational efficiency of the integrated reliability evaluation, two acceleration approaches are introduced in this work to speed up the convergence process of the MCS and the TDS for dynamic security evaluation. Two widely used commercial software packages for power system analysis, Siemens PSS/E OPF and GE PSLF, are used as analytical tools. The overall procedure in the SMCS framework is implemented in Python.

5.1   Adequacy and Dynamic Security Integrated Reliability Evaluation

5.1.1   Procedure

The SMCS provides an iterative process to perform the reliability assessment. The method includes the following four steps:

1. Selecting a system state

2. Analyzing the system state to determine if it is an unreliable state

3. Updating cumulative indices

4. Generating reliability indices after the SMCS converges

The flow chart for the integrated reliability evaluation procedure is provided in Figure 5.1. For each iteration of the SMCS, the system states are generated and incorporated with an annual 8760-hour load curve and wind speed curve. In this process, the correlation between load and wind speed variations is automatically considered. State evaluation is then conducted for each state. TDS and AC power flow are used to determine the dynamic security and adequacy of each state. The state is further evaluated using an AC OPF if the AC power flow determines that system steady-state operating limits are violated. From the TDS, if the system is unstable during the transition after the contingency, the amount of load curtailment resulting from the activation of protection systems to maintain system stability is generated. A tolerance threshold of 20 MW for load curtailment is set in the TDS for determining dynamically insecure cases. When the load curtailment results from TDS are greater than the load curtailment threshold, the state is considered to be dynamically insecure, and the load curtailment results indicate the severity of system insecurity. If the state is transiently stable, an AC power flow is conducted to simulate the outage stage and examine the post-disturbance SEP. When any system operating limits are violated, the AC OPF is used to reschedule generation and alleviate constraint violations, while avoiding load curtailment if possible or to minimize the total load curtailment if unavoidable. When a system state is determined to be steady-state unreliable or dynamically insecure from

TDSs, the system state is classified as an unreliable state. In this situation, the load curtailment resulting from either steady-state evaluation or dynamic security evaluation is used to quantify the unreliability of the system state.
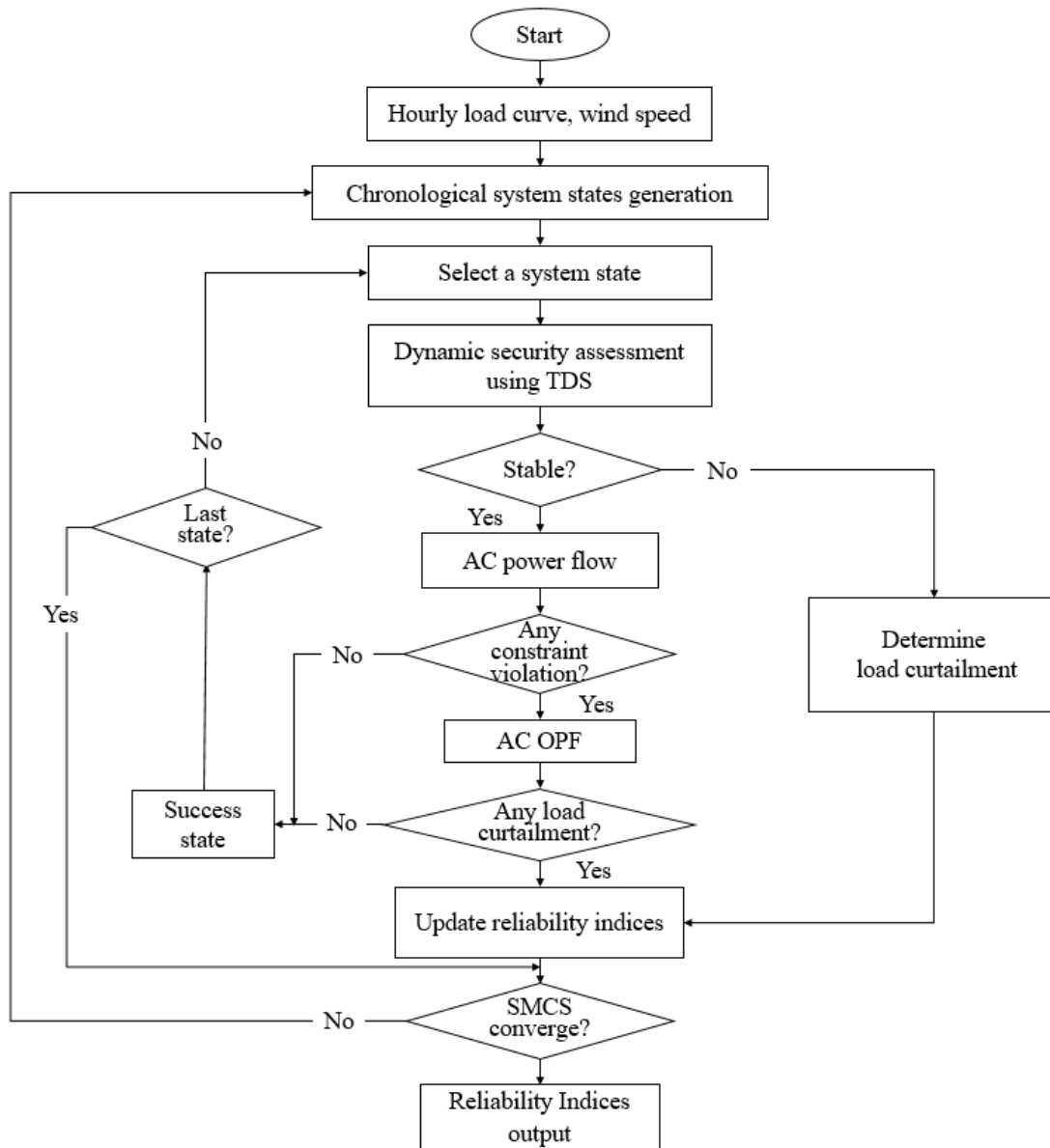
Figure 5.1 Flow Chart for Reliability Evaluation with Adequacy and Dynamic Security Integrated

After evaluating all sampled system states in one iteration of the SMCS, the reliability indices are updated based on the evaluation results of all system states. The convergence of SMCS needs to be determined after an SMCS iteration. The convergence is based on the coefficient of variation (COV) of a selected reliability index. The final reliability indices are computed after the SMCS converges.

5.1.2 Adequacy Assessment Methods

The objective of adequacy assessment is to determine whether the system is capable of supplying the electric load under the specified contingency without violations of the operating constraints. The evaluation addresses the steady-state system condition after a contingency. The power flow study is used to assess system steady-state conditions. As stated in Chapter 3, either DC power flow or AC power flow can be used as adequacy assessment technique. However, for a composite system reliability study in a realistic power system, the system condition, including the bus voltage and transmission flow limits, should be evaluated. Therefore, the AC power flow is used as the steady-state analysis technique in this work.

Following the procedure in Figure 5.1, after system state selection, a set of contingency is specified for each system state. AC power flow will be performed to study the post-contingency steady-state system condition. When the AC power flow results show that there is a violation of operating limits, then remedial actions, including generation rescheduling and load curtailment, are considered to correct the abnormal system conditions. The remedial actions reschedule generation first, without curtailing any load. If the

operating constraint violations still exist, the remedial actions with load shedding capability are then applied to determine where and how much load shedding will be needed to alleviate operating constraint violations, which is recorded as a system failure. The results of the contingency evaluations are stored and subsequently used by the reliability calculation model to calculate the reliability indices. AC OPF is used as the technique to assess the system adequacy when the operating limits are violated.

As discussed previously, the objective of the adequacy assessment is to determine whether a system is capable of supplying the electric demand considering possible generator and transmission contingencies while not violating any operating constraints. Evaluation of system adequacy is based on the alternating current optimal power flow (ACOPF) solution that analyzes whether load curtailment is required to maintain the system within operating limits during generator or transmission line contingencies. These contingencies are selected in the SMCS process based on the probability of fault occurrence and consideration of the repair rate.

In this work, remedial actions modeled in the ACOPF formulation include the generator active and reactive power adjustment, bus voltage magnitude adjustment, transformer tap ratio, and switched shunt admittance controls. As a consequence of a generator or transmission equipment outage, the remedial actions are incorporated to maintain the system within operating limits. If operating constraints violations still exist after the remedial actions, load curtailments are invoked as a last resort to bring the system back within limits. The system is considered to be adequate when the operating limits are satisfied, and no load needs to be curtailed. The minimum load curtailment is the quantitative

metric of system adequacy. The objective function of the ACOPF model in this work is given in (5.1). The formulation of the constraints including the load adjustment limits, node power balance, line flow limits, generation output limits, voltage magnitude and angle limits are given in (5.2) - (5.11):

$$Min : \sum_{\forall L} P_{L0}(1-\psi_L) \tag{5.1}$$

$$\psi_{L,MIN} \le \psi_L \le \psi_{L,MAX} \tag{5.2}$$

$$S_L = \psi_L \cdot S_{L0} \tag{5.3}$$

$$S_G - S_L = diag(\overline{V}Y_{bus}^* \overline{V}^*) \tag{5.4}$$

$$\left| \overline{V}_m Y_{line}^* \overline{V}_n^* \right| \le S_{mn,Max} \tag{5.5}$$

$$\left| \overline{V}_n Y_{line}^* \overline{V}_m^* \right| \le S_{mn,Max} \tag{5.6}$$

$$P_{G,MIN} \le P_G \le P_{G,MAX} \tag{5.7}$$

$$Q_{G,MIN} \le Q_G \le Q_{G,MAX} \tag{5.8}$$

$$S_G = \sqrt{P_G^2 + Q_G^2} \tag{5.9}$$

$$V_{MIN} \le V \le V_{MAX} \tag{5.10}$$

$$\theta_{MIN} \le \theta \le \theta_{MAX} \tag{5.11}$$

where, ψ_L is the load adjustment factor, $\psi_{L,MIN}$ and $\psi_{L,MAX}$ are the minimum and maximum load adjustment factor respectively, P_{L0} is the initial active power of load, S_{L0} is the initial load MVA value, S_L is the MVA value of load, S_G is the MVA value of generator, $\overline{V}$ represents bus voltage phasor, Y_{bus} is the system bus admittance matrices and Y_{bus}^* is the conjugate transpose of Y_{bus}, $\overline{V}_m$ and $\overline{V}_n$ are bus voltage phasor of bus m and bus n, and $\overline{V}_m^*$ and $\overline{V}_n^*$ are the conjugate of $\overline{V}_m$ and $\overline{V}_n$, Y_{line} is the complex admittance of line connecting bus m and bus n, Y_{line}^* is the conjugate transpose of Y_{line}, $S_{mn,MAX}$ is the maximum MVA flow on the line connecting bus m and bus n, P_G is the active power output of generator, $P_{G,MIN}$ and $P_{G,MAX}$ are the minimum and maximum limits of generator active power output, Q_G is the reactive power output of generator, $Q_{G,MIN}$ and $Q_{G,MAX}$ are the minimum and maximum limits of generator reactive power output, V is bus voltage magnitude, V_{MIN} and V_{MAX} is the lower and upper limits of bus voltage magnitude, θ is voltage angle, θ_{MIN} and θ_{MAX} are the lower and upper limits of voltage angle.

As a widely used commercial power system analysis software, PSSE has the OPF function that allows users to customized objective and constraints. In this work, the OPF is modeled and solved using the PSS/E OPF software tool. By using the software tool, the algorithm for finding the optimal solution is based on a Lagrangian relaxation method. The adequacy evaluation results are quantified by the minimum load curtailment from the optimization problem, as represented in (5.12),

$$P_{loadshed} = Min\{\sum\nolimits_{\forall L} P_{L0}(1-\psi_L)\} \tag{5.12}$$

5.1.3 Dynamic Security Assessment Methods

While adequacy assessment evaluates the post-contingency steady-state conditions, the DSA estimates whether the system can maintain stability during the transition period after a contingency. If the transition is stable and a new equilibrium point is reached, the system is termed dynamically secure. Otherwise it is judged to be insecure. TDS is widely recognized as the most accurate method to describe power system transient behavior and therefore is the method of choice to perform the DSA in this work. An accurate system dynamic performance with the protection systems actions can be simulated in the TDS. The protection systems including under-frequency load shedding, under-voltage load shedding, over-frequency and under-frequency generator tripping, over-voltage and under-voltage generator tripping as described in Chapter 4 are modeled in the TDS, so that by activating these protections, following a contingency the system should be transiently stable. The dynamic security is quantified by the MW load shedding due to security preserving corrective protection system actions, as represented in (5.13),

$$P_{loadshed} = P_{L,pre-fault} - P_{L,post-fault}$$ (5.13)

where $P_{loadshed}$ is the assessment result in terms of the MW load curtailment, $P_{L,pre-fault}$ is the total active power of all loads at the pre-fault SEP of the system, and $P_{L,post-fault}$ is the total active power of all loads in the post-fault SEP.

The drawback of TDS is the computational burden, especially when simulating a large system with a significant number of scenarios. A pruning process for TDS is hence introduced in this work to reduce the computational burden. This pruning process will be

discussed in section 5.2.

5.1.4   Reliability Indices

The most important outcome of the probabilistic reliability assessment is the quantified reliability indices. Different from the deterministic methods that give qualitative results, the probabilistic reliability indices provide quantitative indications of the overall system reliability. From the integrated reliability evaluation approach in this work, the quantitative results demonstrate the reliability level that considers both resource adequacy and dynamic security. For a distribution system, reliability indices such as the system average interruption duration index (*SAIDI*), customer average interruption duration index (*CAIDI*), system average interruption frequency index (*SAIFI*), custom average interruption frequency index (*CAIFI*), and the average service availability index (*ASAI*) are commonly used. On the other hand, reliability indices such as the *LOLP*, *LOLE*, *EPNS*, *EENS*, *LOLP*, and *LOLD* are more widely used in resource adequacy evaluation for the transmission level system. They provide an effective means to include all the system states from MCS into the reliability calculation based on probability distribution. From SMCS, in each sampled year, the reliability can be calculated based on state duration time and load curtailment results from state assessment. *LOLP*, *EPNS*, and *LOLF*, which are the probability index, energy index, and frequency and duration of loss of load index, respectively, are three critical indices used in this work. Most importantly, since the dynamic behavior is quantified in terms of loss of load from protection actions, the measures using *LOLP*, *EPNS*, and *LOLF* represent system reliability include both adequacy and dynamic security. The calculation of *LOLP*, *EPNS*, and *LOLF* are as shown below:

1) *LOLP* represents the probability of failure of the system to meet the demand. The *LOLP* index in the i th simulation year is calculated according to (5.13), and the expected value of *LOLP* from the SMCS is calculated according to (5.14):

$$LOLP_i = (1/T_i)\sum_{j=1}^{N_j} H_{ij} \cdot \tau_{ij}$$ (5.14)

$$LOLP = \frac{1}{N_y}\sum_{i=1}^{N_y} LOLP_i$$ (5.15)

2) *EPNS* measures the magnitude of system failure to meet the demand, in terms of mega-watts. The *EPNS* index in the i th simulation year is calculated according to (5.16) and the expected value of *EPNS* is calculated according to (5.17):

$$EPNS_i = (1/T_i)\sum_{j=1}^{N_j} \tau_{ij} \cdot P_{ns,ij}$$ (5.16)

$$EPNS = \frac{1}{N_y}\sum_{i=1}^{N_y} EPNS_i$$ (5.17)

3) *LOLF* represents the frequency of a system failure to meet the demand. The *LOLF* index in the i th simulation year is calculated according to (5.18) and the expected value of *LOLF* is calculated according to (5.19):

$$LOLF_i = (1/T_i)\sum_{j=1}^{N_j} H_{ij} \cdot 8760$$ (5.18)

$$LOLF = \frac{1}{N_y} \sum_{i=1}^{N_y} LOLF_i \tag{5.19}$$

where, N_y is the number of simulation iterations in MCS, i is the index of simulation itera-

tions of the SMCS, T_i is the sum of the durations of states in simulation iteration i, N_j is

the number of states in a simulation iteration, x_{ij} is system state j in the simulation iteration

i, τ_{ij} is the duration time of state x_{ij}, H_{ij} is 1 if there is load not supplied in state x_{ij}, other-

wise H_{ij} is 0, $P_{ns,ij}$ is the amount of load not supplied in state x_{ij}.

The above indices measure system reliability considering both adequacy and dy-

namic security. Impacts from system reliability that is caused by either inadequate resource

or dynamic insecurity are incorporated in the calculation of indices.

The convergence of MCS is normally based on the value of *COV* as it represents

the extent of variability of the index in each simulation iteration in relation to the mean. I_i

is the reliability index obtained from the simulation for the i th iteration in SMCS, $\hat{I}$ is the

estimate of the expected value of the index I. The calculation of $\hat{I}$ and the variance of $\hat{I}$ are

given in (5.20) - (5.21). The *COV* can be calculated according to (5.22),

$$\hat{I} = \frac{1}{N_y} \sum_{i=1}^{N_y} I_i \tag{5.20}$$

$$Var(\hat{I}) = \sum_{i=1}^{N_y} (I_i - \hat{I})^2 / N_y \tag{5.21}$$

$$COV = \frac{\sqrt{Var(\hat{I})}}{\hat{I}} \tag{5.22}$$

Equation (5.22) shows that the *COV* is a normalized measure of the dispersion of probability distributions. Hence, the lower its value, the better is the accuracy of the estimate of $\hat{I}$. To reach a demanding accuracy of SMCS, the criteria for *COV* is normally set to be 1% - 5%. Once the *COV* value attains the convergence criterion, the SMCS is completed and the expected values of reliability indices which are calculated based on (5.20) are the final reliability indices results.

5.2   Reliability Evaluation Acceleration Methodology

The reliability evaluation is a composite of two parts: states selection and the assessment of the selected states. By using SMCS as the probabilistic method of state selection, it is easy to include chronological aspects of the power systems into the simulation. However, the computational efficiency is the critical issue for SMCS. A large number of system states need to be sampled to assure accurate estimates of the reliability indices. To improve the computational efficiency of the SMCS, an importance sampling based on the Cross-Entropy method is introduced in this work.

Using TDS as the dynamic security assessment method also introduces a computational burden. A pruning process is proposed to reduce the volume of cases goes through TDS. The pruning process classifies the states based on two metrics. One is the kinetic energy gained due to the fault, and the other is the change in the magnitude of the Thévenin impedance (Z_{th}) at the point of interconnection (POI) of the generators in the post-contingency network. These two acceleration methodologies are discussed in this section.

5.2.1 CE based Importance Sampling

The number of samples required by the MCS methods can be reduced using variance reduction techniques (VRTs). Importance sampling (IS) has proved to be an effective means of improving the MCS method. The application of IS is based on the idea that certain variables have more significant impact on the estimation process of a target quantity. Thus, if these 'important' values are sampled more often based on an optimized PDF $g_{opt}(\cdot)$, the variance of the estimator should be reduced, and the convergence can be reached faster.

The selection of the new $g_{opt}(\cdot)$ is a difficult task, and for this reason, the application of IS has been largely limited. However, this problem has been overcome by the CE method since it provides a simple adaptive procedure to obtain the optimal probability density function. In this work, the IS based on the CE method is used to accelerate the convergence of SMCS. A mathematical illustration is discussed below.

Consider the original PDF $f(\cdot)$ based on $\vec{u} = (u_1, \ldots, u_j, \ldots, u_n)$ which represents the original unavailability vector of each component, $X_i = (x_{i,1}, \ldots, x_{i,j}, \ldots, x_{i,n})$ are the states of each component sampled based on $f(\cdot)$ in the ith simulation iteration, and H_i as the test function of a reliability index. Assuming that SMCS converges after N iterations, let l be the expected value of a reliability index, the estimation of the reliability index is calculated as:

$$l = E_u(H(x)) = \int H(x)f(x)dx \approx \frac{1}{N}\sum_{i=1}^{N}H(X_i)$$

(5.23)

where the subscript u means that the expectation is taken with respect to u. When the system failures are rare, the estimation process via (5.23) is then very computational demanding. By using IS which introduces a new PDF $g(\cdot)$ in the form of a new unavailability vector $\vec{v} = (v_1,\ldots,v_j,\ldots,v_n)$, a system state sample X_i is drawn based on $\vec{v}$, and the reliability index is estimated according to (5.24),

$$l = \int H(x)\frac{f(x)}{g(x)} g(x)dx = E_v(H(x))\frac{f(x)}{g(x)} \tag{5.24}$$

where the subscript v means that the expectation is taken with respect to the new availability parameter vector v. The estimation of l is:

$$\hat{l} = \frac{1}{N}\sum_{i=1}^{N} H(X_i)W(X_i) \tag{5.25}$$

$$W(X_i) = \frac{f(X_i)}{g(X_i)} \tag{5.26}$$

the $W(X_i)$ is the likelihood ratio and X_i is a random sample from $g(\cdot)$ with the characteristic parameter $\vec{v}$. $W(X_i)$ also be represented as $W(X_i;n,\vec{u},\vec{v})$ is the ratio of distribution $f(\cdot)$ with parameter $\vec{u}$ and distribution $g(\cdot)$ with the parameter $\vec{v}$. The calculation of the likelihood ratio is given in (5.27),

$$W(X_i;n,\vec{u},\vec{v}) = \frac{\prod_{j=1}^{n}(1-u_j)^{x_{i,j}} u_j^{(1-x_{i,j})}}{\prod_{j=1}^{n}(1-v_j)^{x_{i,j}} v_j^{(1-x_{i,j})}} \tag{5.27}$$

The problem now consists of finding the optimal $\vec{v}$ for $g(\cdot)$ that minimizes the variance of $\hat{l}$ with respect to $g(\cdot)$ to reduce the computational effort of the SMCS. The mathematical representation of the problem is given in (5.28). It has been verified in [86] that the solution of the problem (5.28) can be based on (5.29) and (5.30):

$$\min_{g} Var_g \left\{ H(X) \frac{f(X)}{g(X)} \right\} \tag{5.28}$$

$$g^*(X) = \frac{H(X)f(X)}{l} \tag{5.29}$$

$$Var_{g^*}(\hat{l}) = Var_{g^*}(H(X)W(X)) = Var_{g^*}(l) = 0 \tag{5.30}$$

The problem of finding the $g^*(\cdot)$ becomes complicated since apparently in order to derive $g^*(\cdot)$, l is needed. But l is the precisely the quantity we want to estimate from the simulation. To solve this problem, an assumption is made that the distribution $f(\cdot)$ belongs to some parametric family. Let $f(\cdot, \vec{u})$ represent the original distribution function, and limit the choice of $g(\cdot)$ to those from the same parametric family as $f(\cdot)$. So $g(\cdot)$ differs from the original distribution $f(\cdot, \vec{u})$ only by a single parameter $\vec{v}$. Now (5.26) can be rewritten as (5.31), and (5.25) can be rewritten as (5.32):

$$W(X_i; u, v) = \frac{f(X_i; u)}{f(X_i; v)} \tag{5.31}$$

$$\hat{l} = \frac{1}{N} \sum_{i=1}^{N} H(X_i) W(X_i; \vec{u}, \vec{v}) \tag{5.32}$$

The estimation of the optimal parameter $\vec{u}$ in (5.32) can be based on the *Kullback-Leibler* cross-entropy (CE), which defines the distance between two distributions. The *Kullback-Leibler* CE distance between the $g(\cdot)$ and the optimal $g_{opt}(\cdot)$ is defined as shown in (5.32). The solution for the minimization of (5.33) is equivalent to the solution for (5.34).

$$
\begin{aligned}
D(g_{opt}(X), g(X)) &= E_g \ln \frac{g_{opt}(X)}{g(X)} \\
&= \int g_{opt}(X) \ln g_{opt}(X) dX - \int g_{opt}(X) \ln g(X) dX
\end{aligned}
\tag{5.33}
$$

$$
\max \int g_{opt}(X) \ln g(X) dX
\tag{5.34}
$$

From the above derivations, we obtain that: $f(X)=f(X;\vec{u})$, $g(X)=f(X;\vec{v})$, $g_{opt}(X)=\frac{H(X)f(X)}{E_u(H(X))}$. Then, (5.34) can be rewritten as (5.34). The optimal vector of parameters $\vec{v}_{opt}$ is the outcome of this optimization process. Assume now that IS can be used iteratively to solve (5.35). In the first iteration of this procedure, IS will use a new sampling function $f(X;\vec{v}_0)$ with different parameters from $f(X;\vec{u})$ and $f(X;\vec{v})$. Accordingly, (5.35) is rewritten as (5.35). The respective optimal vector of reference parameters v_{opt} is calculated according to (5.36),

$$
\max_v \int \frac{H(x) f(X;\vec{u})}{E_u(H(x))} \ln f(X;\vec{v}) dx \rightarrow \max_v E_u(H(x)) \ln f(X;\vec{v})
\tag{5.35}
$$

$$
\max_v E_w(H(x)) \frac{f(X;\vec{u})}{f(X;\vec{v}_0)} \ln f(X;\vec{v})
\tag{5.36}
$$

$$v_{opt} = \arg\max{}_v E_w(H(x))W(X;\vec{v}_0,\bar{u})\ln f(X;\vec{v}) \tag{5.37}$$

where $W(X;v_0,\vec{u})=f(X;\vec{u})/f(X;\vec{v}_0)$.

Reference [60] shows that the vector v can be calculated using (5.38).

$$v_j = \frac{\sum_{i=1}^{N} H(x_i)W(x_i;\bar{w},\bar{u})x_{ij}}{\sum_{i=1}^{N} H(x_i)W(x_i;\bar{w},\bar{u})} \tag{5.38}$$

Based on the details discussed above, the process for the CE IS variance reduction algorithm for composite system reliability assessment is presented as follows. The corresponding flow chart is shown in Figure 5.2.

Step 1) Specify the CE optimization parameters: a multilevel ρ=0.1 to determine a rare event percentage, a maximum sample size N_{MAX} and *COV* criterion β_{MAX} for IS SMCS, and the iteration counter k=1.

Step 2) Define $\vec{v}_0=\vec{u}$, i.e., $\vec{v}_0$ is equal to the vector of the original unavailability. Determine the rare event criteria $\gamma=R_{max}$. R_{max} is assumed to be 1 MW representing the maximum acceptable load curtailment from state evaluation.

Step 3) Generate composite system states for the current iteration X_1, X_2, ..., X_N based on $\vec{v}_{k-1}$. N is the total number of system states in the current iteration, therefore X_j consists of the states of each element in the system, i.e., $X_j = (x_{j,1},x_{j,2},\ldots,x_{j,m})$, assuming m

is the number of the elements. Evaluate states performance $S(X_i)$ in the form of load curtailment needed to maintain the system within operating limit. Sort $S(X_i)$ in the descending order so that $S = [S_{[1]}, S_{[2]}, \ldots, S_{[N]}]$ and $S_{[1]} \geq S_{[2]} \geq \ldots \geq S_{[N]}$.

Step 4) Access the state performance value at the rare event multilevel $S_{[\rho N]}$. If $S_{[\rho N]} \geq \gamma$, exit the CE optimization process. If $S_{[\rho N]} < \gamma$, evaluate the test function $H(X_i)$ for all states X_i. If $S(X_i) > \gamma$, $H(X_i) = 1$; otherwise, $H(X_i) = 0$.

Step 5) $k = k + 1$, go back to step 3) for the next iteration.

Step 6) after the CE optimization is completed, say after k iterations, the $\vec{v}_{opt} = \vec{v}_k$ gives the optimal PDF parameters.

Initialization
- Initialize Reliability Data of Components: μ
- Initialize Importance Sampling Parameters
- Optimized fault rate $v_0 = \mu$, iteration count = 0

Iteration Count + 1

CE Optimization Process

SMCS for System State Samples
- Generate system states for a year based on SMCS with yearly load curve and wind speed: $X_1, X_2, ..., X_N$

Evaluate System State Samples
- A optimal power flow analysis is conducted for each system state considering voltage and transmission limits
- Performance function $S(X_1)$ is used to evaluate system state: $S(X_1)$= load curtailments that is need to keep system variables within limits

Distorted fault rate calculation
- Rank system state performance in ascending order
- Evaluate test function $H(X_i)$, if $S(X_1)<1$, $H(X_i)=0$; else, $H(X_i)=1$
- Evaluate the importance weight $W(X_i)$

Optimization Index Update
- $\gamma=1$,
- If $S_{[(1-\rho)N]}>\gamma, \gamma_k=\gamma$

$\gamma_k=\gamma$?

No

Yes

Optimized Fault Rate Update
- $v_{opt} = v_{last\ iteration}$

Figure 5.2 The Flow Chart for the CE-IS Optimization Procedure

The optimal PDF parameter $\vec{v}_{opt}$ that is obtained from the CE IS process is then used as the input parameters in the integrated reliability evaluation process. Based on the new availability data, the fault rate of each element can be calculated based on (5.39):

$$\lambda^* = \frac{v_{opt}}{1 - v_{opt}} \tag{5.39}$$

To avoid the bias, the reliability indices calculated from the SMCS based on the optimal unavailability v_{opt} are based on (5.40) - (5.42). The reliability indices from the i-th SMCS iteration are calculated according to (5.43) – (5.45):

$$T_{down} = \sum t_i \cdot W(X_i; n, \vec{u}, \vec{v}) \tag{5.40}$$

$$EPS = \sum t_i \cdot \Delta P(X_i) \cdot W(X_i; n, \vec{u}, \vec{v}) \tag{5.41}$$

$$OCC = \sum 1 \cdot W(X_i; n, \vec{u}, \vec{v}) \tag{5.42}$$

$$LOLP_i = \frac{T_{down}}{8760} \tag{5.43}$$

$$EPNS_i = \frac{EPS}{8760} \tag{5.44}$$

$$LOLF_i = \frac{OCC}{8760} \tag{5.45}$$

5.2.2   Metrics based Pruning Process for TDS

The dynamic security of system states that are selected from SMCS is assessed in TDS. It is well known that the TDS while providing accurate results, has a significant computational burden. A screening tool for TDS is, therefore, investigated in this work to

make the evaluation process more efficient. The proposed screening tool classifies all system states based on a two-stage approach. Firstly, an early terminated TDS is conducted for each system state to obtain system operating conditions after a fault is cleared (assuming it is 5 cycles after the fault occurred). The system states are classified to be critical or non-critical based on the kinetic energy gained by the machines due to the fault and the maximum change in the magnitude of Thévenin impedance seen at the point of interconnection (POI) of a generator.

The reason for using these two metrics is that the stability of a power system during a fault depends on the kinetic energy gained by the system due to the fault, and the robustness of the post-disturbance network [61]. During a fault, the ability of the network to export electrical power is severely restricted, causing the machine to accelerate. Once the fault is cleared by opening the faulted line, the machine can export electrical power, and it decelerates. The stability of the machine is dependent on its ability to decelerate in the post-disturbance condition and to reach a steady state. To estimate the ability of the system to decelerate, the change in the magnitude of Z_{th} looking into the system at the POI of the generator due to the opening of the faulted line is computed. A review of the swing equation [61] indicates that a large change in the magnitude of Z_{th} results in a substantial reduction in the peak of the post-fault swing curve as compared to the pre-faulted condition. A reduction in the peak of the post-fault swing curve limits the ability of the generator to decelerate, thereby making it prone to instability.

The kinetic energy and Thévenin impedance can be calculated from simulation results from the early terminated TDS that lasts to fault clearing time. In this work, faults are

assumed to be cleared in 5 cycles. Detailed TDSs are conducted for critical cases. Load curtailment can be calculated from TDS for each system scenario and serves as a system reliability index.

From the early terminated TDS, the angular speed of generators at the end of the fault can be obtained. The calculation of corrected kinetic energy gained during the fault is as follows:

$$\omega_{coi} = \frac{\sum_{gens} M_i \omega_i}{\sum_{gens} M_i} \tag{5.46}$$

$$M_{cr} = \sum_{critical\_gens} M_{i\_cr} \tag{5.47}$$

$$M_{non\_cr} = \sum_{noncritical\_gens} M_{inon\_cr} \tag{5.48}$$

$$\tilde{\omega}_{cr} = \frac{\sum_{critical\_gens} M_{i\_cr} (\omega_{icr} - \omega_{coi})}{M_{non\_cr}} \tag{5.49}$$

$$\tilde{\omega}_{non\_cr} = \frac{\sum_{noncritical\_gens} M_{inon\_cr} (\omega_{inon\_cr} - \omega_{coi})}{M_{non\_cr}} \tag{5.50}$$

$$M_{eq} = \frac{M_{cr} * M_{non\_cr}}{(M_{cr} + M_{non\_cr})} \tag{5.51}$$

$$\tilde{\omega}_{eq} = \tilde{\omega}_{cr} - \tilde{\omega}_{non\_cr} \tag{5.52}$$

$$KE_{corr} = \frac{1}{2} M_{eq} (\tilde{\omega}_{eq})^2 \tag{5.53}$$

where, ω_{coi} is the angular velocity of the center of inertia, ω_i is the angular velocity of the i th generator, M_i is the inertia constant of the i th generator, M_{cr} is the inertia constant of the critical generators inertial center, M_{non_cr} is the inertia constants of the non-critical generators inertial center, $\widetilde{\omega}_{cr}$ is the angular speed of the inertial center of the critical generator group, $\widetilde{\omega}_{non\_cr}$ is the angular speed of the inertial center of the non-critical generator group, M_{eq} and $\widetilde{\omega}_{eq}$ is the equivalent inertia constant and angular speed of the system, KE_{corr} is the corrected kinetic energy.

For the pre-fault condition, the Thévenin impedance at POI can be directly obtained by the pre-fault network. The change in the magnitude of Z_{th} can be calculated by removing faulted components based on the Z_{th} in the pre-fault network. The maximum change ΔZ_{thmax} in the magnitude of Z_{th} and the corresponding bus number of the POI where it occurs are recorded.

5.3   Integrated Reliability Evaluation Procedure with Accelerating Process

Previously, the overall integrated reliability assessment method with the computation accelerating methods have been discussed and the integrated procedure is shown in Figure 5.3.
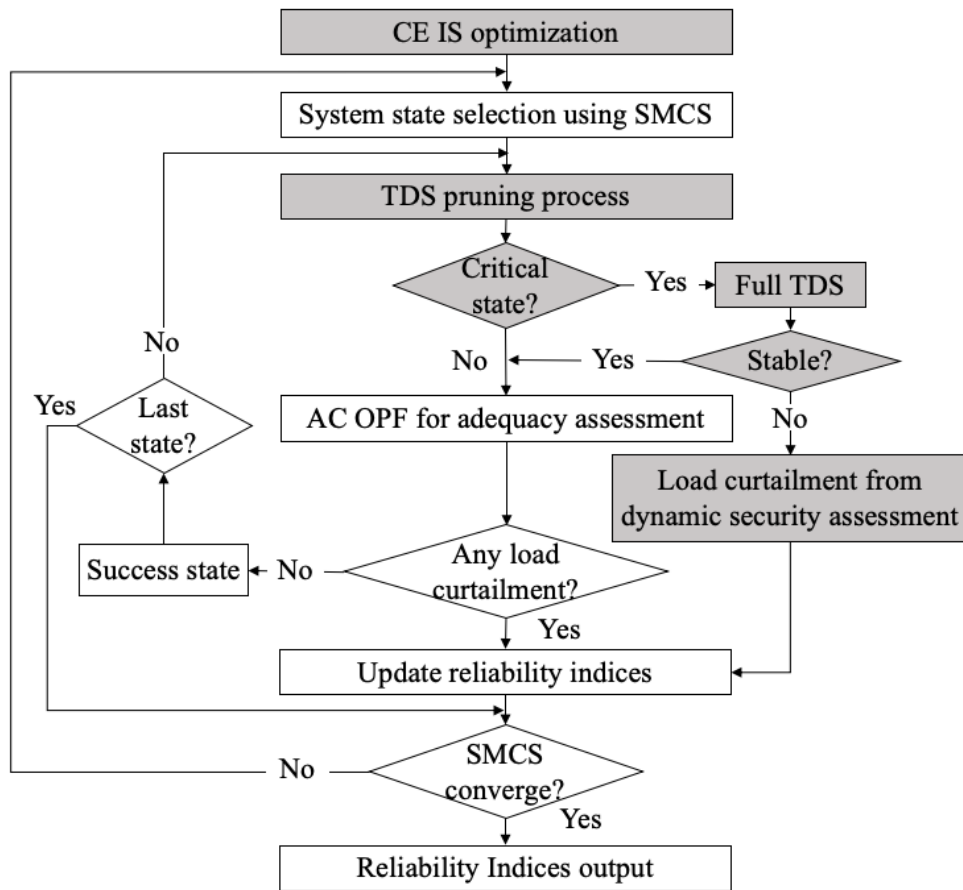
Figure 5.3 Integrated Reliability Evaluation Procedure with Accelerating Process

5.4   Summary

In this chapter, the integrated reliability evaluation procedure is presented. The assessment methods for system steady-state reliability and dynamic security are discussed. The approach evaluates the system response for each selected contingency, examines transient stability in the transition from the pre-contingency to the post-contingency period, and evaluates the post-contingency steady-state equilibrium where all flow limits and voltage limits are satisfied. Stochastic characteristics, including renewable resources, component failures, and load variations, are taken into consideration in probabilistic sampling and dynamic performance modeling. System adequacy and dynamic security are

quantified in terms of MW load curtailment from the respective assessment processes and are incorporated into the calculation of the integrated reliability indices. The outcome of the integrated reliability evaluation provides the probability, frequency, and magnitude of system reliability represented as well-known indices such as *LOLP*, *LOLF*, and *EENS*.

Two accelerating techniques are presented in this chapter with the objective of improving the computational efficiency of the MCS process and the TDS process, respectively. The proposed approach is tested on a synthetic system. The test results are presented and discussed in chapter 6.

Chapter 6

INTEGRATED RELIABILITY EVALUATION RESULTS AND DISCUSSION

Reliability evaluation results using the proposed integrated reliability evaluation approach are discussed in this chapter. The reliability evaluations are conducted on the test system that has been described in chapter 4. The evaluation results that only consider system adequacy are described firstly, then following these results, the results from the integrated reliability evaluation are presented. The results from the two approaches are compared, as an illustration of the merits of the proposed method. The effects of the introduced acceleration approaches for the evaluation process are illustrated in this chapter. The evaluations are conducted using the software tool developed from this work, which utilizes commercial power system analysis tools including GE PSLF and Siemens PSS/E OPF. The software tool is developed using Python.

6.1   Parameters for Reliability Studies

The synthetic test system described in chapter 4 is used to perform the reliability evaluation studies. With detailed positive sequence generator, governor and exciter models for synchronous generators, generator, and converter control models for WTGs incorporated in the test system, it is suitable for conducting reliability evaluations that include the assessment of both adequacy and dynamic security.

Reliability parameters for conventional generators, WTGs, transmission lines are assembled before conducting the reliability studies.

6.1.1 Generation Availability Data

For conventional generators, reliability parameters are assembled base on the data from the IEEE Reliability Test System-1996 [87]. Unit availability data of conventional generators and WTGs in terms of *MTTF* and *MTTR* are given in Table 6.1.

Table 6.1 Generation Availability Data of the Test System

Type	Rating (MVA)	MTTF (hour)	MTTR (hour)
Synchronous generators	≥2200	1150	100
	1800	1100	150
	1500	1500	120
	1200	1500	100
	900	1100	100
	600	960	40
WTGs	33.4	800	40
	23.4	800	40

6.1.2 Transmission Availability Data

The fault rates for transmission lines are assembled based on the data in the CEA 2012 annual report [72]. The CEA report provides the transmission line statistics for line-related transient forced outages data in terms of the frequency of outage of transmission lines for different voltage levels in number per 100 mile-annum. The transmission availability data are given in Table 6.2.

Table 6.2 Transmission Reliability Data of the Test System [72]

No.	Voltage level (kV)	MTTR (hour)	Failures rate (failures/year/km)
1	110	20.7	0.3982
2	500	27.2	1.4722

6.1.3 Load Curve Data

The chronological load curve with a 1-hour resolution in a year is introduced to represent the load stochasticity in the system. The hourly load data in a year is based on the load curve data from IEEE Reliability Test System-1996 [87]. The data include weekly peak loads in percent of the annual peak load, the daily peak load in percent of the weekly peak load, and the hourly load in percent of the daily peak load. Once the system annual peak load is assigned, the 8760-hour load curve in the year can be calculated. The hourly load curve data is given in appendix B.

6.2 Evaluation of System Adequacy

Adequacy assessment examines system steady-state conditions and determines whether load can be supplied with existing generation and transmission resources, and no operating constraints are violated. Therefore, the assessment evaluation is conducted using techniques including AC power flow and AC OPF in this work. Detailed considerations of operating constraints and remedial actions have been described in chapter 5. The flowchart of the procedure for the adequacy evaluation is shown in Figure 6.1.
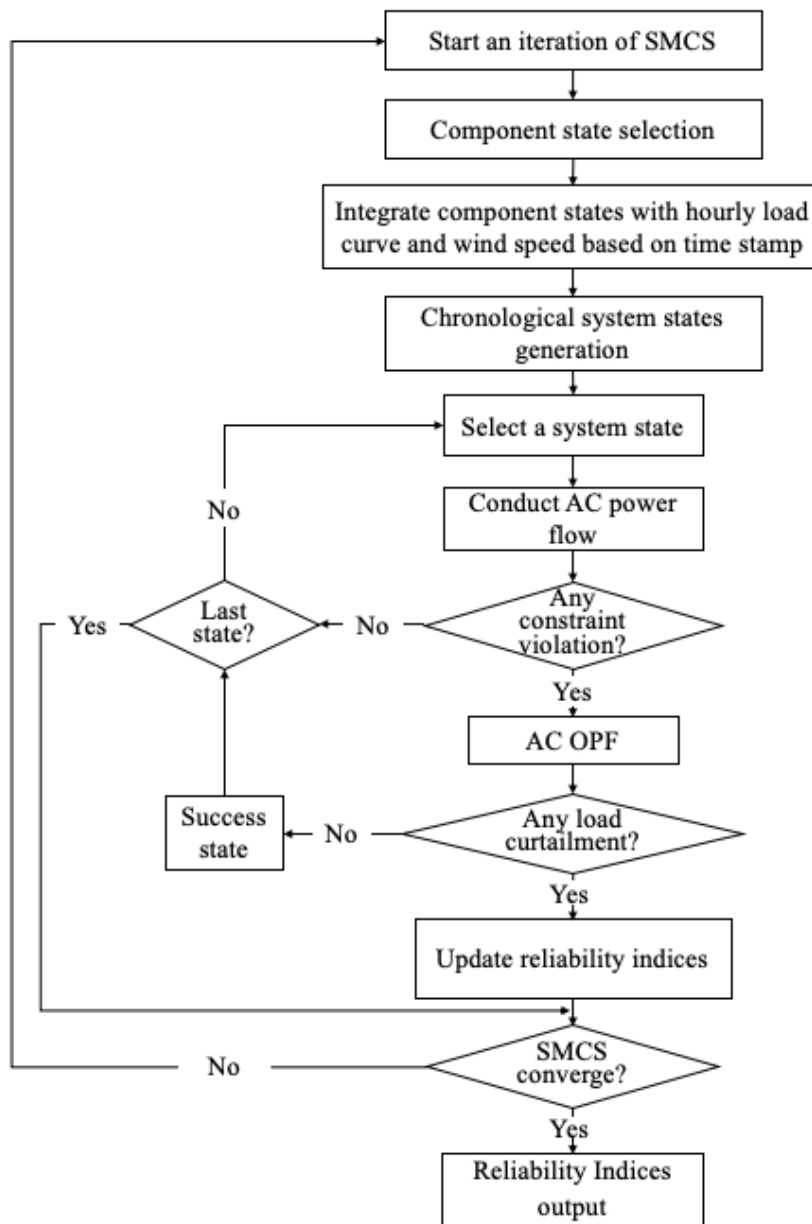
Figure 6.1 Flowchart of the Procedure for Adequacy Assessment

In each iteration of SMCS, chronological components states are selected based on the availability data that are given in Table 6.1 and Table 6.2. These states are then integrated with the chronological load curve and wind speed curve that have a 1-hour resolution. After the integration with the load curve and wind speed curve, the system states at each hour in a year are generated. Generation dispatch is needed for each generated system state to get a converged power flow case for further studies. The mismatch between the generation and load is calculated first. Then based on the mismatch, the output of conventional generators that are operating within generation limits will be re-scheduled.

To determine the adequacy of each system state, power flow is conducted for the state to evaluate whether the system is within operating limits. AC OPF is conducted if operating limits are violated to assess whether load curtailment is needed to bring the system back within operating limits. In the SMCS, the *COV* of the *LOL*P index (β_{LOLP}) is chosen as the convergence criterion. The simulation stops when β_{LOLP} is less than 0.05 or simulation years reach the upper limits of 5000 years.

Simulation results show that, for this test system, the SMCS process of the adequacy evaluation converges after 746 iterations. The total simulation time of 8.95×10^5 seconds, approximately 248 hours. The reliability indices after the SMCS of adequacy evaluation are given in Table 6.3.

After the convergence of the SMCS, adequacy evaluation found a *LOLP* index around 0.0015, an *EPNS* index around 0.0087 MW, and a *LOLF* index around 2.7663 occ/ year. This simulation provides reference values of the reliability indices for the test system.

Figure 6.2 - Figure 6.5 show the convergence trajectory of the *COV* and reliability indices of *LOLP*, *EPNS*, and *LOLF*, respectively. Because of the low probability of unreliability states in the test system, the SMCS process was slowly reaching its convergence.

Table 6.3 Reliability Indices from Reliability Evaluation Considering System Adequacy

# Iteration	β_{LOLP}	COV	LOLP	EPNS (MW)	LOLF (occurrence/year)
746	5%	4.98%	0.0015	0.0087	2.7663

Figure 6.2 Convergence Trajectory of *COV* from Adequacy Assessment Based on SMCS

Figure 6.3 Convergence Trajectory of *LOLP* from Adequacy Assessment Based on SMCS

Figure 6.4 Convergence Trajectory of EPNS from Adequacy Assessment Based on SMCS

Figure 6.5 Convergence Trajectory of *LOLF* from Adequacy Assessment Based on SMCS

6.3   Impact of Accelerating Techniques

As illustrated in section 5.2.1, the CE IS method is introduced in the SMCS to improve simulation efficiency. In this section, the reliability results from CE-IS based SMCS is presented, and a comparison with the traditional SMCS is discussed. To illustrate the accuracy of the CE-IS based SMCS algorithm, the simulation is conducted on the same test system with identical peak load, annual load curve, and yearly wind speed curve, as well as the same availability parameters for elements. The parameter settings of the CE-IS SMCS are as follows: the rare event percentage $\rho = 0.1$, the maximum sample size $N_{MAX} = 5000$, and the *COV* convergence criteria $\beta_{MAX} = 5\%$. Table 6.4 shows the comparison between the adequacy evaluation results for the test system using the crude SMCS and

96

the SMCS with the CE-IS acceleration method. The comparison of the convergence trajectory of the *COV*, *LOLP*, *EPNS*, and *LOLF* indices using the two methods are as shown in Figure 6.6 - Figure 6.9.

The evaluation based on SMCS with CE-IS obtains a *LOLP* value of 0.0014, which is within a 0.01% deviation from the crude SMCS method result. Given that both values are the mathematical estimates of the true value, the difference is negligible. However, the CE-IS SMCS method reaches convergence much faster. The simulation with the acceleration method implemented converges after 81 iterations with a computation time of 0.98×10^5 seconds while the evaluation without CE-IS takes 8.95×10^5 seconds to complete. By applying the CE-IS acceleration method in SMCS, a speed-up factor of 9.13 in elapsed time is achieved, while maintaining approximately equal evaluation results. It can be concluded that the effect of CE-IS method is verified.

Table 6.4 Reliability Indices Comparison Between Traditional SMCS and CE-IS SMCS

Method	LOLP	EPNS	LOLF (occurrence/yr)	Number of iterations	Computation time
Crude SMCS	0.0015	0.0087	2.7663	746	8.95×10^5s (248 h)
CE-IS SMCS	0.0014	0.0079	2.7650	81	0.98×10^5s (27 h)
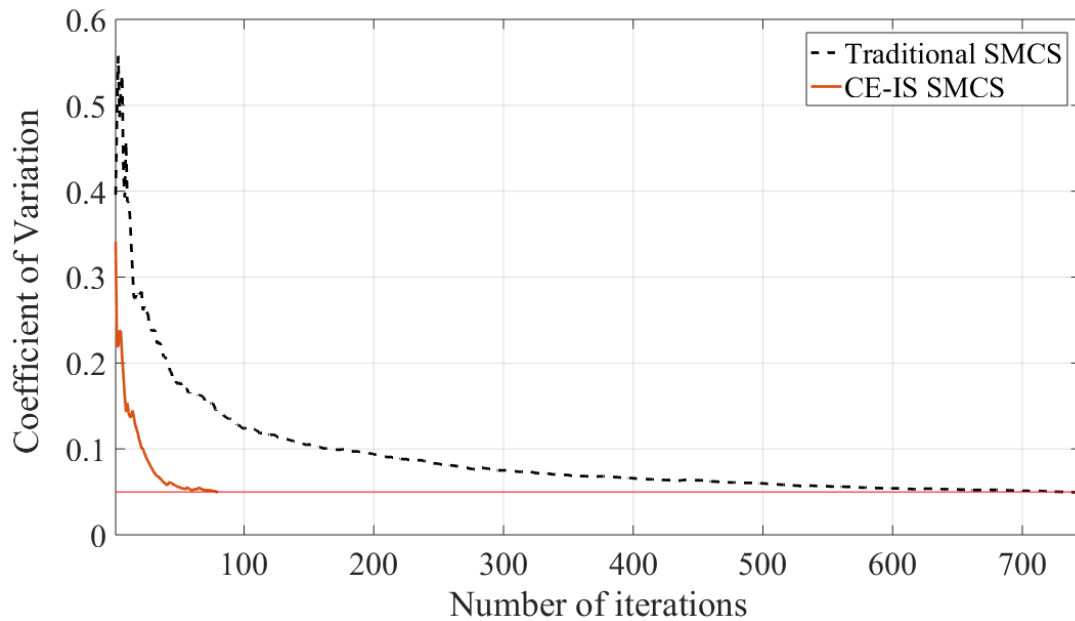
Figure 6.6 Convergence Trajectory of COV from Adequacy Assessment Based on CE-IS SMCS
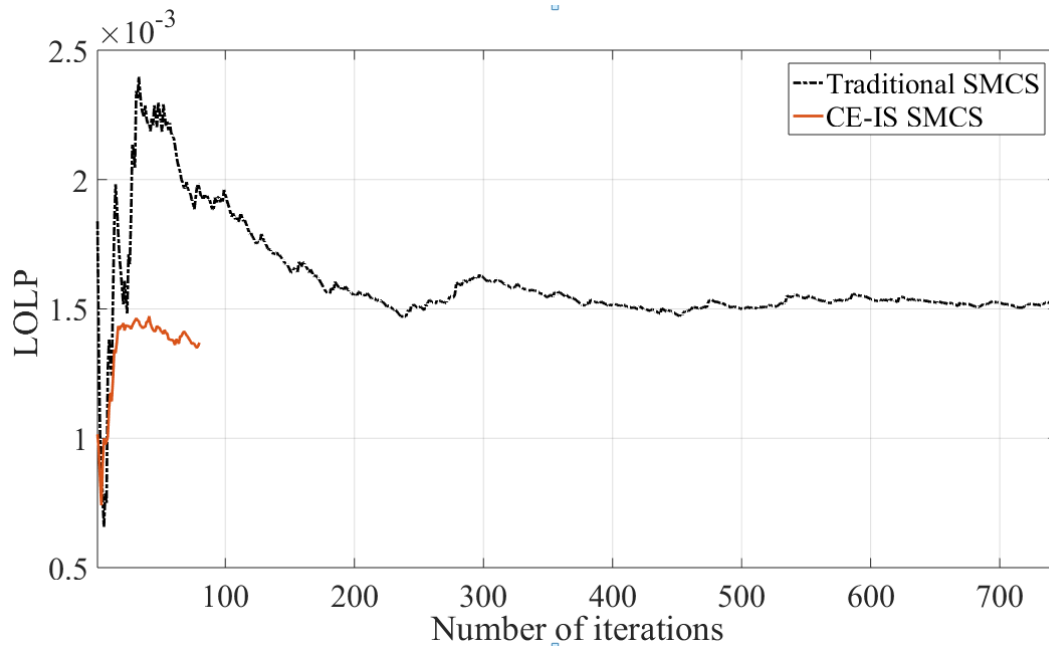
Figure 6.7 Convergence Trajectory of *LOLP* from Adequacy Assessment Based on CE-IS SMCS
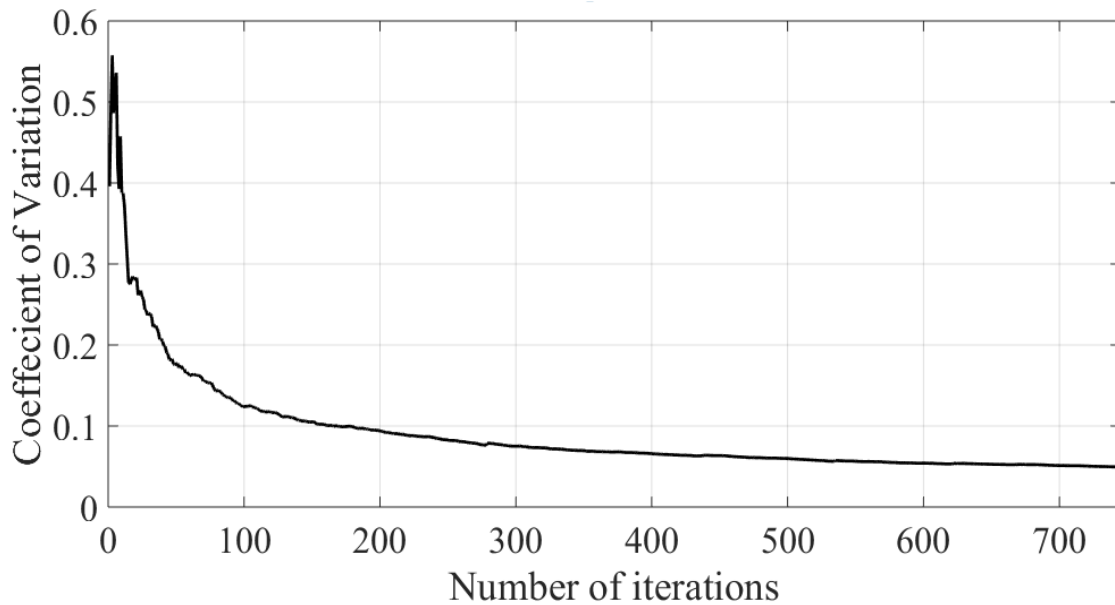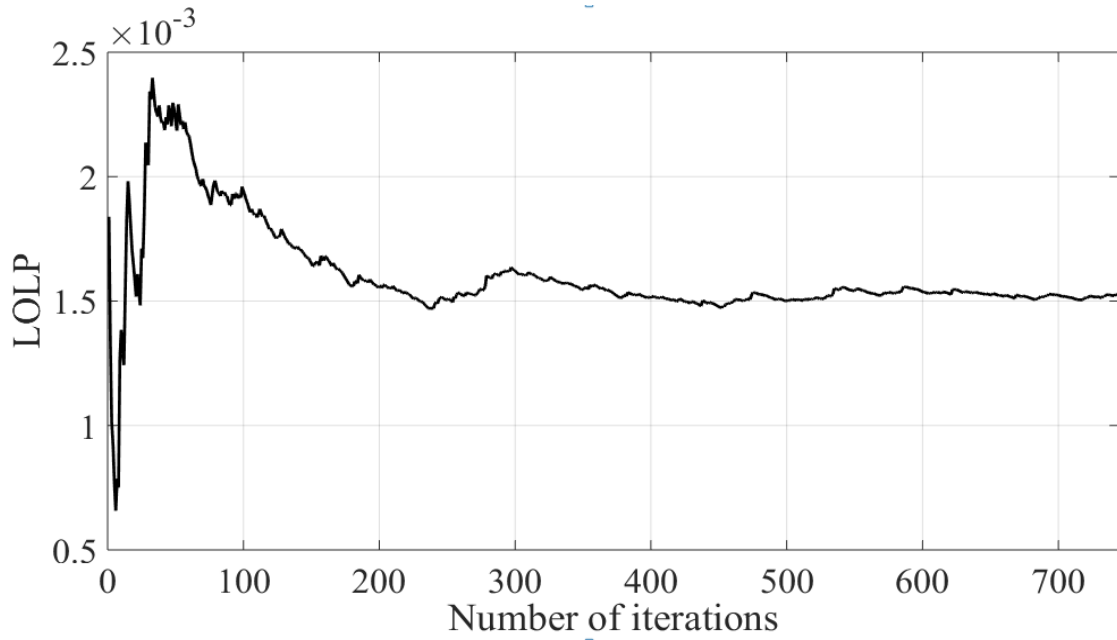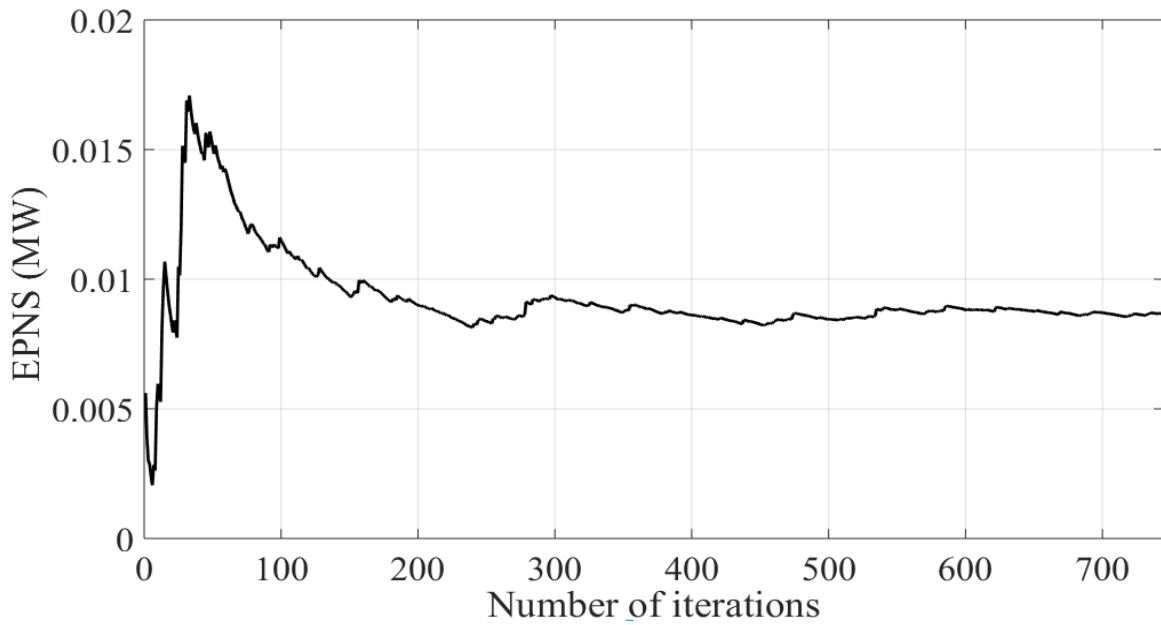
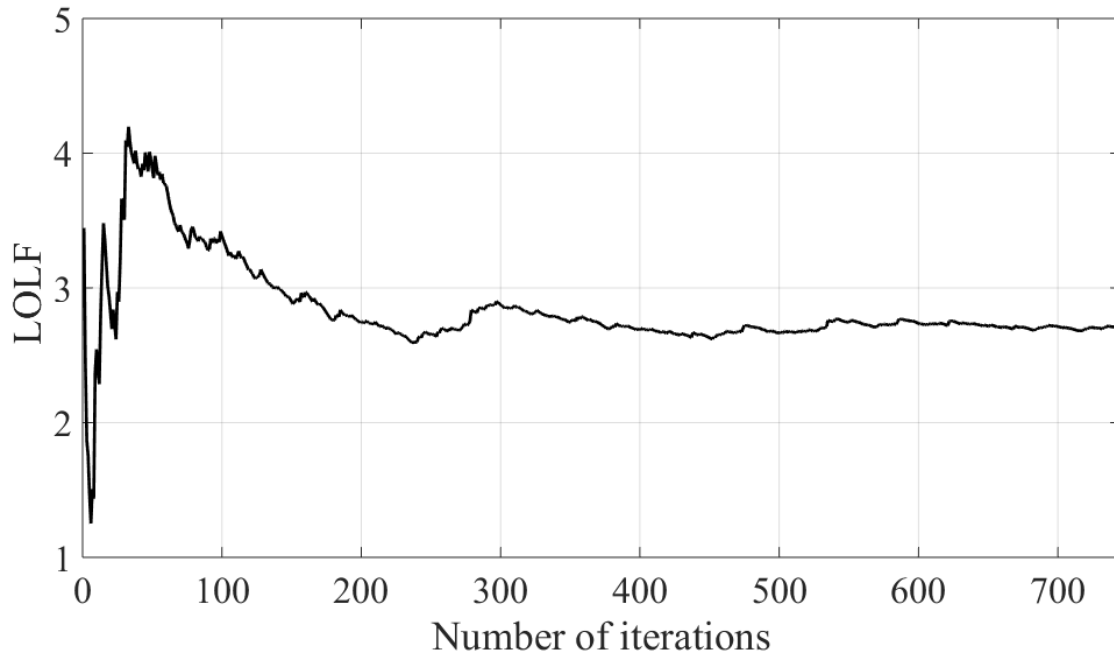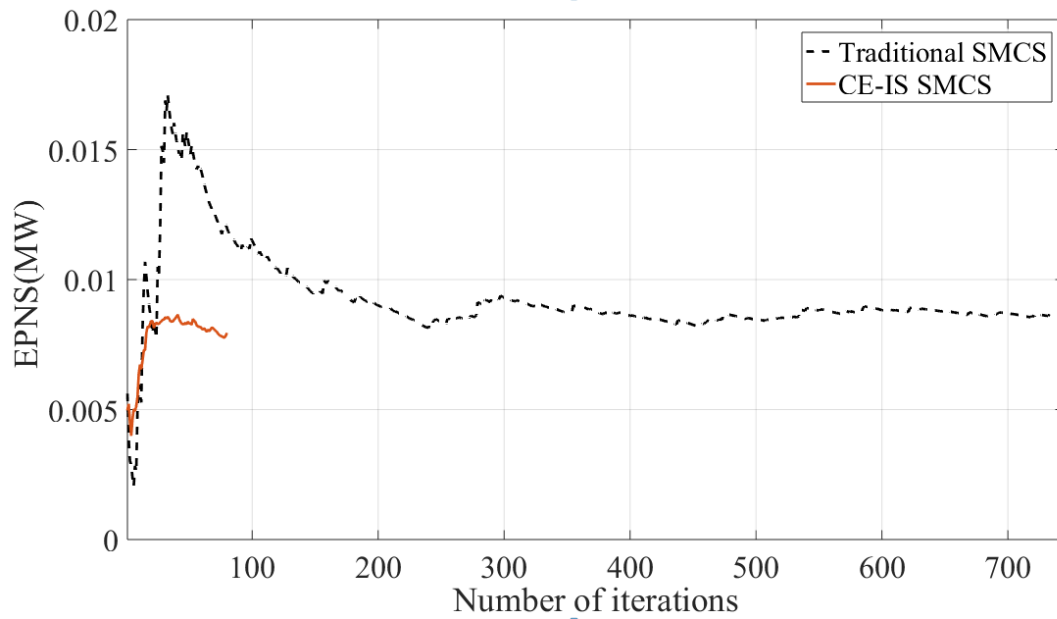Figure 6.8 Convergence Trajectory of EPNS from Adequacy Assessment Based on CE-IS SMCS
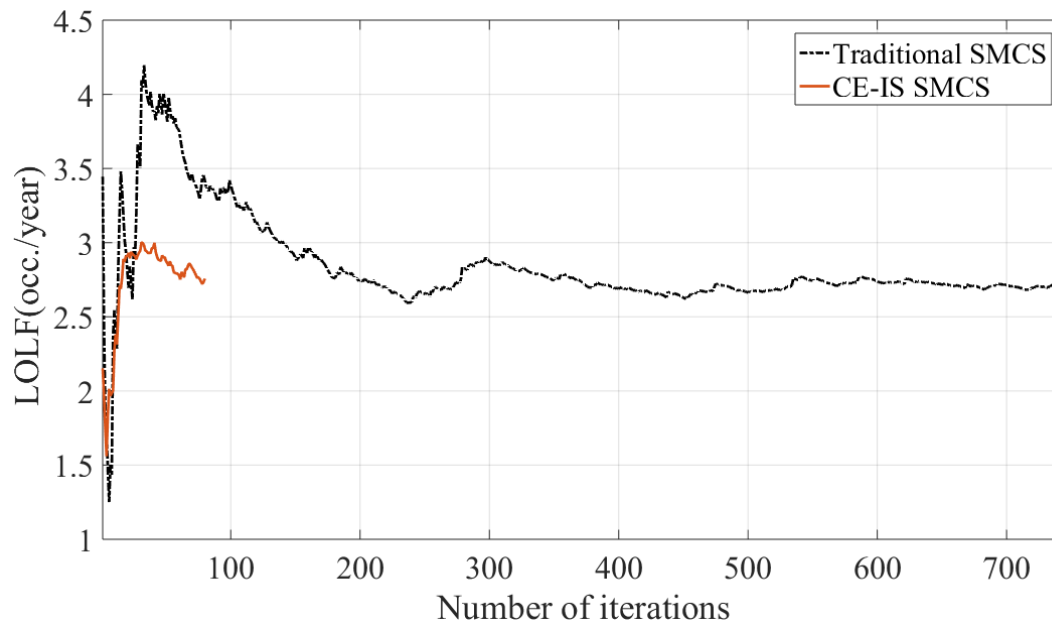
Figure 6.9 Convergence Trajectory of LOLF from Adequacy Assessment Based on CE-IS SMCS

6.4   Integrated Reliability Evaluation Results

From the comparison between the reliability indices obtained using traditional

SMCS method and the CE IS based SMCS in the last section, it can be seen that both

methods reached a very close reliability index associated with *LOLP*. However, the CE-IS

based SMCS demonstrated a computational speed-up of 9.13 times. Based on the proposed

speed-up of the SMCS, this section will discuss the integrated reliability results considering

both system adequacy and dynamic security. The integrated reliability results provide a

measure of both steady-state and dynamic evaluation of the ability of the system to meet

electrical demand. The reliability results are compared in Table 6.5.

Table 6.5 Reliability Indices Comparison Between Integrated Reliability Evaluation and
Adequacy Evaluation

Method	LOLP	EPNS	LOLF (occurrence/yr)	Number of iterations	Computation time
Integrated reliability evaluation	0.0939	72.80	35.6944	20	3.89×10^5 s (108 h)
Adequacy evaluation	0.0014	0.0079	2.7650	81	0.98×10^5 s (27 h)

With system dynamic security being quantified by load shedding from the stability

preserving protection systems, the proposed method provides the quantitative integrated

reliability evaluation results considering both system adequacy and dynamic security. The

comparison between the results from the two approaches reflects the influence of including

the impact of dynamic security in the reliability evaluation.

From Table 6.5, it can be observed that for this test system, accounting for dynamic security has a significant impact on the overall reliability indices resulting in an increase in the *LOLP*, *EPNS*, and *LOLF* indexes. The *LOLP* index and *LOLF* index increase from 0.0014 to 0.0939 and from 2.7650 to 35.6944, respectively. The increase of these two indices indicates that among all sampled states in a year, there are a large portion of cases and longer duration for which the system cannot provide reliable power supply because of dynamic security problems. The increase of the *EPNS* index is due to the fact that the load shedding value from DSA is included in the *EPNS* index calculation. Theoretically, the increase of the three reliability indices, namely *LOLP*, *EPNS* and *LOLF*, was to be expected because a stable transition to post-fault SEP is not always guaranteed after contingencies.

If a stable transition cannot be made after a disturbance in the system, this behavior cannot be captured by the steady-state analysis in adequacy evaluation. By incorporating the DSA in the reliability evaluation process, unstable transitions are captured, which works as a counterbalance to the adequacy evaluation. The unstable transitions are quantified in the evaluation process, and it provides not only the information on the existence of instability but also the severity of the instability. This information can be beneficial for system planners to pinpoint the weaknesses in the system. Results in Table 6.5 also show that the number of iterations for the SMCS to converge is significantly reduced in the integrated approach. The reason for the faster convergence is that for this test system, with DSA considered, the values of indices increase, and the number of iterations is inversely proportional to the index being calculated. However, despite the fewer iterations, the computation time is still much higher than the adequacy evaluation computation time because of the computational burden introduced by TDS for DSA. The simulation of integrated

reliability evaluation converges after 20 iterations while the simulation of adequacy evaluation with the CE-IS acceleration method implemented needs to run 81 iterations to converge. However, the computation time for the integrated reliability evaluation is 3.89×10^5 seconds, while the adequacy evaluation with the CE-IS acceleration method implemented takes 0.98×10^5 seconds to complete.

A statistical summary of the evaluation in a randomly selected iteration of SMCS shows that: in this iteration, 11992 system states are sampled representing the chronological system operating conditions in the year. The reliability evaluation shows that among all these system states, there are 408 cases that are steady-state unreliable based on adequacy assessment, 5002 cases labeled as dynamically insecure, and 4603 cases labeled as steady-state reliable yet dynamically insecure. Among the 4603 cases, 8 cases are N-1 contingencies, and 4595 cases are N-k contingencies with $k > 1$. The statistical data confirms that the reliability study will give optimistic results if the DSA is not considered in the evaluation process. It is important to note that for a different system with different load conditions and availability parameters for generators and transmission lines, the reliability evaluation results could be quite different. Hence for a system that has less dynamic security issues, the integrated reliability evaluation results could be very similar to the adequacy evaluation results. This proposed integrated reliability evaluation approach is more important for systems that have a potential dynamic security problem. Given the undergoing transformation in the power systems, the dynamic behavior of systems can be very different from how it was. The integrated reliability evaluation approach provides a solution to comprehensively identify the dynamic insecurities along with the potential inadequacy of system resources.
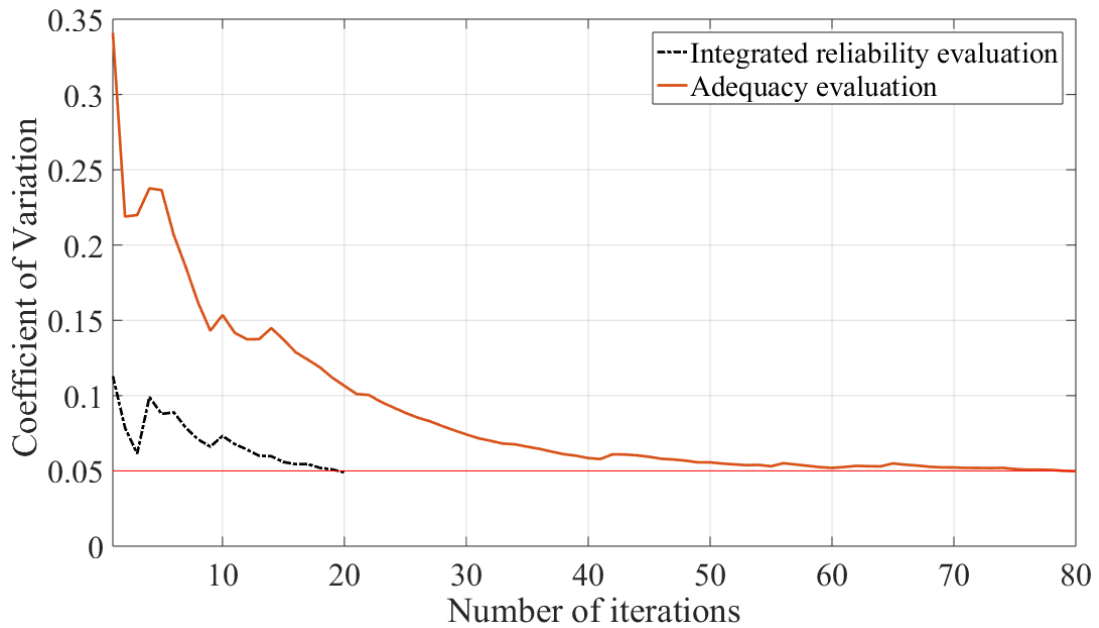
Figure 6.10 Convergence Trajectory of COV Comparison Between Adequacy Evaluation and Integrated Reliability Evaluation
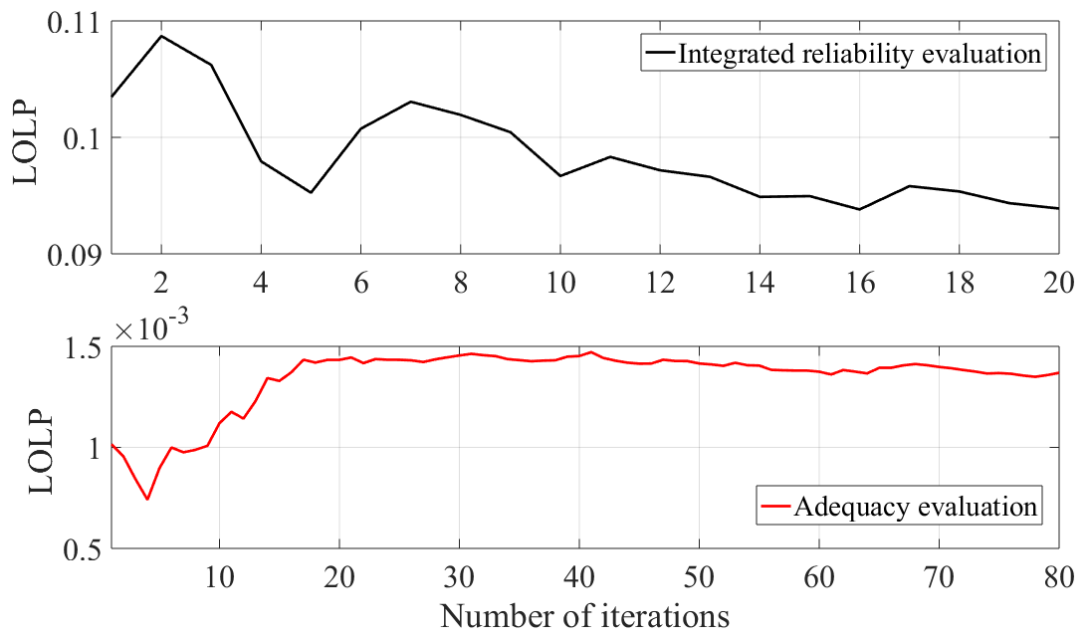
Figure 6.11 Convergence Trajectory of LOLP Comparison Between Adequacy Evaluation and Integrated Reliability Evaluation
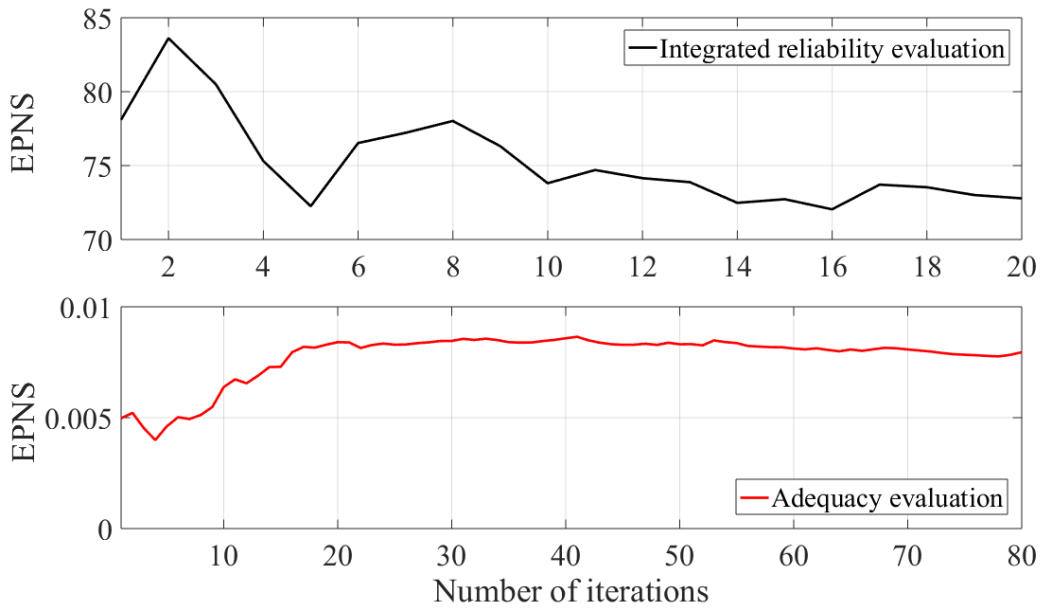
Figure 6.12 Convergence Trajectory of *EPNS* Comparison Between Adequacy Evaluation and Integrated Reliability Evaluation
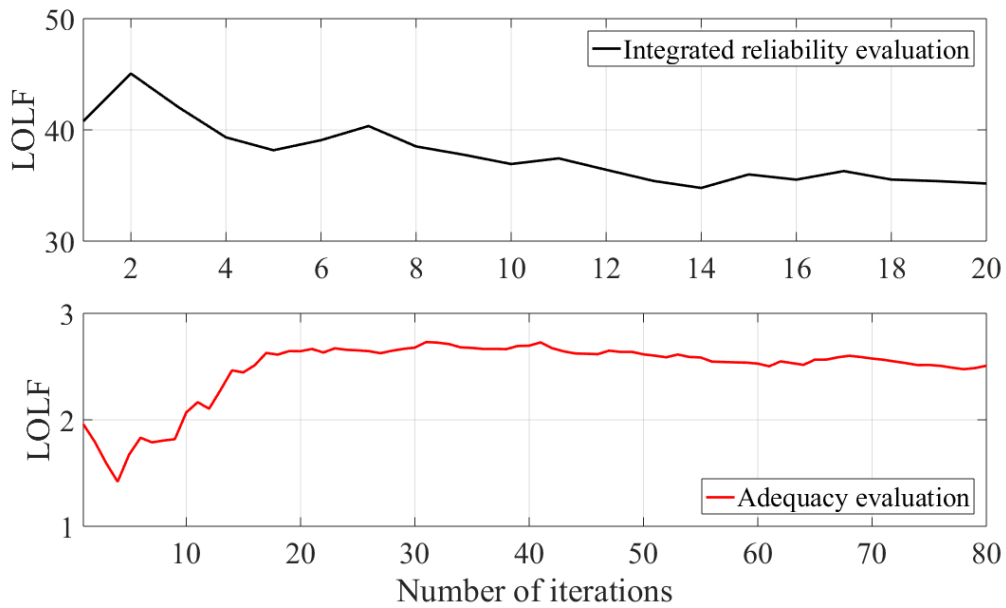
Figure 6.13 Convergence Trajectory of LOLF Comparison Between Adequacy Evaluation and Integrated Reliability Evaluation

The trajectories of COV and the values of the three reliability indices are compared in Figure 6.10 - Figure 6.13 to show the impact on reliability assessment when dynamic security is considered. As shown in Figure 6.10, the simulation of the integrated reliability evaluation converges faster than that without dynamic security. The reason for this is that with dynamic security considered, more cases are detected to be unreliable and are therefore considered in the reliability calculation. With a larger number of unreliable cases being viewed as important, the variance is reduced which provides the same effect as importance sampling.

The analysis of a specific case is essential to understand the states that are steady-state reliable but dynamically insecure. A state with 6375 MW load and 6581 MW generation in the pre-fault condition is selected to conduct this analysis. The set of contingencies in this selected state are listed in Table 6.6.

Table 6.6 Pre-fault and Post-fault Condition of Outage Components

No.	Outage component	Rating (MVA)	Pre-fault condition	Fault at time
1	Gen6 on bus 24	4500	1849.3 MW generation	1 s
2	Gen8 on bus 26	1200	405.9 MW generation	1 s
3	Wind farm on bus 808	33.4	9.80 MW generation	1 s
4	Wind farm on bus 3404	23.4	6.90 MW generation	1 s
5	Wind farm on bus 3405	23.4	6.90 MW generation	1 s
6	Line from bus 13 to bus 18	1500	488.6 MW flow	1 s

In this case, the adequacy analysis based on AC OPF gives a load curtailment of 0.185 MW. This assessment result indicates that the system state is steady-state reliable. By contrast, the results from TDS for DSA show that 1554.4 MW load needs to be shed to maintain stability. The load shedding protection actions are listed in Table 6.7. From Table 6.7, it can be observed that two stages of under-frequency load shedding protection are activated after the fault. The first stage protection was activated at around 2.5 s when the load bus frequency dropped to 59.5 Hz, and the second stage of protection action was initiated between 4.2 s-4.3 s when the load bus frequency dropped to 59.2 Hz, as shown in Figure 6.14. The two stages of protection action brought the system back to a stable operating condition.

Figure 6.15 shows the active power output of the 11 synchronous generators in the system. Since the generators at bus 24 and bus 26 are the contingency components, the loads at bus 23 and bus 25, which were primarily supplied by generators at bus 24 and bus 26, suddenly lost their power supply. Also, the transmission outage from bus 13 to bus 18 limited the power supply from the generator at bus 14 to the heavy load area in zone 4 and zone 5. The resulting system frequency decline, therefore, quickly triggered the load shedding corrective actions. Noticeably, this unreliability, which has a significant impact, cannot be captured by the steady-state assessment. This case study illustrates the importance of incorporating DSA in system reliability evaluation.
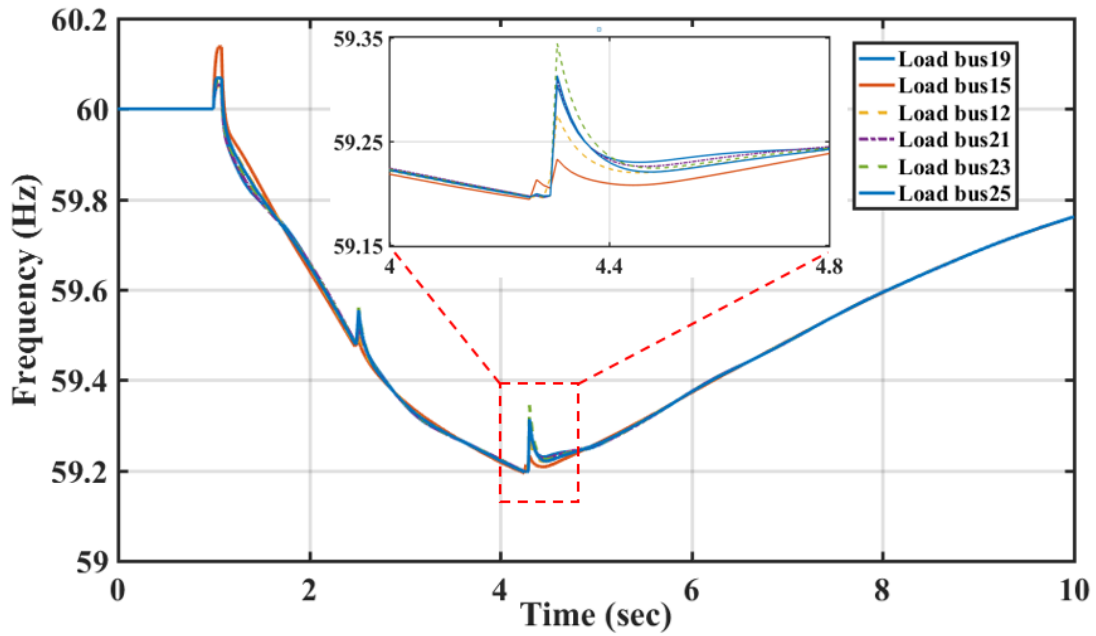
Figure 6.14 Load Bus Frequency Under Contingency
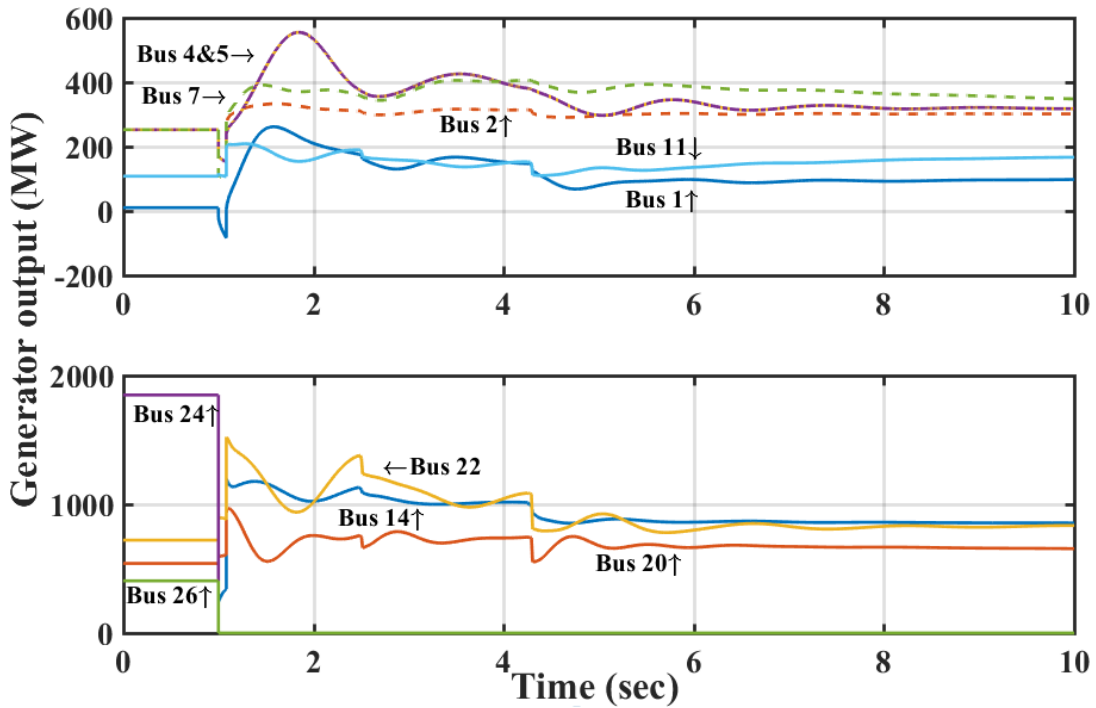
Figure 6.15 Generator Output Under Contingency

107

Table 6.7 Post-contingency Protection Action Report

Time (s)	Switching Action	Details
2.4835	Stage 1 tripped	Load at bus 15
2.4960	Stage 1 tripped	Load at bus 12
2.5044	Stage 1 tripped	Load at bus 25
2.5127	Stage 1 tripped	Load at bus 23
2.5169	Stage 1 tripped	Load at bus 19
2.5169	Stage 1 tripped	Load at bus 21
4.2629	Stage 2 tripped	Load at bus 15
4.2875	Stage 2 tripped	Load at bus 12
4.3004	Stage 2 tripped	Load at bus 23
4.3045	Stage 2 tripped	Load at bus 19
4.3045	Stage 2 tripped	Load at bus 21
Total Load shedding:		1554.4 MW

6.5   Transient Stability Pruning Effects

Previous simulation results show the reliability indices obtained from the traditional SMCS method and the CE IS based SMCS. Both methods reached a similar result. In this section, the reliability evaluation results with the accelerating process applied are discussed. Results from two reliability evaluation are compared and discussed. One is a reliability evaluation with the pruning process from TDS, and the other is with no pruning process applied in TDS. Different load shed values LS_{TDS} are used to determine whether a system is stable in the transient period after disturbance and should be considered in the reliability indices calculation. If the load curtailment of a state from the TDS is higher than

LS_{TDS}, then the state is insecure, and the amount of load curtailment, as well as state duration, are introduced in the index calculation.

For a chosen iteration, the pruning process eliminated 3842 states among 11992 states from the detailed TDS analysis, with a 32.04% speed-up of the DSA. The criteria for the two stability estimation metrics are KE_{cr}=0.5×10^{-5}pu and ΔZ_{th}=0.005 pu obtained by conducting a sensitivity study. Table 6.8 gives the comparison of *LOLP* results from the evaluation process with and without the TDS pruning process. The LS_{TDS} in Table 6.8 represents the criteria for determining dynamically insecure cases. When the load shedding results from TDS are larger than LS_{TDS}, the state is considered to be dynamically insecure. Simulation results show that the reliability evaluation with the pruning process gives similar results compared with no pruning process be applied. The deviations vary from 2.4494%-4.9645%. Additionally, from the sensitivity study of the different load shed threshold value, it can be seen that when LS_{TDS} is equal to 20 MW, 100 MW, and 200 MW, the *LOLP* results are very close to each other. Thus, we can choose any of the three values to be the load shed threshold to determine whether a state is transiently unstable from TDS.

Table 6.8 Comparison of LOLP Indices Results: With and Without Pruning Process

LS_{TDS} criteria (MW)	Without Pruning Process	With Pruning Process	Deviation (%)
20	0.0939	0.0916	2.4494
100	0.0939	0.0916	2.4494
200	0.0936	0.0913	2.4573
400	0.0753	0.0721	4.2497

Table 6.8 (Continued)

LS$_{TDS}$ criteria (MW)	Without Pruning Process	With Pruning Process	Deviation (%)
500	0.0564	0.0536	4.9645
600	0.0388	0.0375	3.3505
700	0.0269	0.0259	3.3457
800	0.0264	0.0257	2.2727
Average deviation:			3.1924

6.6   Summary

The probabilistic reliability evaluation gives a quantitative indication of overall system reliability condition, which is rather different from the traditional deterministic approach. Different simulation cases are presented in this chapter to draw a conclusion of the proposed integrated reliability evaluation approach. Simulation results show that when addressing both adequacy and dynamic security in the reliability evaluation, the evaluation differs with the traditional method of reliability evaluation with only the adequacy considered. The reliability indices are relatively higher when the dynamic security assessment is integrated because of the fact that under some disturbances system cannot stably transfer to a post-disturbance steady state.

The integrated reliability evaluation has a high computational burden due to a large number of TDSs and SMCS involved. Simulation has been conducted to show the effect of the two proposed accelerating method. Both methods show a decent speed-up effect.

Chapter 7

IMPACT OF HIGH WIND POWER PENETRATION ON INTEGRATED SYSTEM

RELIABILITY

With the changing resource mix, the frequency and voltage support that were pri-
marily provided by nuclear and coal-fired generators are reducing. The frequency and
voltage support are known to be crucial parts of essential reliability services (ERSs), and
their reduction could have a significant impact on system reliability. Concerns have been
raised, however, that the existing studies mainly treat the assessment of the frequency or
voltage support individually and do not incorporate these assessments in the long-term re-
liability evaluation. A systematic analysis addressing the impact of the changing ERSs on
system reliability is still missing. Besides, while inverter-based resources with advanced
controls can provide ERSs such as frequency and voltage support, the effect on long-term
reliability needs to be examined.

The integrated reliability evaluation approach proposed in this work provides a
means to incorporate the assessment of ERSs in the reliability evaluation process. The fre-
quency control and voltage control can be evaluated in detail in the TDSs, where the
frequency and voltage controls and associated protection systems are modeled. From the
TDSs, the impact of the ERSs can be quantified by load curtailment and generator tripping
from protection actions to maintain system stability after contingencies. Moreover, the ef-
fect of increasing wind power penetration on system reliability and the effect of WTGs
providing frequency and voltage support can be evaluated using this approach. The results
are illustrated in this chapter. To study the impact of increasing wind power penetration on

system reliability, scenarios with different levels of wind power penetration in the test system that is described in chapter 4 are developed. The scenario development procedure is illustrated in this chapter.

7.1   High Wind Power Penetration Scenarios Development

To study the impact of incremental wind power penetration on system reliability, four scenarios with gradually increasing wind power penetration levels are derived from the base case scenario. The base case scenario is modified based on the base case of the test system that was described in chapter 4. The objective of the modification is to represent a power plant with several smaller generation units so that the convergence of power flow solutions in high wind power penetration cases can be obtained. The modification is shown in the power flow solution table in Appendix C. In this base case scenario, there is a peak demand of 14463 MW and a wind power generation of 1680 MW, making it a 10% wind power penetration of the system load. For the convenience of description, this base case scenario is labeled as scenario #1. The four scenarios with incremental wind power penetration are labeled as scenario #2, scenario #3, scenario #4, and scenario #5, with around 20%, 40%, 60%, and 80% wind power penetration, respectively at peak load with the WTGs operating at maximum output.

In the power flow cases, either a WTG or a synchronous generator can be modeled as a conventional source with specified active power and reactive power, and a bus voltage to regulate. Although a wind plant typically consists of a number of WTGs and a collector system, it is reasonable to approximate a wind plant with a single WTG. This simplification

is known as the aggregate WTG model. In developing the power flow cases with incre-mental wind power penetration, the capacity of the synchronous generators should be de-committed with the wind power capacity in the system is increased. And generation needs to be re-dispatched according to wind power output. The strategy used here is the '2/3 decommitment, 1/3 redispatch' approach [88]. Following the strategy, every additional 3 MW of wind power generation, there is a 2 MW reduction in synchronous generator unit commitment and a 1 MW reduction in the synchronous generator unit dispatch. As an ex-ample, assume that 500 MW of wind production with a rating of 750 MVA needs to be accommodated in a system that has 1500 MW synchronous generation with a rating of 1800 MVA. 333 MVA of the synchronous generation needs to be de-committed. The sys-tem will have 750 MVA rated wind generation with 500 MW output, and 1000 MW output and a rating of 1467 MVA from synchronous generation. After determining the output and rating of WTGs and conventional generators, the rating of all transformers needs to be adjusted accordingly.

The four power flow scenarios are developed based on this rule to study the impact of high wind power penetration on system reliability. It is worthwhile to note that, in high wind power penetration cases, such as scenario #5 with 80% wind power penetration, the power flow case needs to be further adjusted to ensure the convergence of power flow solution such as the tuning on the output of static VAR compensators in the system. The developed power flow scenarios, as well as the base power flow scenario #1, are summa-rized in Table 7.1. Detailed power flow solutions of each scenario are provided in Appendix B.

113

The procedure for reliability evaluation of the system with a certain level of wind power penetration is depicted in Figure 7.1.
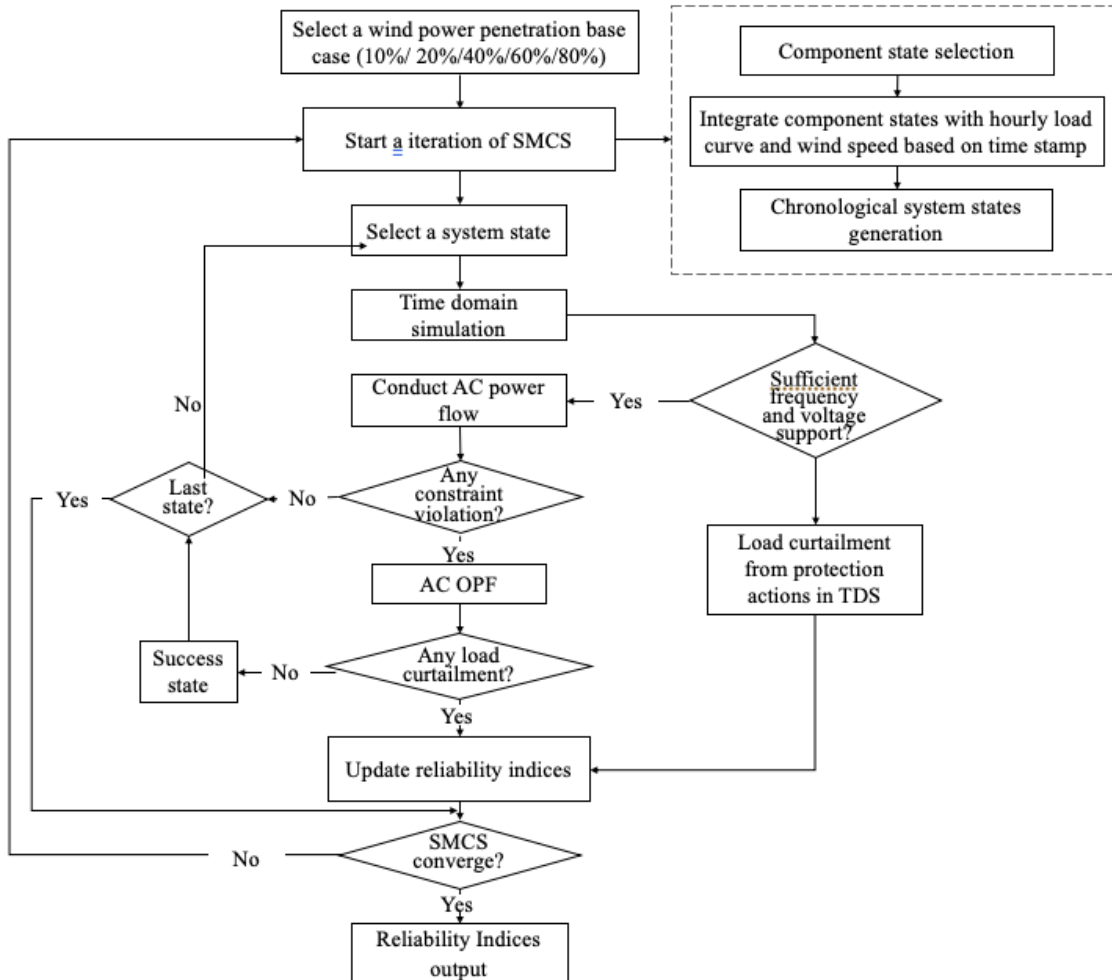
Figure 7.1 Flow Chart for Reliability Evaluation Including ERSs Assessment

To conduct the reliability assessment, one of the five scenarios listed in Table 7.1 is selected as the base case, so that system operating conditions are generated incorporating components status, load level and wind speed sampled from the SMCS. As shown in Figure

7.1, the frequency support and voltage support capability of the system is evaluated in the TDS and incorporated in the process of reliability evaluation.

Table 7.1 Scenarios with Increasing Wind Power Penetration

Scenario	Wind turbine generators	Synchronous generators	Load (MW)	Wind power penetration (%)
	Output (MW)/ Rating (MVA)	Output (MW)/ Rating (MVA)		
# 1	1680/ 1871	12956/ 19900	14463.7	11.4
# 2	3360/ 3742	11265/ 18700	14463.7	22.9
# 3	6720/ 7481	7891.1/ 16500	14463.7	45.9
# 4	10080/ 11223	4638.9/ 14400	14463.7	68.4
# 5	13440/ 14962	1398.7/ 14900	14463.7	90.5

Innovative indices to measure system dynamic behavior from the aspects of frequency support and voltage support capabilities to maintain system frequency and voltage stability are proposed in this work. The proposed indices are given as follows:

1) *UFOC* represents the expected number of under-frequency load shedding actions. It can be calculated using (7.1):

$$UFOC = \frac{1}{N_y}\sum_{i=1}^{N_y}\sum_{j=1}^{N_j} UFLS(x_{ij}) \qquad (7.1)$$

2) *UFENS* represents the expected power not supplied after under-frequency load shedding actions. It can be calculated using (7.2):

$$UFENS = \frac{1}{N_y}\sum_{i=1}^{N_y}\sum_{j=1}^{N_j} P_{UFLS,ij} \cdot UFLS(x_{ij}) \qquad (7.2)$$

3) *EOAF* represents the expected occurrence of abnormal frequency at generator terminals (occ./yr). It can be calculated using (7.3):

$$EOAF = \frac{1}{N_y}\sum_{i=1}^{N_y}(OOF_i + OUF_i) \qquad (7.3)$$

4) *EGAF* represents the expected generator tripping caused by abnormal frequency (MW). It can be calculated as (7.4):

$$EGAF = \frac{1}{N_y}\sum_{i=1}^{N_y}\left[(1/T_i)\sum_{j=1}^{N_j}(P_{trip\_OF,ij} \cdot \tau_{ij} + P_{trip\_UF,ij} \cdot \tau_{ij})\right] \qquad (7.4)$$

5) *EOAV* represents the expected occurrence of abnormal voltage at generator terminals (occ./yr). It can be calculated using (7.5):

$$EOAV = \frac{1}{N_y}\sum_{i=1}^{N_y}(OOV_i + OUV_i) \qquad (7.5)$$

6) *EGAV* represents the expected generator tripping caused by abnormal voltage (MW). It can be calculated as (7.6):

$$EGAV = \frac{1}{N_y} \sum_{i=1}^{N_y} \left[(1/T_i) \sum_{j=1}^{N_j} (P_{trip\_OV,ij} \cdot \tau_{ij} + P_{trip\_UV,ij} \cdot \tau_{ij}) \right] \qquad (7.6)$$

where, N_y is the number of simulation years in the SMCS, i is the index of simulation year of the SMCS, T_i is the summation of the duration of states in simulation year i, N_j is the number of states in a simulation year, x_{ij} is system state j in the simulation year i, τ_{ij} is the duration time of state x_{ij}, $UFLS(x_{ij})$ is 1 if there is under-frequency load shedding relay action in state x_{ij}, otherwise $UFLS(x_{ij})$ is 0, $P_{UFLS,ij}$ is the MW value of load shedding triggered by under-frequency load shedding relay in state x_{ij}, OOF_i and OUF_i are the number of occurrence of over-frequency generator tripping actions and under-frequency generator tripping actions in simulation year i, OOV_i and OUV_i are the number of occurrence of over-voltage and under-voltage generator tripping actions in simulation year i, $P_{trip\_OF,ij}$ and $P_{trip\_UF,ij}$ are the MW value of generation trip results from over-frequency and under-frequency protection, and $P_{trip\_OV,ij}$ and $P_{trip\_UV,ij}$ is the MW value of generation trip results from over-voltage and under-voltage protection.

7.2   Impact of Increasing Wind Power Penetration on System Reliability

The approach proposed in this work provides a framework to include the ERSs assessment in reliability evaluation. Using this approach, ERSs can be included in the reliability indices calculation. Two evaluations, based on the power flow scenario #1, have been conducted to illustrate the effect of considering the ERSs in reliability evaluation. The

first evaluation considers only adequacy assessment and finds a *LOLP* index around 0.0013 and an *EPNS* index around 0.0085 MW. The second reliability evaluation considers both ERSs assessment and adequacy assessment. The results from the second evaluation are given in Table 7.2. In both these evaluations, the WTGs are set to not provide frequency and voltage support.

Table 7.2 Reliability Indices with ERSs Assessment Considered

LOLP	EPNS (MW)	UFOC	UFENS
0.0829	70.9181	57.9825	70.8614
EOAF	EGAF (MW)	EOAV	EGAV (MW)
0.1228	0.2414	0.9298	1.0551

Table 7.2 shows that when the evaluation considers the ERS assessment in conjunction with adequacy assessment, the total system *LOLP* increases from 0.0013 to 0.0829, and *EPNS* increases from 0.0085 MW to 70.9181 MW. The significant increase of the reliability indices shows that the system reliability level is worse if the sufficiency of ERSs is also evaluated. The under-frequency load shedding related indices *UFOC* and *UFENS* are 57.9825 MW and 70.8614 MW, respectively, whereas the generator frequency and voltage protection related indices *EOAF*, *EGAF*, *EOAV*, and *EGAV* are 0.1228, 0.2414 MW, 0.9298 and 1.0551 MW respectively. The indices related to under-frequency load shedding are much higher than the indices that relate to generator protection. The results demonstrate that the insufficiency of frequency support is the main reason for the system unreliability.

The above results illustrate the efficacy of using the integrated reliability evaluation approach to consider ERSs assessment in conjunction with adequacy assessment. Further simulations are conducted to study the impact of increasing wind power penetration on system reliability using the proposed approach. Representing the increasing wind penetration, scenarios #2 – scenario #5 in Table 7.1 are used as the base case in the simulation independently to evaluate system reliability with 20%, 40%, 60%, and 80% wind penetration levels. All simulations are conducted with ERSs assessment considered while WTGs do not participate in the frequency and voltage regulation. The reliability indices of the test system under the five scenarios are summarized in Table 7.3.

Table 7.3 Reliability Indices with ERSs Assessment (WTGs Not Providing ERSs)

Scenario	LOLP	EPNS (MW)	UFOC	UFENS
# 1	0.0829	70.9181	57.9825	70.8614
# 2	0.0941	80.0636	67.4667	79.9666
# 3	0.1110	102.2281	97.6552	101.7636
# 4	0.1578	149.2959	144.1923	149.0271
# 5	0.2023	200.7808	207	200.5203
Scenario	EOAF	EGAF (MW)	EOAV	EGAV (MW)
# 1	0.1228	0.2414	0.9298	1.0551
# 2	0	0.0134	0.1556	0.1693
# 3	0.0345	0.0113	0	0
# 4	0.0385	0.1149	0.0385	9.3462
# 5	8.8000	13.8817	7.4667	3.9480

It can be observed that, when wind power penetration level increases, the system reliability gradually deteriorates. For instance, the *LOLP* is 0.0829 when wind power penetration is 10%, then the index increases to 0.0941, 0.1110, 0.1578 and 0.2023 at 20%, 40%, 60% and 80% wind penetration level respectively. System reliability is greatly impacted at high wind power penetration scenarios. The results also show that the generator protection related indices *EOAF*, *EGAF*, *EOAV*, *EGAV* are relatively smaller compared to *UFOC* and *UFENS*. This behavior indicates that for the test system, the low frequency support is the dominant cause of the deteriorating reliability at high wind penetration conditions. Results show that the voltage related reliability support is sufficient in the test system, partly because constant impedance load models are used in the simulations. The frequency-related indices provide important information on system reliability.

The convergence trajectories of the reliability index *LOLP* in the evaluation of the test system with different levels of wind power penetration are as shown in Figure 7.2 - Figure 7.6. When the evaluation is based on the scenario with 10%, 20%, 40%, 60%, and 80% wind power penetration, the SMCS takes 56, 44, 28, 25, 16 iterations of simulation to reach the convergence. The reason for the decreasing simulation iterations needed for SMCS to converge is that more cases are evaluated to be unreliable with the increasing of wind power penetration. The values of indices increase, and the number of iterations is inversely proportional to the index being calculated.

The decline in frequency support with increasing wind power penetration, as observed from Table 7.3, was expected. Since in all the simulations, WTGs are not enabled with frequency and voltage control, these generators do not participate in system control.

Synchronous generators solely contribute to the frequency support in the system; hence, the frequency support is reduced with the decommitment of synchronous generators. The decommitment of synchronous generators leads to the decline in system inertia, which is important to maintain frequency stability after sudden disturbances.
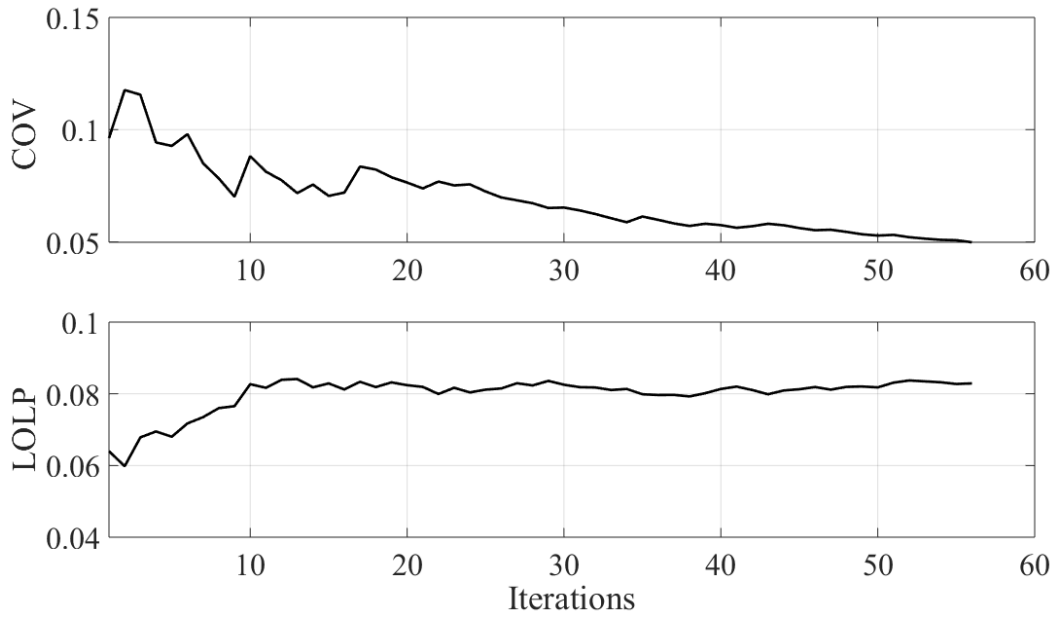
Figure 7.2 Convergence of *LOLP* in the Evaluation on System with 10% Wind Power Penetration
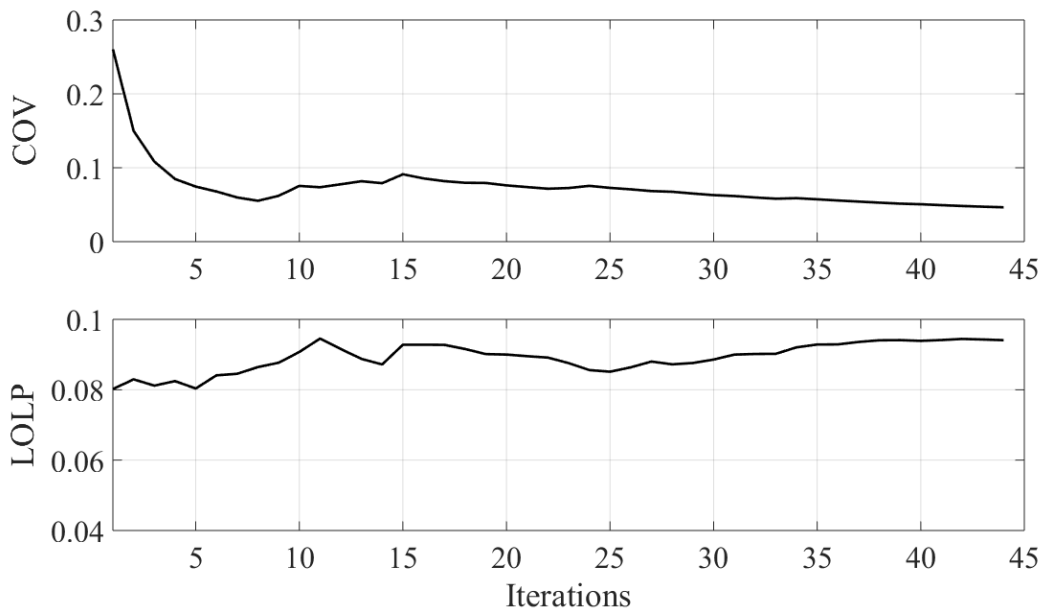
Figure 7.3 Convergence of *LOLP* in the Evaluation on System with 20% Wind Power Penetration
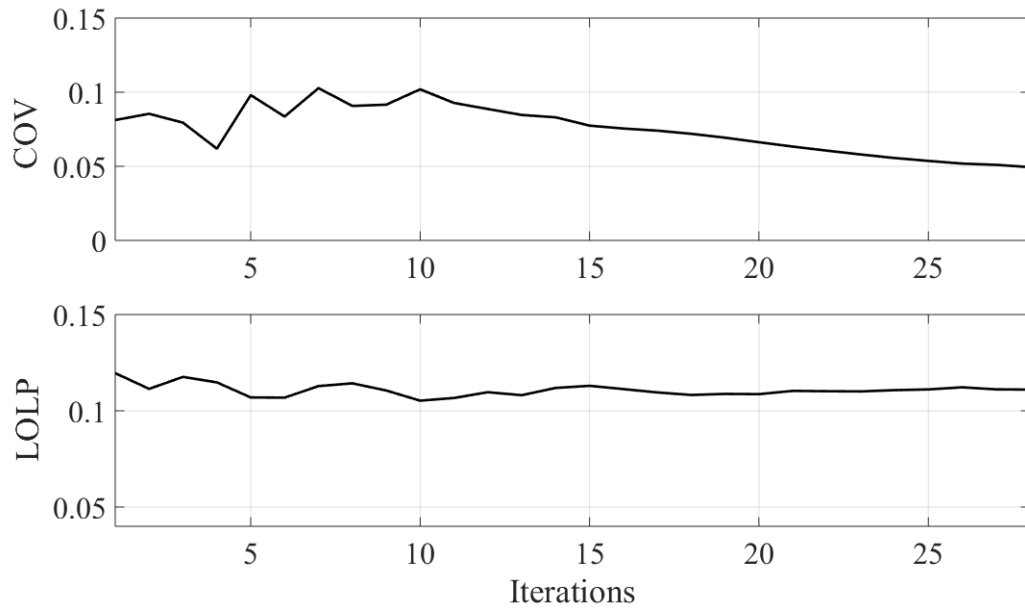
Figure 7.4 Convergence of *LOLP* in the Evaluation on System with 40% Wind Power Penetration
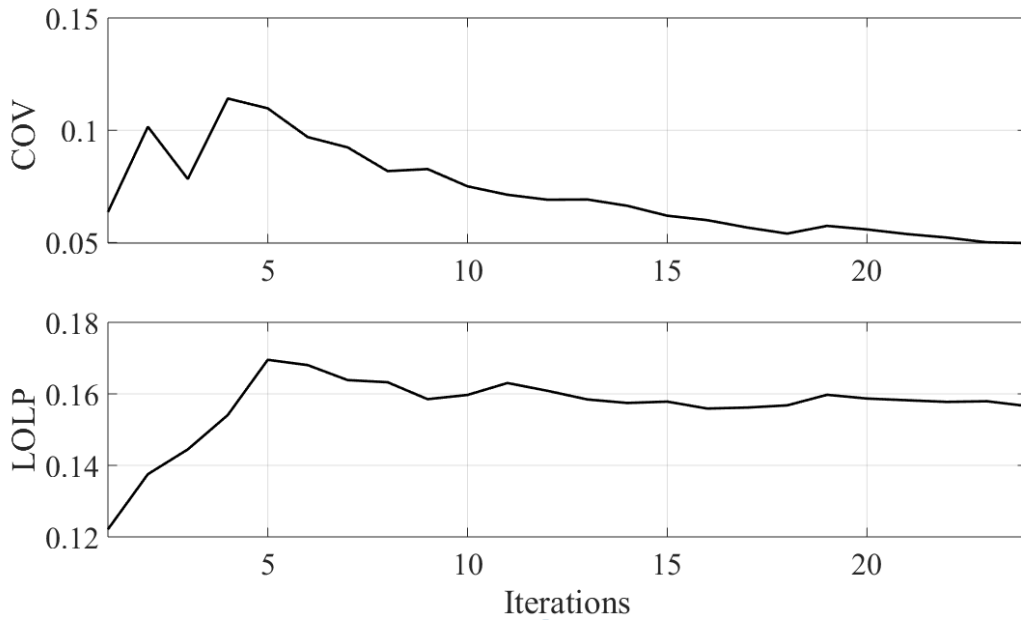
Figure 7.5 Convergence of *LOLP* in the Evaluation on System with 60% Wind Power Penetration
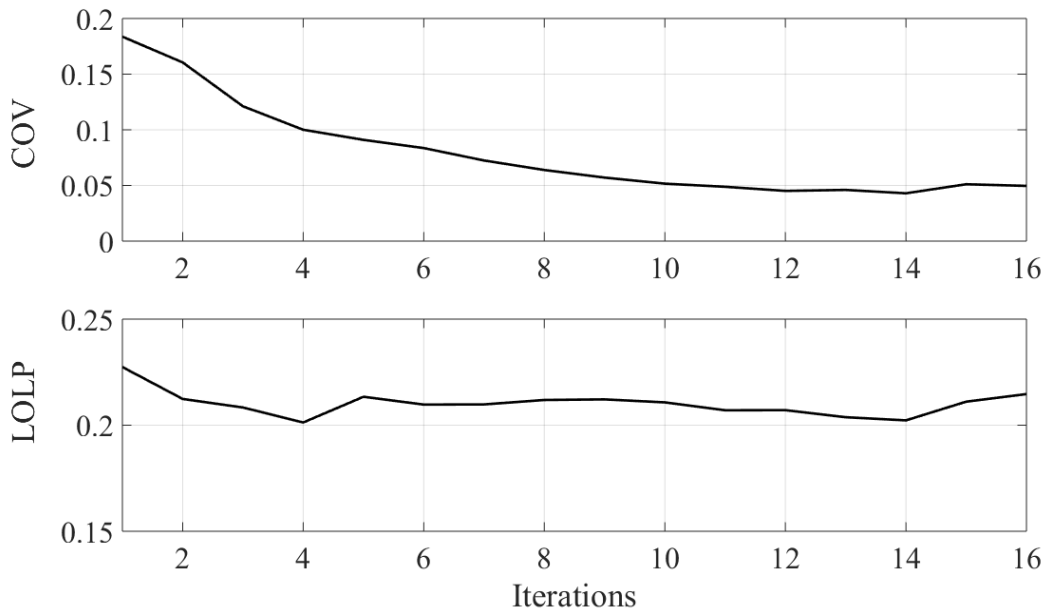
Figure 7.6 Convergence of *LOLP* in the Evaluation on System with 80% Wind Power Penetration

Figure 7.7 shows the trends of *LOLP* and the average system inertia versus the wind power penetration level. The average system inertia is the mean value of system inertia of system states sampled from SMCS in the evaluation. It can be observed that the average system inertia declines with the increasing wind power penetration level. The decline in system inertia causes the deterioration of the frequency support in the system as less inertia leads to faster frequency decrease. The frequency of three selected buses during a loss of generation contingency with different wind power penetration is shown in Figure 7.8 - Figure 7.13. The pre-contingency system operating conditions and the contingency information is given in Table 7.4. In the five scenarios, system loads are the same with different wind power output; hence, the conventional generator output varies accordingly. The five pre-contingency conditions have 10%, 20%, 40%, 60% and 80% instantaneous wind penetration. The contingency is the same in five scenarios, which is a 1024.4 MW generation loss.
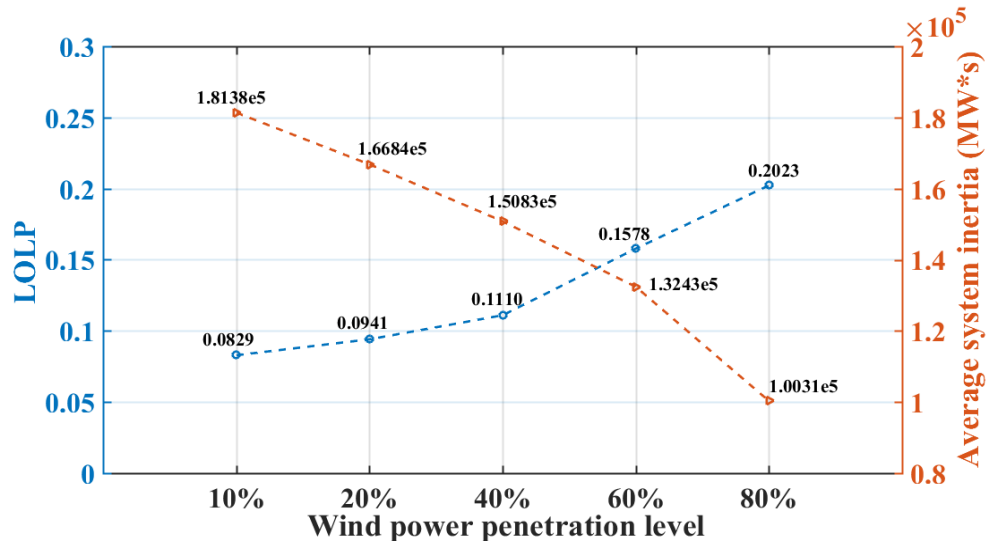
Figure 7.7 *LOLP* Index and Average System Inertia Change with Wind Penetration
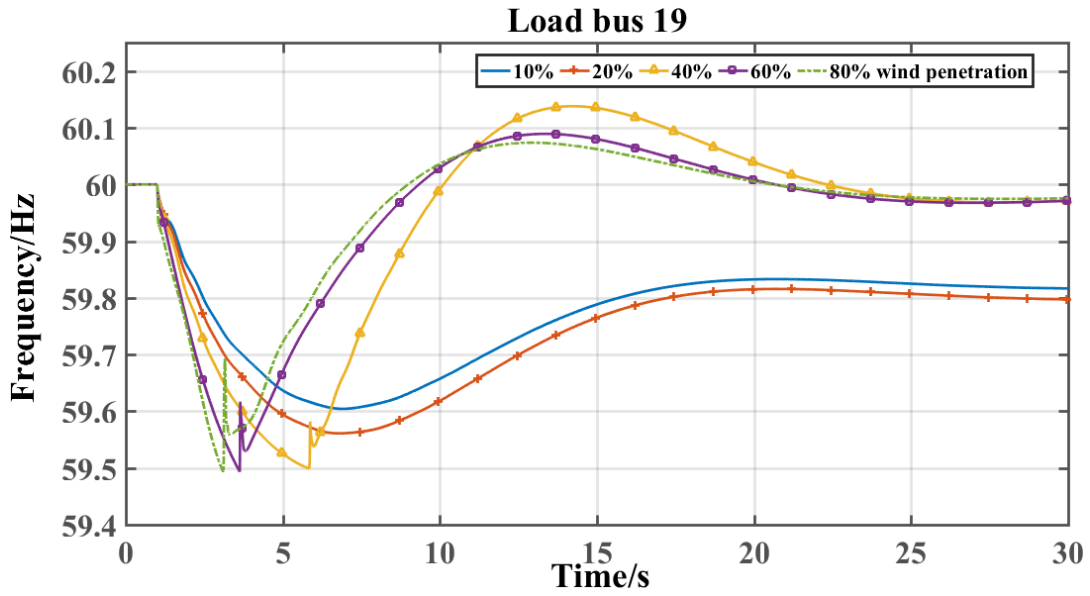
Figure 7.8 Frequency of Load Bus 19 After Loss of Generation
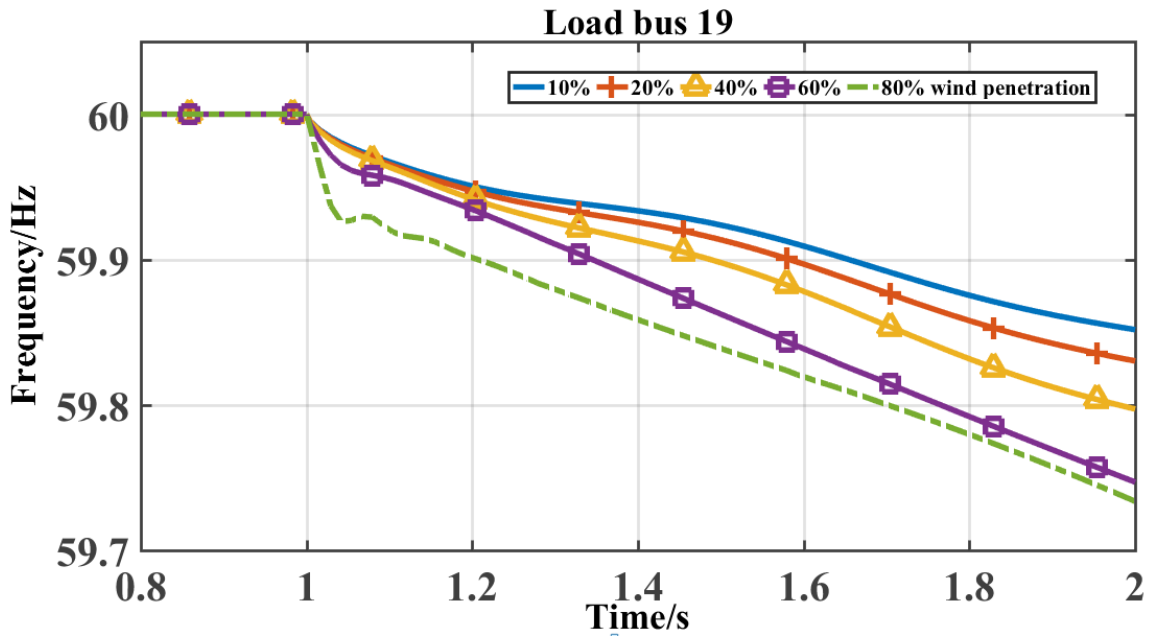
Figure 7.9 Frequency of Load Bus 19 After Loss of Generation (Zoom-in)
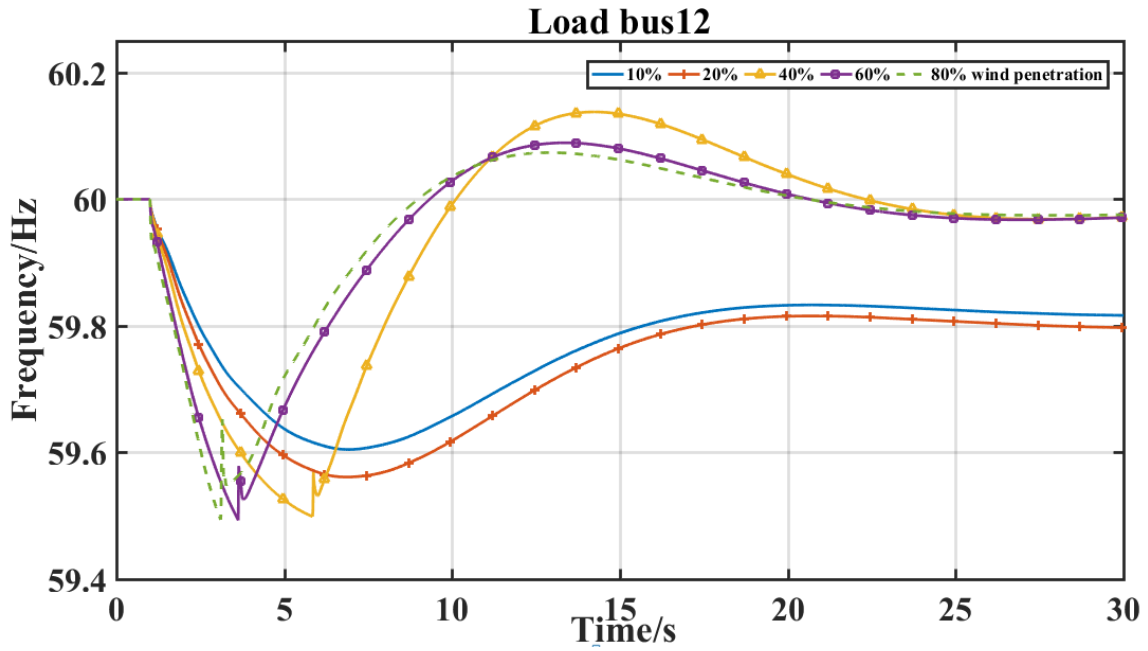
Figure 7.10 Frequency of Load Bus 12 After Loss of Generation
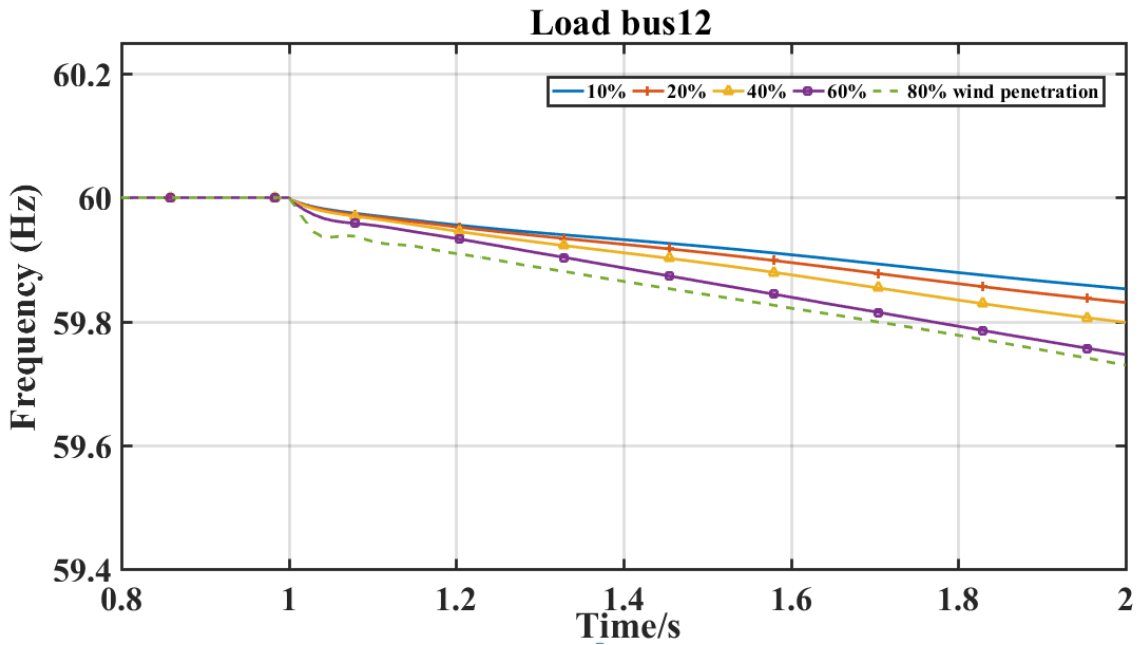
Figure 7.11 Frequency of Load Bus 12 After Loss of Generation (Zoom-in)
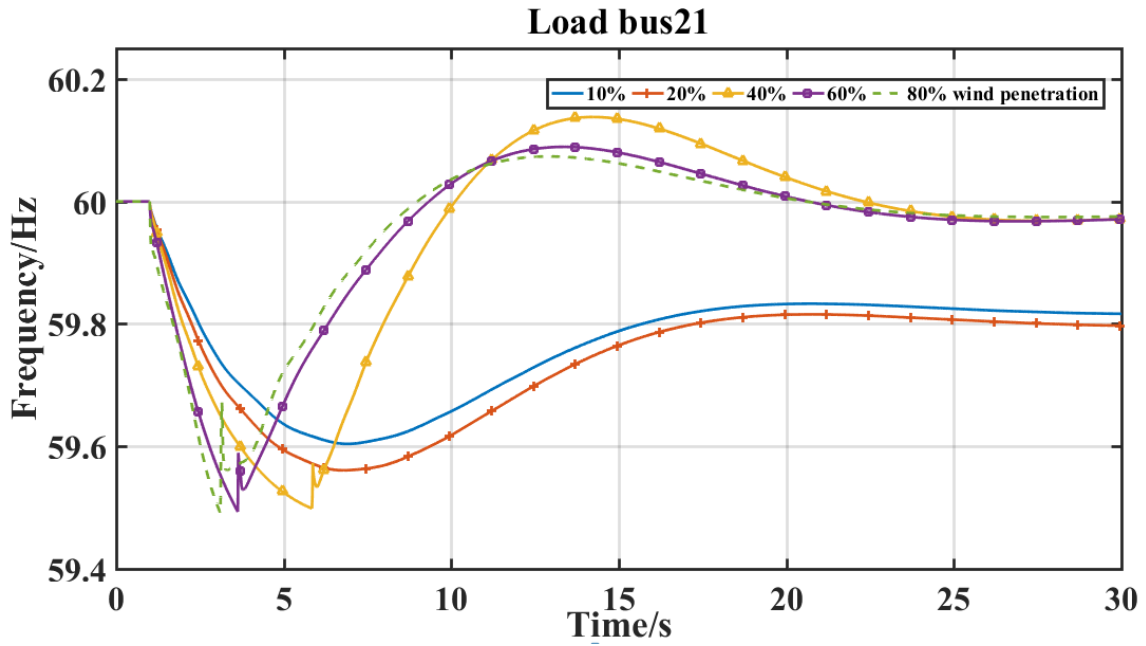
Figure 7.12 Frequency of Load Bus 21 After Loss of Generation
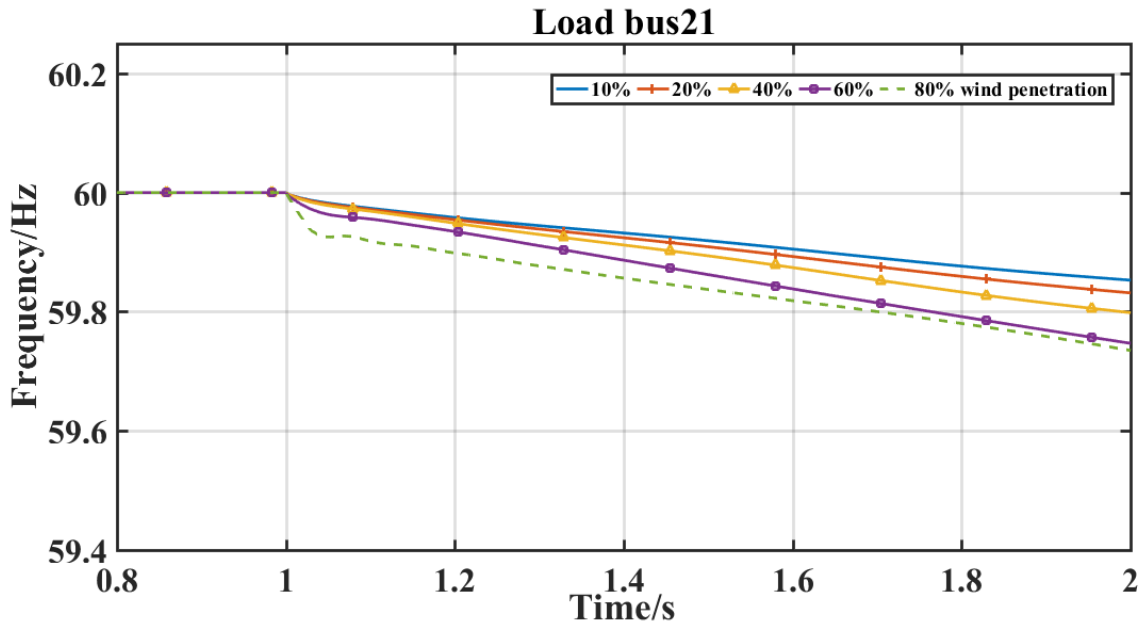
Figure 7.13 Frequency of Load Bus 21 After Loss of Generation (Zoom-in)

127

Table 7.4 Pre-contingency Condition and Fault Setting

Instantaneous wind penetration	Wind generation (MW)	Synchronous generation (MW)	Total load (MW)	Loss of generation (MW)
10.1%	1093.5	9713.4	10712.6	1024.4
20.2%	2187.5	8612.6	10712.6	1024.4
40.5%	4374.5	6409.4	10712.6	1024.4
60.5%	6562	4269.4	10712.6	1024.4
80.3%	8752.5	2142.2	10712.6	1024.4

Consider the frequency of load bus 19 as an example. Simulations show that with 10% and 20% wind power penetration in pre-contingency conditions, the system experiences a frequency decline to 59.62 Hz and 59.56 Hz, respectively. The frequency then gradually recovers to 59.82 Hz and 59.80 Hz, respectively. There is no load curtailment in the two simulations. By contrast, if the same contingency is conducted on the same system with 40%, 60%, and 80% wind power penetration in the pre-contingency conditions, the frequency decreases more severely and triggers the under-frequency load shedding protections. The load shed occurred at 5.842s, 3.629s, and 3.104s, respectively. The frequency in the three simulations settled at 59.98 Hz. The initial rate of change of frequency (ROCOF) of the five simulations is around 0.15 Hz/s, 0.17 Hz/s, 0.2 Hz/s, 0.25 Hz/s, and 0.26 Hz/s correspondingly. The simulations confirmed that system frequency support capability decreases with the growing wind power penetration in the system. While the traditional reliability evaluations of the five cases without considering the ERSs assessment showed

the system is reliable after the loss of generation, the simulations demonstrate the value of considering the ERSs in the reliability evaluation process.

For this test system, the frequency at different buses are very similar, the frequency at all load buses goes as low as 59.5 Hz and under-frequency load shedding protection at all buses are activated. However, it can be observed that the frequency rises after the load shedding protection tripped at load bus 19 and bus 12 are different. The reason is that load bus 19 has heavier load which is around 3000 MW of load while bus 12 has only around 300 MW of load.

7.3 Impact of WTGs Providing Essential Reliabilty Services on System Reliability

Since most modern WTGs are equipped with frequency and voltage control functions to participate in frequency and voltage regulation, it is necessary to include these ERSs capabilities of WTGs in the reliability evaluation. To evaluate the effects, reliability evaluations are conducted to the test system under the same five wind penetration level scenarios, as given in Table 7.1. In the simulations, the frequency and voltage control functions of WTGs are enabled to allow the WTGs providing ERSs. The reliability indices are given in Table 7.5. The convergence trajectories of the reliability index *LOLP* in the evaluation of the test system considering WTGs providing ERSs are as shown in Figure 7.14 - Figure 7.18. The comparison of reliability indices from the evaluation process with and without WTGs providing the ERSs are shown in Figure 7.19.

Table 7.5 Reliability Indices with ERSs Assessment (WTGs Providing ERSs)

Scenario	LOLP	EPNS (MW)	UFOC	UFENS
# 1	0.0629	53.1593	49.7258	53.1169
# 2	0.0585	48.2155	51.5588	48.1589
# 3	0.0681	60.2351	71.4179	59.9616
# 4	0.0886	83.6518	104.4884	83.5219
# 5	0.1109	114.7830	143.8636	114.6268
Scenario	EOAF	EGAF (MW)	EOAV	EGAV (MW)
# 1	0.2097	0.2324	0.9839	1.2059
# 2	0	0.0179	0.2941	0.2299
# 3	0	0	0	0
# 4	0.2791	0.1942	12.0465	5.7316
# 5	7.7727	10.2299	10.5227	5.9157
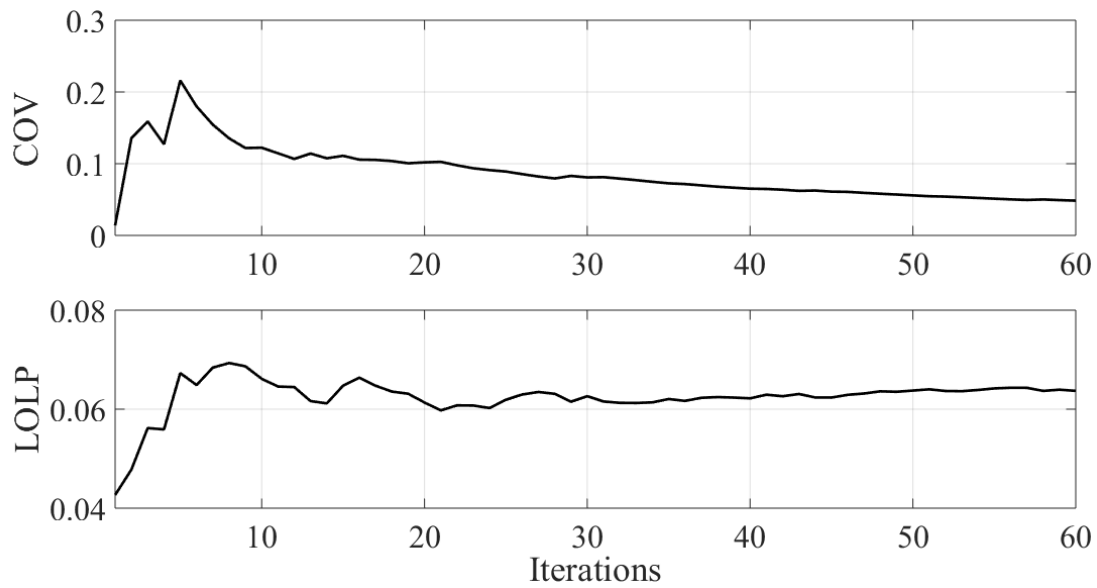
Figure 7.14 Convergence of *LOLP* in the Evaluation on System with 10% Wind Power Penetration (WTGs Providing ERSs)
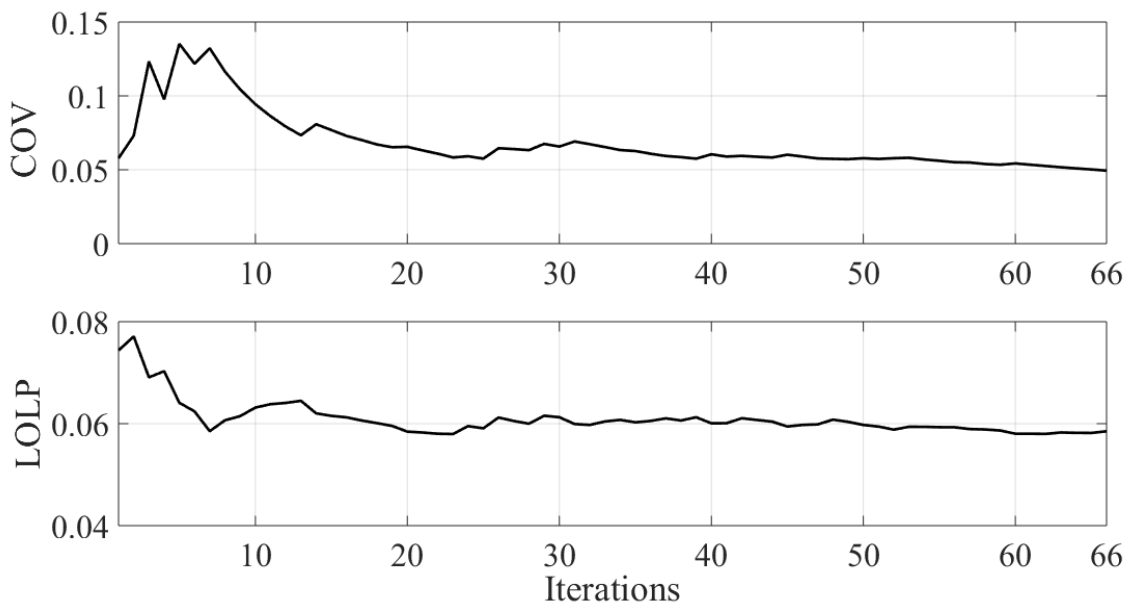
Figure 7.15 Convergence of *LOLP* in the Evaluation on System with 20% Wind Power Penetration (WTGs Providing ERSs)
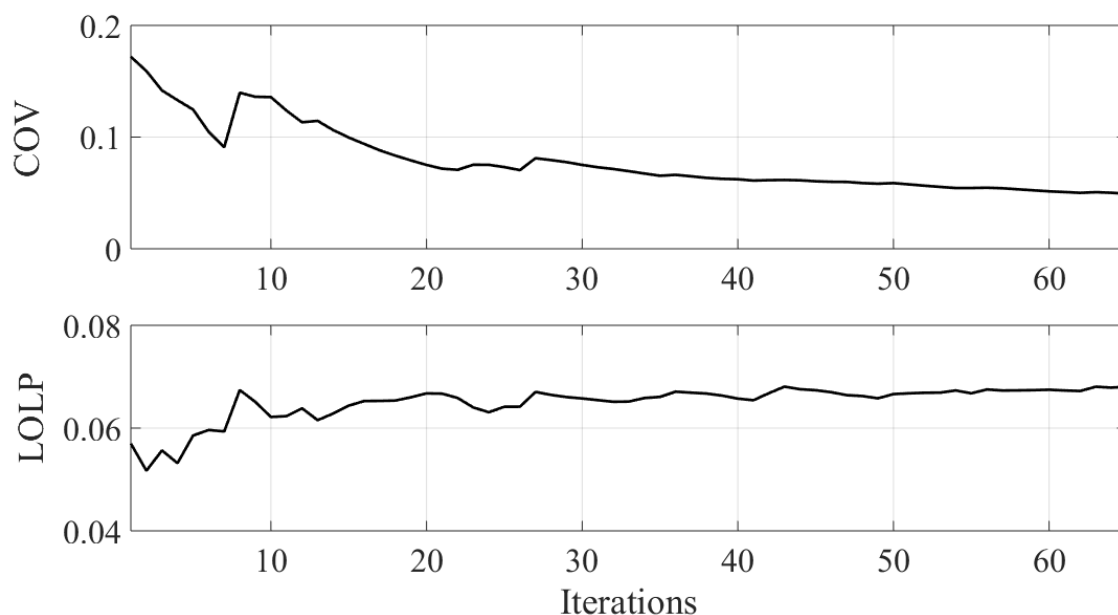
Figure 7.16 Convergence of *LOLP* in the Evaluation on System with 40% Wind Power Penetration (WTGs Providing ERSs)
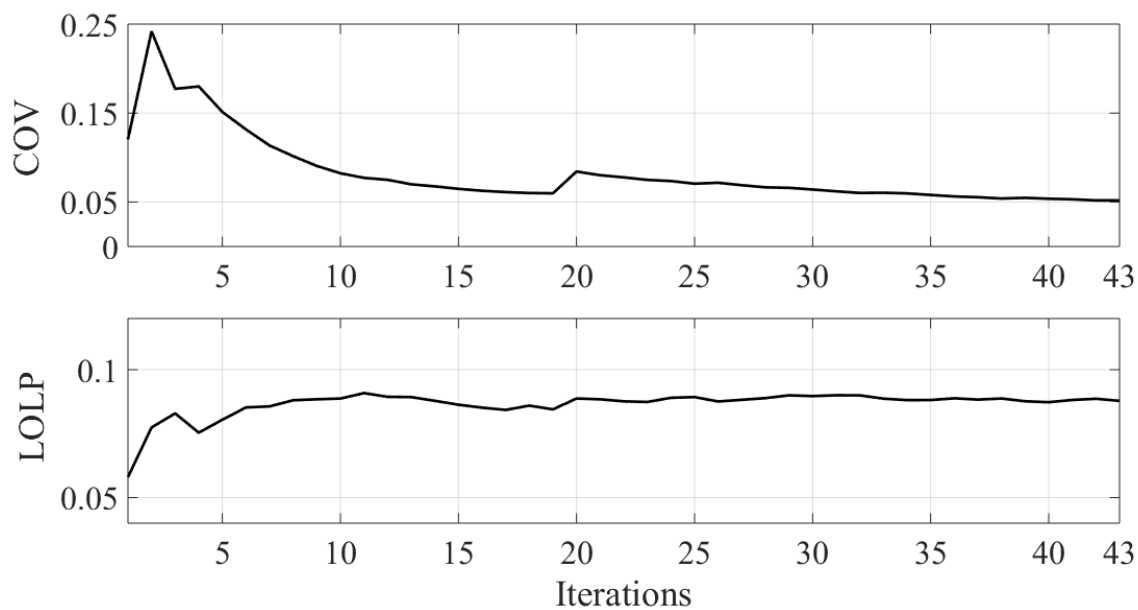
Figure 7.17 Convergence of *LOLP* in the Evaluation on System with 60% Wind Power Penetration (WTGs Providing ERSs)
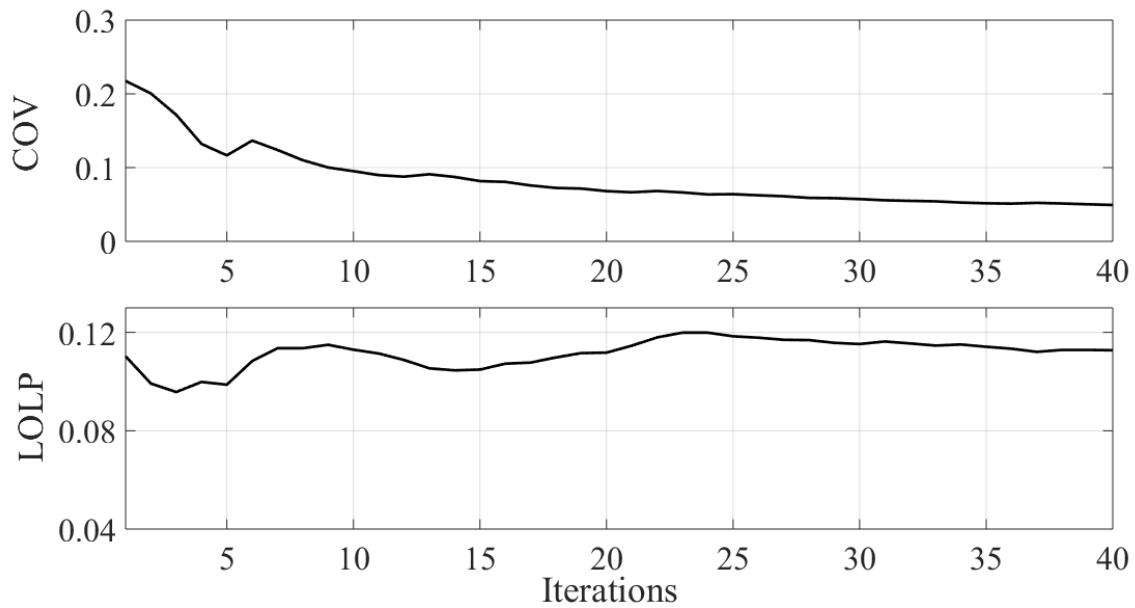
Figure 7.18 Convergence of *LOLP* in the Evaluation on System with 80% Wind Power Penetration (WTGs Providing ERSs)
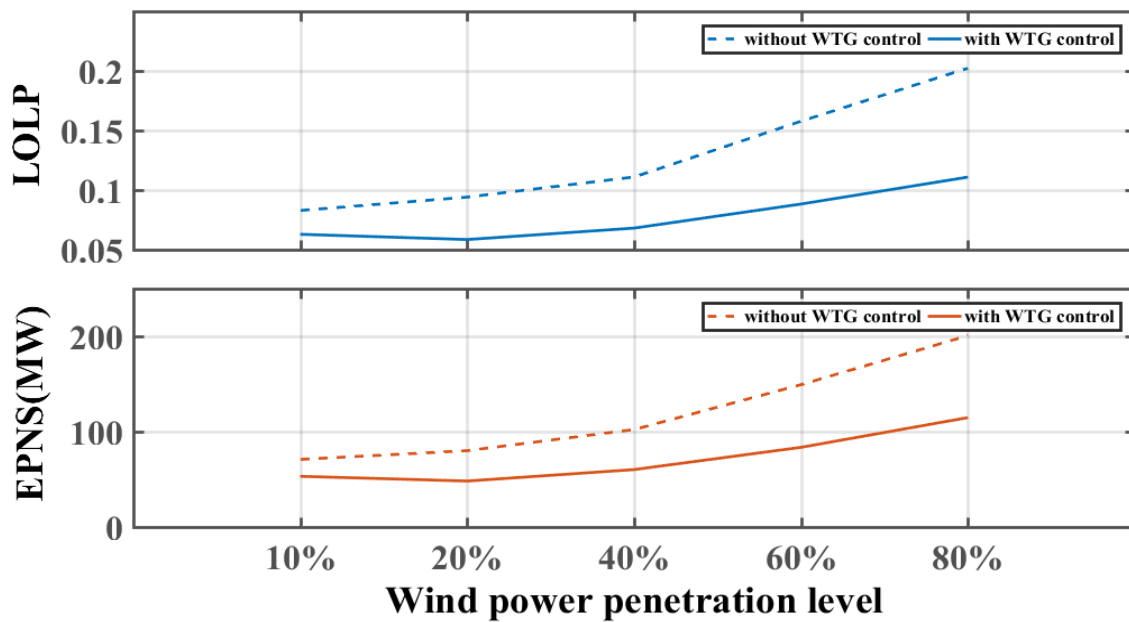
Figure 7.19 LOLP and EPNS Results Comparison of WTGs With/Without ERSs

It can be observed that whether WTGs provide ERSs or not, the system reliability indices rise when wind power penetration increases. However, the comparison shows that, with the same level of wind power penetration, when WTGs provide ERSs, system reliability is improved compared to when WTGs do not provide ERSs. Additionally, the reliability improvement is more significant when wind power penetration in the system is higher.

The case studies with WTGs providing ERSs are conducted based on the same pre-contingency system operating conditions and the loss of generation contingency that is provided in Table 7.4. The frequency of load bus 19 from the case studies is shown in Figure 7.20. It is observed that these plots are different from the results shown in Figure 7.8, where under-frequency load shedding was triggered in the 40%, 60%, 80% wind power penetration scenarios, no load shedding occurred in this set of simulations with all five wind power penetration levels. After the loss of generation occurred, with WTGs providing ERSs, the frequency nadirs are 59.63 Hz, 59.61 Hz, 59.61 Hz, 59.57 Hz, and 59.59 Hz respectively, for the scenarios with 10%, 20%, 40%, 60% and 80% wind power penetration. System reliability is improved when WTGs contribute to providing ERSs.
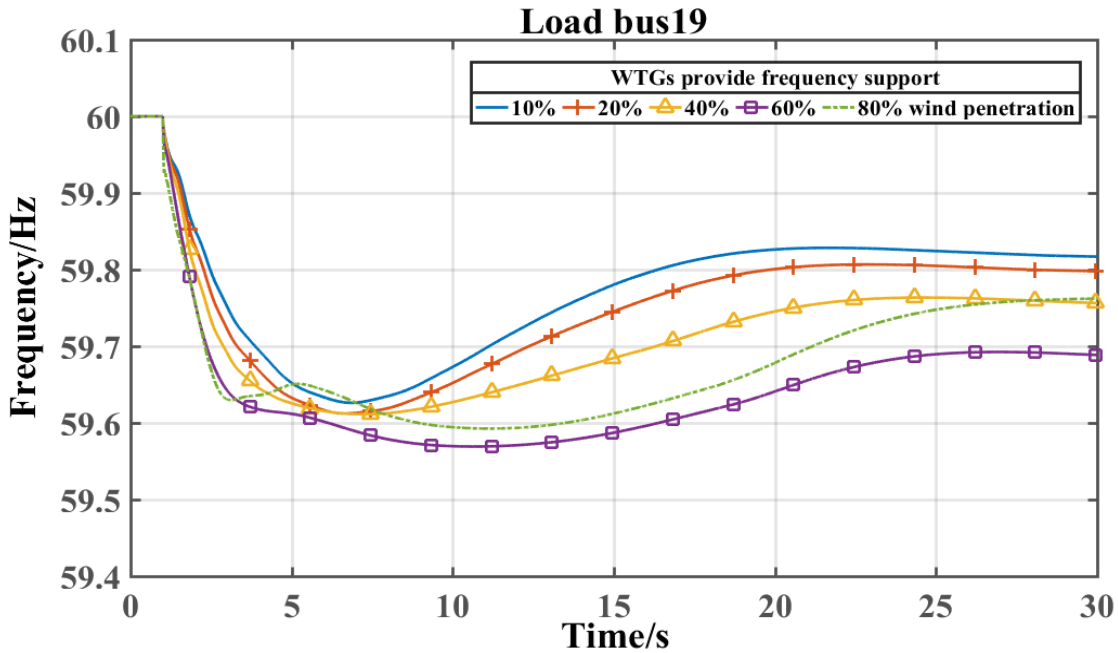
Figure 7.20 Frequency of Load Bus 19 After Loss of Generation

Figure 7.21 - Figure 7.23 show the frequency trajectories of load bus 19, load bus 12, and load bus 21 respectively. Each figure includes the frequency change under three wind power penetration, i.e., 20%, 40%, and 80%. In Figure 7.21, it can be observed that frequency behavior on load bus 19 is significantly different when WTGs are providing and not providing ERSs. The frequency improvement in the 20% penetration scenario is subtle. However, the ERSs contributed by WTGs are critical to avoid load shedding in the scenarios with 40% and 80% wind power penetration. The output of a synchronous generator and a wind farm in the 80% wind penetration scenario are shown in Figure 7.24. In response to the system frequency drop, the wind farm increased its power output. Since WTGs are interfaced with the synchronous power system via converters, they are capable of providing fast control. The increase of wind farm power output is initiated 0.5s after the contingency

occurred and lasted for about 20s. The capability is varied among different WTGs and different settings, however, the results demonstrate that this interim reliability support is crucial to guarantee reliable power supply when the ERSs provided by synchronous machines are insufficient. It is important to note that the frequency does not violate the UFLS threshold but settles at a lower than normal frequency level. Secondary frequency controls should then bring the system back to the nominal operating frequency.
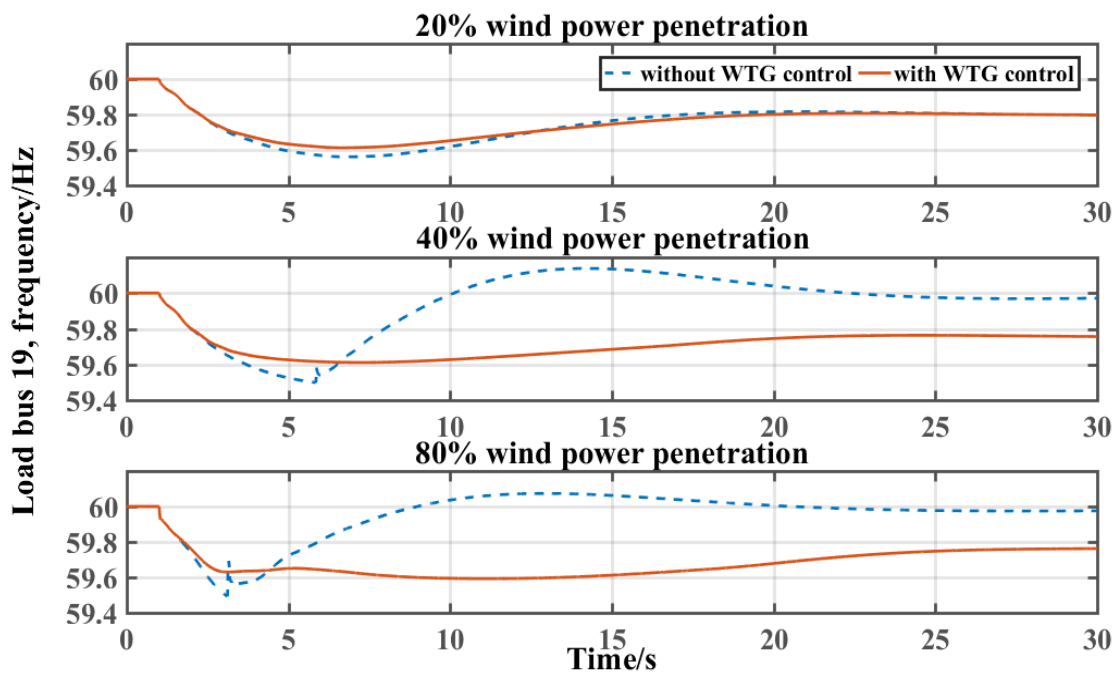
Figure 7.21 Comparion of Frequency on Bus 19 Under Different Wind Penetration
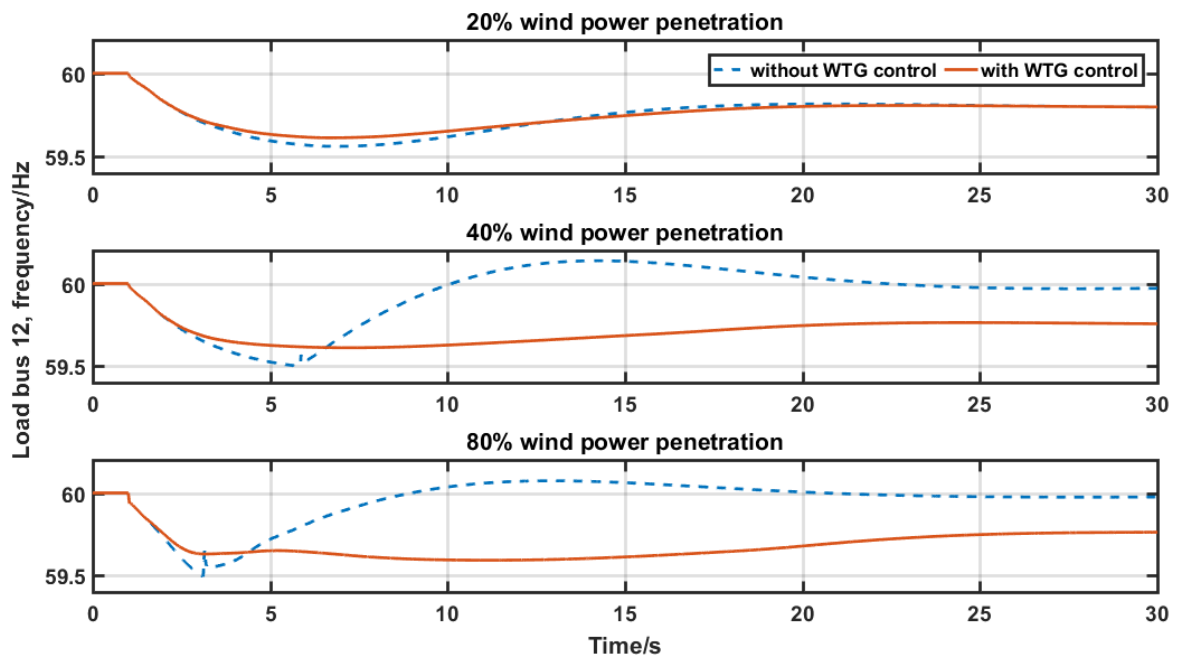
Figure 7.22 Comparion of Frequency on Bus 12 Under Different Wind Penetration
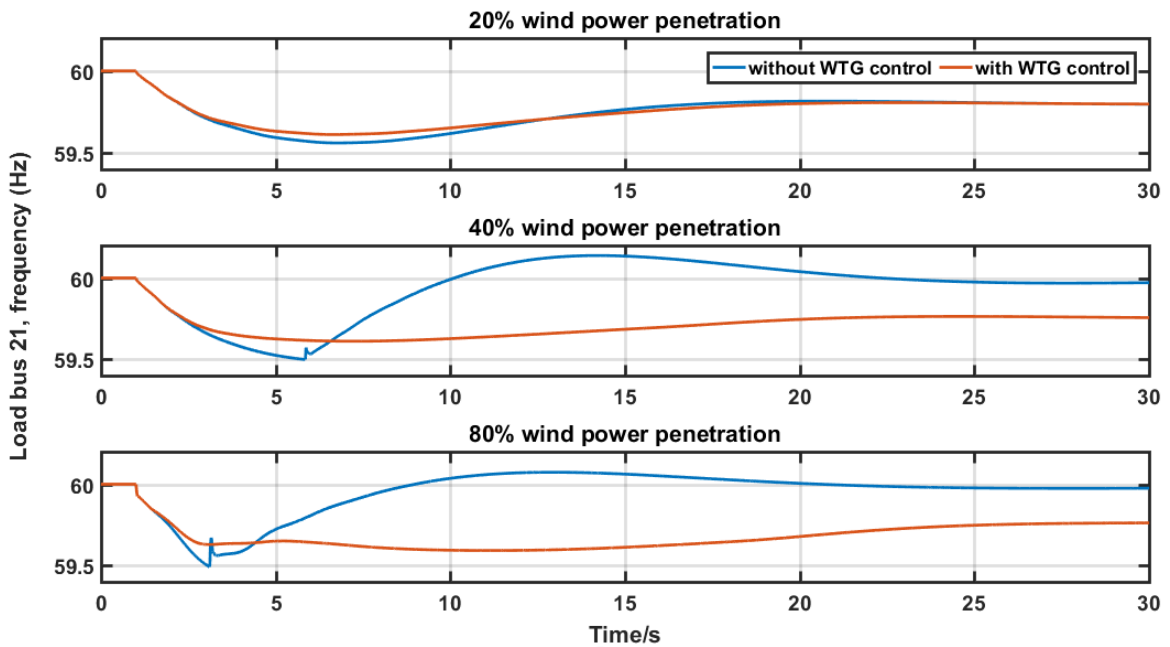
Figure 7.23 Comparion of Frequency on Bus 21 Under Different Wind Penetration
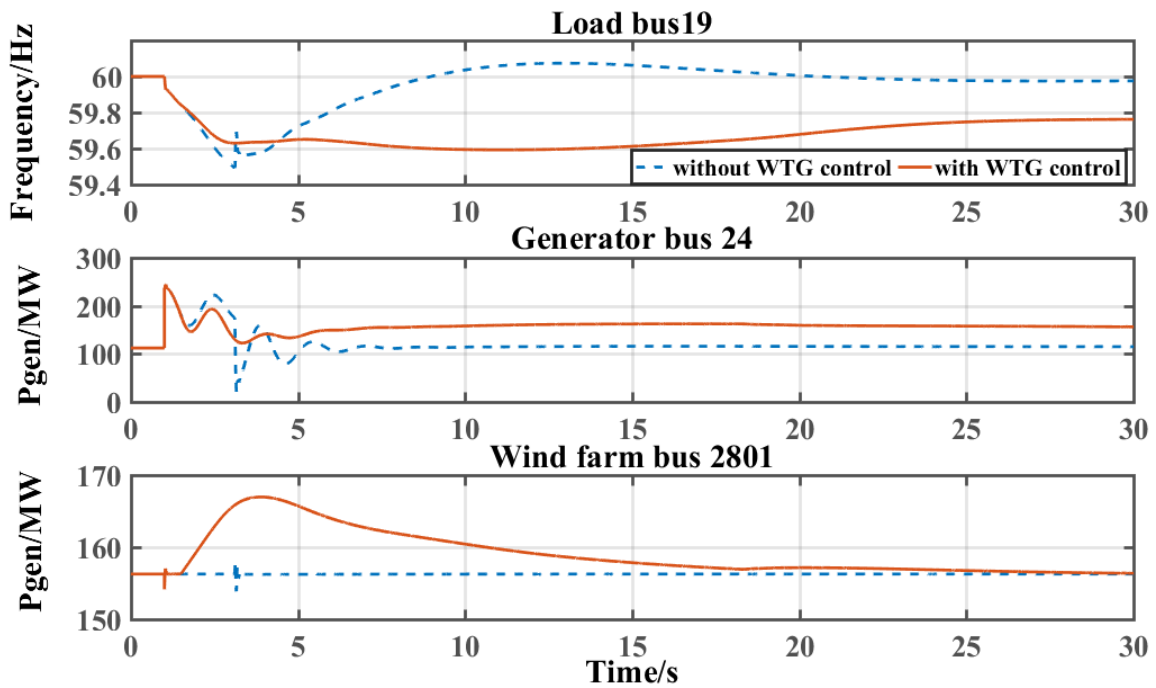
Figure 7.24 Frequeny Response of Generators Under 80% Wind Power Penetration

7.4   Summary

Using the integrated reliability evaluation approach that is proposed in this work,

the assessment of the ERSs, namely the frequency and voltage support capability, is incor-

porated in the system reliability evaluation. The frequency control and voltage control can

be evaluated in detail in the TDSs, where the frequency and voltage controls and protection

systems are modeled. From the TDSs, the impact of the inadequacy of ERSs can be quan-

tified by load curtailment and generator tripping from protection actions to maintain system

stability after contingencies. Reliability indices that represent system reliability with ERSs

capability are discussed in this chapter. The probabilistic analysis framework allows vari-

ous system operating conditions being considered in the ERSs assessment.

The reliability evaluation with the ERSs assessment incorporated is conducted on the same test system that earlier studies were conducted. The simulation results show the importance of representing the ERSs in the evaluation process to measure whether a system has sufficient frequency or voltage support, which is crucial to system reliability. The results also show that system reliability deteriorates when increasing wind power is integrated into the system if there are no additional ERSs contribution from WTGs. Simulation results demonstrate the importance of WTGs providing ERSs which improve system reliability significantly, especially when the system has high wind power penetration. Results also illustrate the necessity of the new approach to consider ERSs assessment and include the capability of WTGs providing reliability services in system reliability evaluation.

Chapter 8

CONCLUSIONS AND FUTURE RESEARCH

8.1   Conclusions

This research proposes a probabilistic reliability evaluation method with resource adequacy and DSA integrated into a single framework. Sequential MCS was used because it provides a flexible approach for considering time-variant stochastic characteristics in the system. Stochastic characteristics have been considered in this work and include components outages, different transmission fault types, chronological load variance, and stochastic wind power output. Compared to the traditional reliability evaluation, which evaluates the adequacy and dynamic security separately, the proposed method provides the reliability indices reflecting both adequacy and dynamic security based on the quantification of the two aspects of reliability in terms of load curtailments.

The quantification of the impact of dynamic security is included by the load curtailment from protection action to maintain system stability after contingencies. By including this value of load curtailment into the calculation of reliability indices, the integrated system reliability can be represented using the well-recognized reliability indices, which are *LOLP*, *EPNS*, and *LOLF*. The proposed method is tested on a synthetic test system and the results show the importance of considering the two reliability aspects together since both the steady-state and transient system performance need to be analyzed in reliability studies. Also, the computational effort in the evaluation process is significant

because of the sequential MCS and the TDS for dynamic security assessment. Two acceleration methods are introduced to lighten the computational burden. In practical applications, the computational time could be substantially reduced further by using parallel or distributed computing as the SMCS is amenable to such implementations.

The proposed integrated reliability evaluation method is further extended to incorporate the assessment of ERSs, including the frequency support and voltage support capability in the system. Simulation results show the efficiency of including the ERSs assessment in the proposed approach. The impact of increasing wind power penetration on system reliability as analyzed using the proposed approach and the decline of the reliability level in the test system has been observed with the increased wind power penetration. Also, the effect of WTGs providing the frequency and voltage support is studied. Evaluation results demonstrate the importance of WTGs providing the frequency and voltage support. In some cases, this capability has avoided the system from shedding load. The main conclusions of the study are as follows:

1. The proposed reliability evaluation approach provides an effective method of integrating adequacy and dynamic security into a single framework. Stochastic and time-variant characteristics in the system can easily be considered in the evaluation using SMCS.

2. The dynamic security of a system state is quantified by the amount of load shed that is needed to keep the system stable during the transition. By introducing this value of load shed into the calculation of reliability indices, the overall system reliability can be

represented using the well-recognized reliability indices, which are *LOLP*, *EPNS*, and *LOLF*.

3. The proposed CE-IS method greatly speeds up the convergence process of the MCS, and the pruning process considerably reduces the number of cases that need to be evaluated by TDS. The two acceleration methods were found to be accurate in the sense that they do not introduce bias into the calculation of the reliability indices.

4. The importance of representing the ERSs in the evaluation process to measure whether a system has sufficient frequency or voltage support is illustrated in this research. Quantified indices are proposed to measure the adequacy of frequency and voltage support. The results show that system reliability deteriorates when increasing wind power is integrated in the system if there are no additional ERSs contribution from WTGs.

5. The results demonstrate the importance of WTGs providing ERSs when the system has high wind power penetration. Results also verified the use of the proposed approach to consider ERSs assessment and include the capability of WTGs providing reliability services in system reliability evaluation.

8.2   Future Research

During the work conducted on the project, some ideas have been generated to further improve the proposed approach:

1. Computational efficiency: The substantial computational burden of the reliability evaluation is due to the large number of system states that are needed to reach an expected

value of reliability indices. Although the approach proposed in this work is not targeted on real-time evaluation, computational efficiency is expected to be improved. Since each iteration of the MCS is independent of each other, parallel computing techniques and multiple CPU cores to execute reliability evaluation can be applied to this work.

2. Stochastic relay performance: In this work, it is assumed that the faults on transmission lines are cleared 5 cycles after the relay is tripped. However, in a practical scenario, there is some uncertainty associated with the fault clearing time due to relay misoperation, which can be incorporated into the simulations. Also, if historical data on relay failures are available, the probability of relay failure can be incorporated into the dynamic security assessment.

3. Load modeling: In the current work, a load is modeled as a constant impedance load. Since the frequency and voltage support are evaluated in the approach, it is essential to further develop the load model to be voltage and frequency sensitive and include a portion of the motor model in the system. The sensitivity analysis of system reliability with different load models can be examined in the future.

REFERENCES

[1]   "2018 Long-term reliability assessment," North American Electric Reliability Corporation, Atlanta, GA, Dec, 2018.

[2]   E. Rehman, M. Miller, S. John, and F. Huang, "Dynamic stability assessment of high penetration of renewable generation in the ERCOT grid," ERCOT, Austin, Tx, April, 2018.

[3]   "Transmission system planning performance requirements TPL -001-5," North American Electric Reliability Corporation, Atlanta, GA, J, 2018.

[4]   P. Kundur *et al.*, "Definition and classification of power system stability," *IEEE Trans. Power Syst.*, vol. 19, no. 2, p. 1387, May. 2004.

[5]   R. Billinton and W. Li, *Reliability Assessment of Electric Power Systems using Monte Carlo Methods*. New York: Springer, 1994.

[6]   R. Allan, "Power system reliability assessment-A conceptual and historical review," *Reliab. Eng. Syst. Saf.*, vol. 46, no. 1, pp. 3–13, 1994.

[7]   R. Billinton, "Reliability assessment of composite generation and transmission systems: composite system adequacy assessment - the contingency enumeration approach," in *IEEE Tutorial Course*, 1989.

[8]   C. Singh, "Reliabilty assessment of composite generation and transmission system: basic probability and reliability concepts," in *IEEE Tutorial Course*, 1989.

[9]   R. M and H. A, *System reliability theory: Models, statistical methods and applications*. New Jersey: Wiley, 2ed., 2004.

[10]   W. Li, *Risk Assessment of Power Systems: Models, Methods and Applications*. New York: Wiley, 2004.

[11]   F. Vallée, J. Lobry, and O. Deblecker, "System reliability assessment method for wind power integration," *IEEE Trans. Power Syst.*, vol. 23, no. 3, pp. 1288–1297, Aug, 2008.

[12]   A. Ghaedi, A. Abbaspour, M. Fotuhi-Firuzabad, and M. Moeini-Aghtaie, "Toward a comprehensive model of large-scale DFIG-based wind farms in adequacy assessment of power systems," *IEEE Trans. Sustain. Energy*, vol. 5, no. 1, pp. 55–63, Jan. 2014.

[13]   Y. Zhang and A. A. Chowdhury, "Reliability assessment of wind integration in

operating and planning of generation systems," in *IEEE Power & Energy Society General Meeting*, 2009, pp. 1–7.

[14] R. Billinton and W. Li, "Hybrid approach for reliability evaluation of composite generation and transmission systems using Monte-Carlo simulation and enumeration technique," *IEE Proc. C - Gener. Transm. Distrib.*, vol. 138, no. 3, pp. 233–241, May. 1991.

[15] N. Gubbala and C. Singh, "Models and considerations for parallel implementation of monte carlo simulation methods for power system reliability evaluation," *IEEE Trans. Power Syst.*, vol. 10, no. 2, pp. 779–787, May. 1995.

[16] C. L. T. Borges, D. M. Falcão, J. C. O. Mello, and A. C. G. Melo, "Composite reliability evaluation by sequential Monte Carlo simulation on parallel and distributed processing environments," *IEEE Trans. Power Syst.*, vol. 16, no. 2, pp. 203–209, May. 2001.

[17] M. A. Da Rosa, V. Miranda, L. Carvalho, and A. M. L. Da Silva, "Modern computing environment for power system reliability assessment," *2010 IEEE 11th Int. Conf. Probabilistic Methods Appl. to Power Syst.,* Singapore, 2010, pp. 664–671, 2010.

[18] M. A. Da Rosa, A. M. Leite Da Silva, and V. Miranda, "Multi-agent systems applied to reliability assessment of power systems," *Int. J. Electr. Power Energy Syst.*, vol. 42, no. 1, pp. 367–374, May. 2012.

[19] A. M. Leite da Silva, L. C. de Resende, L. A. da Fonseca Manso, and V. Miranda, "Composite reliability assessment based on Monte Carlo simulation and artificial neural networks," *IEEE Trans. Power Syst.*, vol. 22, no. 3, pp. 1202–1209, Aug. 2007.

[20] J. A. S. Dias and C. L. T. Borges, "Object oriented model for composite reliability evaluation including time varying load and wind generation," *2010 IEEE 11th Int. Conf. Probabilistic Methods Appl. to Power Syst.,* Singapore, 2010, pp. 767–772, 2010.

[21] A. Sankarakrishnan and R. Billinton, "Sequential Monte Carlo simulation for composite power reliablity analysis with time varying loads," *IEEE Trans. Power Syst.*, vol. 10, no. 3, pp. 1540–1545, Aug. 1995.

[22] S. R. Huang and S. L. Chen, "Evaluation and improvement of variance reduction in Monte Carlo production simulation," *IEEE Trans. Energy Convers.*, vol. 8, no. 4, pp. 610–617, Dec. 1993.

[23] R. Billinton and A. Jonnavithula, "Composite system adequacy assessment using

sequential Monte Carlo simulation with variance reduction techniques," *IEE Proc. Gener. Transm. Distrib.*, vol. 144, no. 1, pp. 1–6, Jan. 1997.

[24] G. C. Oliveira, M. V. F. Pereira, and S. H. F. Cunha, "A technique for reducing computational effort in Monte-Carlo based composite reliability evaluation," *IEEE Trans. Power Syst.*, vol. 4, no. 4, pp. 1309–1315, Nov. 1989.

[25] M. V. F. Pereira, M. E. P. Maceira, G. C. Oliveira, and L. M. V. . Pinto, "Combining analytical models and Monte-Carlo techniques in probabilistic power system analysis," *IEEE Trans. Power Syst.*, vol. 7, no. 1, pp. 265–272, Feb. 1992.

[26] S. H. F. Cunha, M. V. F. Pereira, M. V. G. Pinto, and G. C. Oliveira, "Composite generation and transmission reliability evaluation in large hydroelectric systems," *IEEE Trans. Power Appar. Syst.*, vol. PAS-104, no. 10, pp. 2657–2663, Oct. 1985.

[27] A. M. L. Da Silva, R. A. G. Fernández, and C. Singh, "Generating capacity reliability evaluation based on Monte Carlo simulation and cross-entropy methods," *IEEE Trans. Power Syst.*, vol. 25, no. 1, pp. 129–137, Feb. 2010.

[28] R. A. González-Fernández and A. M. Leite Da Silva, "Reliability assessment of time-dependent systems via sequential cross-entropy Monte Carlo simulation," *IEEE Trans. Power Syst.*, vol. 26, no. 4, pp. 2381–2389, Nov. 2011.

[29] R. A. González-Fernández, A. M. Leite Da Silva, L. C. Resende, and M. T. Schilling, "Composite systems reliability evaluation based on Monte Carlo simulation and cross-entropy methods," *IEEE Trans. Power Syst.*, vol. 28, no. 4, pp. 4598–4606, Nov. 2013.

[30] N. Maruejouls, V. Sermanson, S. T. Lee and P. Zhang, "A practical probabilistic reliability assessment using contingency simulation," IEEE PES Power Systems Conference and Exposition, 2004., New York, NY, 2004, pp. 1312-1318 vol.3

[31] D. S. Kirschen, D. Jayaweera, D. P. Nedic, and R. N. Allan, "A probabilistic indicator of system stress," *IEEE Trans. Power Syst.*, vol. 19, no. 3, pp. 1650–1657, Aug. 2004.

[32] E. Vaahedi, W. Li, T. Chia, and H. Dommel, "Large scale probabilistic transient stability assessment using B.C. Hydro's on-line tool," *IEEE Trans. Power Syst.*, vol. 15, no. 2, pp. 661–667, May. 2000.

[33] R. Billinton, P. R. S. Kuruganty and M. F. Carvalho, "An approximate method for probabilistic assessment of transient stability," in *IEEE Transactions on Reliability*, vol. R-28, no. 3, pp. 255-258, Aug. 1979.

[34] J. D. McCalley, A. A. Fouad, V. Vittal, A. A. Irizarry-Rivera, B. L. Agrawal and R.

G. Farmer, "A risk-based security index for determining operating limits in stability-limited electric power systems," in *IEEE Transactions on Power Systems*, vol. 12, no. 3, pp. 1210-1219, Aug. 1997.

[35] V. Van Acker, J. D. McCalley, V. Vittal, and J. A. P. Lopes, "Risk-Based transient stability assessment," *Int. Conf. Electr. Power Eng. PowerTech Budapest 1999*, p. 235, 1999.

[36] M. Ni, J. D. Mccalley, V. Vittal, and T. Tayyib, "Online risk-based security assessment," *IEEE Trans. Power Syst.*, vol. 18, no. 1, pp. 258–265, Feb. 2003.

[37] J. D. McCalley, V. Vittal, and M. Ni, "On-Line Risk-Based Security Assessment,"Iwoa State Univ, 1999.

[38] R. Billinton and P. R. S. Kuruganty, "A probabilistic index for transient stability, " *IEEE Trans. Power Appar. Syst*, vol. PAS-99, no. 1, pp. 195-206, Jan. 1980.

[39] P. R. . K. R.Billinton, "Probabilistic assessment of transient stability in a practical multimachine system," *IEEE Trans. Power Appar. Syst.*, vol. PAS-100, no. 7, pp. 3634–3641, 1981.

[40] S. Aboreshaid, R. Billinton, and M. Fotuhi-Firuzabad, "Probabilistic transient stability studies using the method of bisection," *IEEE Trans. Power Syst.*, vol. 11, no. 4, pp. 1990–1995, Nov. 1996.

[41] R. Billinton and S. Aboreshaid, "Stochastic modelling of high-speed reclosing in probabilistic transient stability studies," *IEE Proc. Gener. Transm. Distrib.*, vol. 142, no. 4, pp. 350–354, July. 1995.

[42] D. Fang, L. Jing, and T. Chung, "Corrected transient energy function-based strategy for stability probability assessment of power systems," *IET Gener. Transm. Distrib.*, vol. 2, no. 3, pp. 424–432, May. 2008.

[43] A. Dissanayaka, U. D. Annakkage, B. Jayasekara, and B. Bagen, "Risk-based dynamic security assessment," *IEEE Trans. Power Syst.*, vol. 26, no. 3, pp. 1302–1308, Aug. 2011.

[44] P. M. Anderson and A. Bose, "A probabilistic approach to power system stability analysis," *IEEE Trans. Power Appar. Syst.*, vol. PAS-102, no. 8, pp. 2430–2439, Aug. 1983.

[45] K. J. Timko, A. Bose, and P. M. Anderson, "Monte carlo simulation of power system stability," *IEEE Trans. Power Appar. Syst.*, vol. PAS-102, no. 10, pp. 3453–3459, Oct. 1983.

[46]   L. Shi, S. Sun, L. Yao, Y. Ni, and M. Bazargan, "Effects of wind generation intermittency and volatility on power system transient stability," *IET Renew. Power Gener.*, vol. 8, no. 5, pp. 509–521, July. 2014.

[47]   P. N. Papadopoulos and J. V. Milanović, "Probabilistic framework for transient stability assessment of power systems with high penetration of renewable generation," *IEEE Trans. Power Syst.*, vol. 32, no. 4, pp. 3078–3088, July. 2017.

[48]   P. N. Papadopoulos, A. Adrees and J. V. Milanovićć, "Probabilistic assessment of transient stability in reduced inertia systems," *2016 IEEE Power and Energy Society General Meeting (PESGM)*, Boston, MA, 2016, pp. 1-5.

[49]   M. Negnevitsky, D. H. Nguyen, and M. Piekutowski, "Risk assessment for power system operation planning with high wind power penetration," *IEEE Trans. Power Syst.*, vol. 30, no. 3, pp. 1359–1368, May 2015.

[50]   H. Ahmadi and H. Ghasemi, "Maximum penetration level of wind generation considering power system security limits," *IET Gener. Transm. Distrib.*, vol. 6, no. 11, pp. 1164–1170, Nov. 2012.

[51]   L. Wu and D. Infield, "Power system frequency management challenges - a new approach to assessing the potential of wind capacity to aid system frequency stability," *IET Renew. Power Gener.*, vol. 8, no. 7, pp. 733–739, Sep. 2014.

[52]   J. F. Zhang, C. T. Tse, K. W. Wang, and C. Y. Chung, "Voltage stability analysis considering the uncertainties of dynamic load parameters," *IET Gener. Transm. Distrib.*, vol. 3, no. 10, pp. 941–948, Oct. 2009.

[53]   A. B. Almeida, E. V. De Lorenci, R. C. Leme, A. C. Z. De Souza, B. I. L. Lopes, and K. Lo, "Probabilistic voltage stability assessment considering renewable sources with the help of the PV and QV curves," *IET Renew. Power Gener.*, vol. 7, no. 5, pp. 521–530, Sept. 2013.

[54]   S. Q. Bu, W. Du, and H. F. Wang, "Probabilistic analysis of small-signal rotor angle/voltage stability of large-scale AC/DC power systems as affected by grid-connected offshore wind generation," *IEEE Trans. Power Syst.*, vol. 28, no. 4, pp. 3712–3719, Nov. 2013.

[55]   J. Muñoz, C. Cañizares, K. Bhattacharya, and A. Vaccaro, "An affine arithmetic-based method for voltage stability assessment of power systems with intermittent generation sources," *IEEE Trans. Power Syst.*, vol. 28, no. 4, pp. 4475–4487, Nov. 2013.

[56]   A. B. Rodrigues, R. B. Prada, and M. D. G. Da Silva, "Voltage stability probabilistic assessment in composite systems: Modeling unsolvability and controllability loss,"

IEEE Trans. Power Syst., vol. 25, no. 3, pp. 1575–1588, Aug. 2010.

[57] A. M. Leite Da Silva, I. P. Coutinho, A. C. Zambroni De Souza, R. B. Prada, and A. M. Rei, "Voltage collapse risk assessment," *Electr. Power Syst. Res.*, vol. 54, no. 3, pp. 221–227, 2000.

[58] S. Aboreshaid and R. Billinton, "Probabilistic evaluation of voltage stability," *IEEE Trans. Power Syst.*, vol. 14, no. 1, pp. 342–348, Feb. 1999.

[59] S. O. Faried, R. Billinton and S. Aboreshaid, "Probabilistic evaluation of transient stability of a power system incorporating wind farms," in *IET Renewable Power Generation*, vol. 4, no. 4, pp. 299-307, July 2010.

[60] M. Abapour and M. R. Haghifam, "On-line assessment of the transient instability risk," *IET Generation, Transmission & Distribution*, vol. 7, no. 6. pp. 602–612, Jun. 2013.

[61] "Essential reliability services whitepaper on sufficiency guidelines," North American Electric Reliability Corporation, Atlanta, GA, Dec. 2016.

[62] "2014 Long-term reliability assessment," North American Electric Reliability Corporation, Atlanta, GA, Nov, 2014.

[63] F. F. Wu, Y. K. Tsai, and Y. X. Yu, "Probabilistic steady-state and dynamic security assessment," *IEEE Trans. Power Syst.*, vol. 3, no. 1, pp. 1–9, Feb. 1988.

[64] A. M. Leite Da, S. J. Endrenyi, and L. Wang, "Integrated treatment of adequacy and security in bulk power system reliability evaluations," *IEEE Transactions on Power Systems*, vol. 8, no. 1, pp. 275-285, Feb. 1993.

[65] G. M. Huang and Y. Li, "Power system reliability indices to measure impacts caused by transient stability crises," *2002 IEEE Power Engineering Society Winter Meeting. Conference Proceedings (Cat. No.02CH37309)*, New York, NY, USA, 2002, pp. 766-771 vol.2.

[66] N. Amjady, "A framework of reliability assessment with consideration effect of transient and voltage stabilities," *IEEE Trans. Power Syst.*, vol. 19, no. 2, pp. 1005–1014, May. 2004.

[67] A. M. Rei, M. Armando, L. Da Suva, J. L. Jardim, and J. C. O. De Mello, "Static and dynamic aspects in bulk power system reliability evaluations," *IEEE Trans. Power Syst.*, vol. 15, no. 1, pp. 189–195, Feb. 2000.

[68] M. Benidris, J. Mitra, and C. Singh, "Integrated evaluation of reliability and stability of power systems," *IEEE Trans. Power Syst.*, vol. 32, no. 5, pp. 4131–4139, Sep.

2017.

[69]   N. Nguyen and J. Mitra, "Reliability of power system with high wind penetration under frequency stability constraint," *IEEE Trans. Power Syst.*, vol. 33, no. 1, pp. 985–994, Jan., Jan. 2018.

[70]   J. A. Momoh and Y. V Makarov, "A framework of voltage stability assessment in power system reliability analysis," *IEEE Trans. Power Syst.*, vol. 14, no. 2, pp. 484–491, May., May 1999.

[71]   C. Liang, P. Wang, X. Han, W. Qin, R. Billinton, and W. Li, "Operational reliability and economics of power systems with considering frequency control processes," *IEEE Trans. Power Syst.*, vol. 32, no. 4, pp. 2570–2580, Jul. 2017.

[72]   "2012 Annual Report Forced Outage Performance of Transmission Equipment," Canadian Electricity Association, 2012.

[73]   V. A. Hines, A. B. Ogilvie, and C. R. Bond, "Continuous Reliability Enhancement for Wind (CREW) Database: Wind Plant Reliability Benchmark," Sandia National Lab., Livermore, California, Sep. 2012.

[74]   N. W. Miller and J. J. Sanchez-gasca, *et al.* "Modeling of GE Wind Turbine-Generators for Grid Studies," General Electric International, Inc., NY, March. 2008.

[75]   R. Karki, P. Hu, and R. Billinton, "A simplified wind power generation model for reliability evaluation," *IEEE Trans. Energy Convers.*, vol. 21, no. 2, pp. 533–540, Jun. 2006.

[76]   R. Billinton, H. Chen, and R. Ghajar, "Time-series models for reliability evaluation of power systems including wind energy," *Microelectron. Reliab.*, vol. 36, no. 9, pp. 1253–1261, 1996.

[77]   R. Billinton and D. Huang, "Incorporating wind power in generating capacity reliability evaluation using different models," *IEEE Trans. Power Syst.*, vol. 26, no. 4, pp. 2509–2517, Nov. 2011.

[78]   N. Abdel-Karim, E. Preston, J. Moura and T. Coleman, "Variable energy resource capacity contributions consistent with reserve margin and reliability," *2017 IEEE Power & Energy Society General Meeting*, Chicago, IL, 2017, pp. 1-5.

[79]   M. Papic *et al.*, "Practical experience in evaluating adequacy of generating capacity in the Western interconnection," *2015 IEEE Power & Energy Society General Meeting*, Denver, CO, 2015, pp. 1-5.

[80]   "SERC 2018 Probabilistic Assessment," SERC Reliability Corporation, Charlotte,

NC, Nov. 2018.

[81]   D. Jager and A. Andreas, "NREL National Wind Technology Center (NWTC): M2 Tower; Boulder, Colorado (Data);," 1996.

[82]   P. M. Anderson and A. A. Fouad, *Power System Control and Stability*, Second Edition. New Jersey: Wiley, 2003.

[83]   "IEEE Recommended Practice for Excitation System Models for Power System Stability Studies, " in *IEEE Std 421.5-2016 (Revision of IEEE Std 421.5-2005)*, vol., no., pp.1-207, 26 Aug. 2016.

[84]   PSLF User's Manual V21, General Electric International, Inc., 2017

[85]   "NERC Protection and Control Standards, PRC-006-1," North American Electric Reliability Corporation, Atlanta, GA, Aug, 2013.

[86]   R. Y. Rubinstein and D. P. Kroese, *The Cross Entropy Method: A Unified Approach To Combinatorial Optimization, Monte-carlo Simulation (Information Science and Statistics)*. Berlin, Heidelberg: Springer-Verlag, 2004.

[87]   Grigg. C and et al., "The IEEE reliability test system-1996. A report prepared by the Reliability Test System Task Force of the Application of Probability Methods Subcommittee," *IEEE Trans. Power Syst.*, vol. 14, no. 3, pp. 1010–1020, Aug. 1999.

[88]   N. W. Miller, K. Clark, and M. Shao, "Frequency responsive wind plant controls: Impacts on grid performance," *2011 IEEE Power and Energy Society General Meeting*, Detroit, MI, USA, 2011, pp. 1-8.

[89]   S. Datta, V.Vittal, "Operational Risk Metric for Dynamic Security Assessment of Renewable Generation", *IEEE Transactions on Power Systems*, vol. 32, no. 2, pp. 1389-1399, Mar. 2017.

[90]   P. Mitra, V. Vittal, B. Keel, J. Mistry, "A systematic approach to n-1-1 analysis for power system security assessment," *IEEE Power and Energy Technology Systems Journal*, vol. 3, no. 2, pp. 71-80, June. 2016.

[91]   C.Singh, J. Jirutitijaroen, J. Mitra, *Electric Power Grid Reliability Evaluation-Models and Methods*, Wiley-IEEE Press, 2018

APPENDIX A

GENERATOR DYNAMIC MODEL DATA

Table A.1 Base Case Power Flow Data

Bus	Name	kV	Pgen	Qgen	Qmax	Qmin	MVA	Pmax	Pmin
1	Gen1	22	205.5	-2.8	750	-600	2200	2000	0
2	Gen2	22	601.4	11.2	325	-250	1200	1000	0
4	Gen11	22	700	12.9	325	-250	1200	1000	0
5	Gen12	22	850	23.1	325	-250	1200	1000	0
7	Gen9	22	850	-13.3	325	-250	1200	1000	0
11	Gen3	22	400	11.4	175	-95	600	500	0
14	Gen7	22	1450	32	850	-750	2400	2000	0
20	Gen4	22	1200	30.8	500	-400	1800	1500	0
22	Gen5	22	1900	52.6	1000	-800	2400	2000	0
24	Gen6	22	3900	168	1500	-1200	4500	4000	0
26	Gen8	22	900	30.8	325	-250	1200	1000	0
8	WTG_8	0.69	300	20	145	-145	334	300	14
28	WTG_28	0.69	150	19.5	72.5	-72.5	167	150	7
29	WTG_29	0.69	150	19	72.5	-72.5	167	150	7
30	WTG_30	0.69	150	19.5	72.5	-72.5	167	150	7
31	WTG_31	0.69	150	10.8	72.5	-72.5	167	150	7
32	WTG_32	0.69	150	25	72.5	-72.5	167	150	7
33	WTG_33	0.69	105	14	50	-50	117	105	5
34	WTG_34	0.69	210	26	100	-100	234	210	10
35	WTG_35	0.69	210	26	100	-100	234	210	10
36	WTG_36	0.69	105	14	50	-50	117	105	5

Note: Pgen, Pmax, Pmin are in MW, Qgen, Qmax, Qmin are in MVAr

Generator, governor, and exciter are modeled for a synchronous generator in this work. Steam turbine, gas turbine, and hydro turbine are modeled with different governors that are represented by TGOV1, GGOV1 and HYGOV respectively in PSLF. The parameters for the three governor models are given in Table A.2 - Table A.4. The parameters of synchronous generator model and exciter model are given in Table A.5 - Table A.6.

Table A.2 Governor Data – TGOV1

R	T1	Vmax	Vmin	T2	T3	Dt
0.05	0.5	1.0	0.0	3.0	10.0	0.0

Table A.3 Governor Data – GGOV1

Rperm	Rtemp	Tr	Tf	Tg	Velm	Gmax
0.04	0.3	5.0	0.05	0.5	0.2	1.0
Gmin	Tw	At	Dturb	Qn1	Ttrip	Tn
0.0	1.0	1.2	0.5	0.08	0	0
Tnp	Db1	Eps	Db2	Gv0	Pgv0	GV1
0	0	0	0	0	0	0
Pgv1	GV2	Pgv2	Gv3	Pgv3	Gv4	Pgv4
0	0	0	0	0	0	0
Gv5	Pgv5	Hdam	Bgv0	Bgv1	Bgv2	Bgv3
0	0	1.0	0	0	0	0
Bgv4	Bgv5	Bmax	Tblade	/	/	/
0	0	0	100	/	/	/

Table A.4 Governor Data – HYGOV

R	Rselect	Tpelec	Maxerr	Miner	Kpgov
0.04	1.0	1.0	0.05	-0.05	10.0
Kigov	Kdgov	Tdgov	Vmax	Vmin	Tact
2.0	0.0	1.0	1.0	0.15	0.5
Kturb	Wfnl	Tb	Tc	Flag	Teng
1.5	0.2	0.1	0.0	1.0	0.0
Tfload	Kpload	Kiload	Ldref	Dm	Ropen
3.0	2.0	0.67	1.0	0.0	0.10
Rclose	Kimw	Pmwset			
-0.1	0.002	80.0			

Table A.5 Synchronous Generator Dynamic Data – GENROU

Tpdo	Tppdo	Tpqo	Tppqo	H	D
7.0	0.025	0.75	0.05	6.0	0.0
Ld	Lq	Lpd	Lpq	Lppd	L1
2.2	2.1	0.22	0.416	0.2	0.147
S1	S12	Ra	Rcomp	Xcomp	/
0.109	0.3	0.0	0.0	0.0	/

Table A.6 Exciter Data – EXST1

Tr	Vimax	Vimin	Tc	Tb	Ka	Ta
0.0	0.1	-0.1	1.0	10.0	100.0	0.02
Vrmax	Vrmin	Kc	Kf	Tf	Tc1	Tb1
5.0	-5.0	0.05	0.0	1.0	1.0	1.0
Vamax	Vamin	Xe	Ilr	Klr	/	/
5.0	-5.0	0.04	2.8	5.0	/	/

The DFAG WTG are modeled using GEWTG, WNDTGE, and EXWTGE in GE PSLF. The dynamic data used in this work are provided in Table A.7 - Table A.9.

Table A.7 Wind Turbine Generator/Converter Model – GEWTG

Lpp	Dvtrp1	Dvtrp2	Dvtrp3	Dvtrp4	Dvtrp5
0.8	-0.25	-0.5	-0.7	-0.85	0.1
Dvtrp6	Dttrp1	Dttrp2	Dttrp3	Dttrp4	Dttrp5
0.15	1.9	1.2	0.7	0.2	1
Dttrp6	Fcflg	Rrpwr	Brkpt	Zerox	/
0.1	0	10	0.9	0.5	/

Table A.8 Wind Turbine and Turbine Control Model – WNDTGE

Spdw1	Tp	Tpc	Kpp	Kip	Kptrq	Kitrq	Kpc
0	0.3	0.05	150	25	3	0.6	3
Kic	Pimax	Pimin	Pwmax	Pwmin	Pwrat	H	Nmass
30	27	0	1.12	0.04	0.45	4.94	1
Hg	Ktg	Dtg	Wbase	Tw	Apcflg	Pa	Pbc
0	0	0	0	1	1	1	0.95
Pd	Fa	Fb	Fc	Fd	Pmax	Pmin	Kwi
0.4	0.96	0.996	1.004	1.04	1	0.2	10
Dbwi	Twowi	Urlwi	Drlwi	Pmxwi	Pmnwi	Wfflg	Td1
0.0025	5.5	0.1	-1	0.1	0	0	0.15
Tpset	Pirat	Tpav	Tlpwi	/	/	/	/
5	10	0.15	1	/	/	/	/

Table A.9 Wind Turbine Converter Control Model – EXWTGE

Varflg	Kqi	Kvi	Vmax	Vmin	Qmax	Qmin	Xiqmax	Xiqmin
-1	0.1	40	1.1	0.9	0.436	-0.436	1.45	0.5
Tr	Tc	Kpv	Kiv	Vl1	Vh1	Tl1	Tl2	Th1
0.02	0.15	18	5	-9999	9999	0	0	0
Th2	Ql1	Ql2	Ql3	Qh1	Qh2	Qh3	Pfaflg	Fn
0	0	0	0	0	0	0	0	1
Tv	Tpwr	Ipmax	Xc	Kqd	Tlpqd	Xqd	Vermn	Vfrz
0.05	0.05	1.22	0	0	5	0	0.1	0.7

APPENDIX B

CHORONOLOGICAL LOAD CURVE DATA

The chronological load curve data is obtained from [87]. The data is listed in Table B.1.

Table B.1 Load Curve Data

Hour	Winter weeks 1 -8 and 44 - 52		Weeks 18 -30		Spring/fall weeks 9-17 & 31 - 43	
	Work day	Weekend	Work day	Weekend	Work day	Weekend
12-1 am	67	78	64	74	63	75
1-2	63	72	60	70	62	73
2-3	60	68	58	66	60	69
3-4	59	66	56	65	58	66
4-5	59	64	56	64	59	65
5-6	60	65	58	62	65	65
6-7	74	66	64	62	72	68
7-8	86	70	76	66	85	74
8-9	95	80	87	81	95	83
9-10	96	88	95	86	99	89
10-11	96	90	99	91	100	92
11-noon	95	91	100	93	99	94
Noon-1pm	95	90	99	93	93	91
1-2	95	88	100	92	92	90

Table B.1 (Continued)

| HOUR | WINTER WEEKS | | WEEKS | | SPRING/FALL WEEKS | |
| | 1 -8 & 44 - 52 | | 18 -30 | | 9-17 & 31 - 43 | |
	WORK DAY	WEEKEND	WORK DAY	WEEKEND	WORK DAY	WEEKEND
2-3	93	87	100	91	90	90
3-4	94	87	97	91	88	86
4-5	99	91	96	92	90	85
5-6	100	100	96	94	92	88
6-7	100	99	93	95	96	92
7-8	96	97	92	95	98	100
8-9	91	94	92	100	96	97
9-10	83	92	93	93	90	95
10-11	73	87	87	88	80	90
11-12	63	81	72	80	70	85

APPENDIX C

HIGH WIND POWER PENETRATION SCENARIOS

Table C.1 10% Wind Power Penetration Case Power Flow Data

Bus	Name	kV	Pgen	Qgen	Qmax	Qmin	MVA	Pmax	Pmin
1	Gen1	22	205.5	-2.8	750	-600	2200	2000	0
2	Gen2	22	300.7	5.6	175	-95	600	500	0
2	Gen2	22	300.7	5.6	175	-95	600	500	0
4	Gen11	22	700	12.9	325	-250	1200	1000	0
5	Gen12	22	850	23.1	325	-250	1200	1000	0
7	Gen9	22	850	-13.3	325	-250	1200	1000	0
11	Gen3	22	400	11.4	175	-95	600	500	0
14	Gen7	22	550	16.2	360	-280	1200	1000	0
14	Gen7	22	900	16.2	360	-280	1200	1000	0
20	Gen4	22	550	15.4	250	-200	900	750	0
20	Gen4	22	650	15.4	250	-200	900	750	0
22	Gen5	22	950	26.3	325	-250	1200	1000	0
22	Gen5	22	950	26.3	325	-250	1200	1000	0
24	Gen6	22	1300	56	500	-400	1500	1350	0
24	Gen6	22	1300	56	500	-400	1500	1350	0
24	Gen6	22	1300	56	500	-400	1500	1350	0
26	Gen8	22	450	15.4	175	-95	600	500	0
26	Gen8	22	450	15.4	175	-95	600	500	0
8	WTG_8	0.69	300	20	145	-145	334	300	14
28	WTG_28	0.69	150	19.5	72.5	-72.5	167	150	7
29	WTG_29	0.69	150	19	72.5	-72.5	167	150	7
30	WTG_30	0.69	150	19.5	72.5	-72.5	167	150	7
31	WTG_31	0.69	150	10.8	72.5	-72.5	167	150	7
32	WTG_32	0.69	150	25	72.5	-72.5	167	150	7
33	WTG_33	0.69	105	14	50	-50	117	105	5
34	WTG_34	0.69	210	26	100	-100	234	210	10
35	WTG_35	0.69	210	26	100	-100	234	210	10
36	WTG_36	0.69	105	14	50	-50	117	105	5

Note: Vbase is in kV, Pgen, Pmax, Pmin are in MW, Qgen, Qmax, Qmin are in MVAr

Table C.2 20% Wind Power Penetration Case Power Flow Data

Bus	Name	Vbase	Pgen	Qgen	Qmax	Qmin	MVA	Pmax	Pmin
1	Gen1	22	280	-2.8	750	-600	2200	2000	0
2	Gen2	22	260	3.7	175	-95	600	500	0
2	Gen2	22	260	3.7	175	-95	600	500	0
4	Gen11	22	600	5.7	325	-250	900	750	0
5	Gen12	22	600	5.7	325	-250	1200	1000	0
7	Gen9	22	600	-46.2	325	-250	1200	1000	0
11	Gen3	22	350	8.1	175	-95	600	500	0
14	Gen7	22	500	13.8	325	-250	1200	1000	0
14	Gen7	22	900	13.8	325	-250	1200	1000	0
20	Gen4	22	550	15.4	325	-250	900	750	0
20	Gen4	22	650	15.4	325	-250	900	750	0
22	Gen5	22	945	26	325	-250	1200	1000	0
22	Gen5	22	945	26	325	-250	1200	1000	0
24	Gen6	22	975	28.9	325	-250	1200	1000	0
24	Gen6	22	975	28.9	325	-250	1200	1000	0
24	Gen6	22	975	28.9	325	-250	1200	1000	0
26	Gen8	22	450	15.3	175	-95	600	500	0
26	Gen8	22	450	15.3	175	-95	600	500	0
801	WTG_8	0.69	600	21	290	-290	668	600	14
2801	WTG_28	0.69	300	34	145	-145	334	300	7
2901	WTG_29	0.69	300	33	145	-145	334	300	7
3001	WTG_30	0.69	300	33	145	-145	334	300	7
3101	WTG_31	0.69	300	32	145	-145	334	300	7
3201	WTG_32	0.69	300	44.5	145	-145	334	300	7
3301	WTG_33	0.69	210	25.5	101.5	-101.5	234	210	5
3401	WTG_34	0.69	420	44	203	-203	468	420	10
3501	WTG_35	0.69	420	44	203	-203	468	420	10
3601	WTG_36	0.69	210	25.5	101.5	-101.5	234	210	5

Note: Vbase is in kV, Pgen, Pmax, Pmin are in MW, Qgen, Qmax, Qmin are in MVAr

Table C.3 40% Wind Power Penetration Case Power Flow Data

Bus	Name	Vbase	Pgen	Qgen	Qmax	Qmin	MVA	Pmax	Pmin
1	Gen1	22	61.1	-1.9	750	-600	1800	1500	0
2	Gen2	22	180	-0.8	175	-95	600	500	0
2	Gen2	22	0	0	0	0	0	0	0
4	Gen11	22	200	-7	325	-250	900	750	0
5	Gen12	22	200	-7	325	-250	900	750	0
7	Gen9	22	200	-67.6	325	-250	900	750	0
11	Gen3	22	200	1.7	175	-95	600	500	0
14	Gen7	22	500	13.9	325	-250	1200	1000	0
14	Gen7	22	900	13.9	325	-250	1200	1000	0
20	Gen4	22	550	15.5	325	-250	900	750	0
20	Gen4	22	650	15.5	325	-250	900	750	0
22	Gen5	22	600	12.5	325	-250	900	750	0
22	Gen5	22	800	12.5	325	-250	1200	1000	0
24	Gen6	22	800	15.3	325	-250	1200	1000	0
24	Gen6	22	800	15.3	325	-250	1200	1000	0
24	Gen6	22	650	15.3	325	-250	900	750	0
26	Gen8	22	300	5.6	175	-95	600	500	0
26	Gen8	22	300	5.6	175	-95	600	500	0
801	WTG_8	0.69	1200	16	581	-581	1336	1200	14
2801	WTG_28	0.69	600	54	290.5	-290.5	668	600	7
2901	WTG_29	0.69	600	52	290.5	-290.5	668	600	7
3001	WTG_30	0.69	600	50.5	290.5	-290.5	668	600	7
3101	WTG_31	0.69	600	50	290.5	-290.5	668	600	7
3201	WTG_32	0.69	600	69.5	290.5	-290.5	668	600	7
3301	WTG_33	0.69	420	44.5	203.5	-203.5	467.5	420	5
3401	WTG_34	0.69	840	69	407	-407	935	840	10
3501	WTG_35	0.69	840	69	407	-407	935	840	10
3601	WTG_36	0.69	420	44	203.5	-203.5	467.5	420	5

Note: Vbase is in kV, Pgen, Pmax, Pmin are in MW, Qgen, Qmax, Qmin are in MVAr

Table C.4 60% Wind Power Penetration Case Power Flow Data

Bus	Name	Vbase	Pgen	Qgen	Qmax	Qmin	MVA	Pmax	Pmin
1	Gen1	22	213.9	-2.7	325	-250	1200	1000	0
2	Gen2	22	105	-1.4	175	-95	600	500	0
4	Gen11	22	210	-7.5	325	-250	900	750	0
5	Gen12	22	210	-7.5	325	-250	900	750	0
7	Gen9	22	210	-64.7	175	-95	600	500	0
11	Gen3	22	90	-0.5	175	-95	600	500	0
14	Gen7	22	600	-4.9	325	-250	900	750	0
20	Gen4	22	500	2.3	325	-250	900	750	0
22	Gen5	22	300	0.4	325	-250	900	750	0
22	Gen5	22	300	0.4	325	-250	900	750	0
24	Gen6	22	500	4	325	-250	900	750	0
24	Gen6	22	500	4	325	-250	1200	1000	0
24	Gen6	22	400	4	325	-250	900	750	0
26	Gen8	22	250	3.3	175	-95	600	500	0
26	Gen8	22	250	3.3	175	-95	600	500	0
801	WTG_8	0.69	1800	22	871	-871	2004	1800	14
2801	WTG_28	0.69	900	66.5	435.5	-435.5	1002	900	7
2901	WTG_29	0.69	900	64	435.5	-435.5	1002	900	7
3001	WTG_30	0.69	900	69	435.5	-435.5	1002	900	7
3101	WTG_31	0.69	900	68	435.5	-435.5	1002	900	7
3201	WTG_32	0.69	900	90.5	435.5	-435.5	1002	900	7
3301	WTG_33	0.69	630	58	305	-305	701.5	630	5
3401	WTG_34	0.69	1260	86	610	-610	1403	1260	10
3501	WTG_35	0.69	1260	86	610	-610	1403	1260	10
3601	WTG_36	0.69	630	57.5	305	-305	701.5	630	5

Note: Vbase is in kV, Pgen, Pmax, Pmin are in MW, Qgen, Qmax, Qmin are in MVAr

Table C.5 80% Wind Power Penetration Case Power Flow Data

Bus	Name	Vbase	Pgen	Qgen	Qmax	Qmin	MVA	Pmax	Pmin
1	Gen1	22	68.7	-2.7	325	-250	2000	1800	0
2	Gen2	22	50	-0.8	175	-95	1200	1000	0
2	Gen2	22	50	-0.8	175	-95	1200	1000	0
4	Gen11	22	150	-11.5	325	-250	900	750	0
5	Gen12	22	0	-6.2	325	-250	600	500	0
7	Gen9	22	50	-51.3	175	-95	600	500	0
11	Gen3	22	0	-0.2	175	-95	600	500	0
14	Gen7	22	300	-7.9	325	-250	600	500	0
14	Gen7	22	0	-2.5	325	-250	600	500	0
20	Gen4	22	400	0.6	325	-250	900	750	0
20	Gen4	22	0	1.7	325	-250	600	500	0
22	Gen5	22	50	-0.8	325	-250	600	500	0
22	Gen5	22	0	-0.1	325	-250	900	750	0
24	Gen6	22	0	-0.6	325	-250	900	750	0
24	Gen6	22	100	-1	325	-250	900	750	0
24	Gen6	22	80	-1	325	-250	600	750	0
26	Gen8	22	50	-0.6	175	-95	600	500	0
26	Gen8	22	50	-0.6	175	-95	600	500	0
801	WTG_8	0.69	2400	53	1162	-1162	2672	2400	14
2801	WTG_28	0.69	1200	75.5	581	-581	1336	1200	7
3001	WTG_30	0.69	1200	83.5	581	-581	1336	1200	7
3101	WTG_31	0.69	1200	86	581	-581	1336	1200	7
3201	WTG_32	0.69	1200	114.5	581	-581	1336	1200	7
3301	WTG_33	0.69	840	69	406.5	-406.5	935	840	5
3401	WTG_34	0.69	1680	101	813	-813	1870	1680	10
3501	WTG_35	0.69	1680	101	813	-813	1870	1680	10
3601	WTG_36	0.69	840	68.5	406.5	-406.5	935	840	5

Note: Vbase is in kV, Pgen, Pmax, Pmin are in MW, Qgen, Qmax, Qmin are in MVAr